Purely Ionic and Molecular Orbital Modelings

of the Bonding

in Mineral Crystal Structures

by

Curtis George Lindsay

Dissertation submitted to the Faculty of the

Virginia Polytechnic Institute and State University

in partial fulfillment of the requirements for the degree of

Doctor of Philosophy

in

Geological Sciences

APPROVED:

G. V. Gibbs, Chairman

F. D. Bloss

M. B. Boisen, Jr.

J. D. Rimstidt

J. W. Viers

August, 1988

Blacksburg, Virginia

Purely Ionic and Molecular Orbital Modelings

of the Bonding

in Mineral Crystal Structures

by

Curtis George Lindsay

G. V. Gibbs, Chairman

Geological Sciences

(ABSTRACT)

The modified electron gas (MEG) model has been used to generate ionic model $CaCO_3$ crystals in the calcite, aragonite, diopside, and perovskite structure types. For calcite and aragonite, the model predicts shorter CO bonds and larger bulk moduli than observed. Modeling of the thermochemistry of $CaCO_3$ does not reproduce the observed thermochemistry even qualitatively. The model predicts that the hypothetical diopside structure type is the most stable form $CaCO_3$ among the four structure types. These discrepancies may illustrate the significance of CO bond covalency in determining the physico-chemical properties of $CaCO_3$.

The MEG model has also been used to generate model alkali halide crystals in the sphalerite, rocksalt, and CsCl types in an exploration of the reliability of the radius ratio rule. The MEG model predicts the correct cation coordination numbers for 13 of 16 alkali halides, whereas the radius ratio rule predicts the correct coordination numbers in at most 9 of the same 16 alkali halides. Analyses of the model crystal structures suggests that energy minimization is more important than packing efficiency in determining the most stable structures for ionic crystals.

The molecular orbital (MO) model has been used to determine minimum-energy geometries and electron density distributions in sulfate hydroxyacid molecules. These molecules have been used to model the bonding in sulfate crystals. SO bond lengths calculated for H_2SO_4 and $H_2S_2O_7$ correlate linearly with fractional s-characters of the bonds, as in sulfate crystals. With increasing S coordination number, the bonded radii of S and O, as determined from electron density maps, increase at the same rate, contrary to the common assumption of constant anion radii. $H_2S_2O_7$ shows a relatively large change in energy as its SOS angle is deformed from its minimum-energy value

(125.6°) to 180°, in conformity with the small variation among observed SOS angles. In contrast, SiOSi and POP angles show relatively wide variations in crystals and molecules. This suggests that polysulfates may be less amenable than polysilicates or polyphosphates to polymorphism or glass formation. Other properties of H_2SO_4 are also calculated and compared with experimental observations and previous calculations.

Acknowledgements

The author expresses his deep appreciation to his major professor, Dr. G. V. Gibbs, for his invaluable guidance, assistance, support, and encouragement through all phases of the work that led to the production of this dissertation. The author also wishes to thank the members of his advisory committee, Dr. F. D. Bloss, Dr. M. B. Boisen, Jr., Dr. J. D. Rimstidt, and Dr. J. W. Viers, for the time and effort they contributed to reviewing this dissertation, for their helpful suggestions for its improvement, and for their overall support of the author's studies. Special thanks are extended to Dr. Mark D. Jackson for instructing the author in the theory and application of the modified electron gas method and for reviewing Chapter II. The author also thanks the other members of his research group, especially Dr. Maureen Julian, Kurt Bartelmehs, and Bob Downs, for their friendship and support during the author's studies. provided numerous helpful suggestions for producing the graphic displays, and she and her assistants are thanked for their prompt and patient service in drafting the figures. Virginia Chapman's assistance in preparing the manuscript is also gratefully acknowledged. The studies reported in this dissertation were supported by the National Science Foundation through grant EAR 82 18743 to and grant EAR 88 03933 to and , for studying bonding and charge density distributions in minerals, and through additional generous support of computations on the CRAY supercomputer at the Pittsburgh Supercomputing Center.

Table of Contents

Chapter I

OVERVIEW

Reliable methods for modeling the bonding in crystals provide the crystal chemist with valuable tools for elucidating the physics of crystals on a scale that cannot be studied by experimental means. It would be gratifying to develop a technique that could be used to calculate the value of any quantitative property of a crystalline material from fundamental physical principles without the aid of experimental measurements; to do so would seem to indicate a thorough understanding of the physics of chemical bonding in crystals. This level of success has not yet been attained insofar as we are aware, but several modeling methods have been quite successful in reproducing the observed values of at least some of the properties of crystals, or structural units within crystals, within limits on chemistry and structure type. Even when a model is not particularly successful at reproducing observed properties, it can provide a means of improving our understanding of bonding in crystals in that it provides an opportunity for isolating the cause of the failure and for modifying the theory underlying the method.

In the next three chapters, we demonstrate two methods for modeling chemical bonding. The first is a method developed by Gordon and Kim (1972) and modified by Waldman and Gordon (1979), called the modified electron gas (MEG) method. The other is the molecular orbital (MO) method. Both methods use isolated-atom wavefunctions determined from a set of basis functions using Hartree-Fock self-consistent field (HF SCF) theory. In the MEG method, the isolated-atom wavefunctions are assumed to retain their forms as atoms approach one another to form a crystal

structure. The electron density distribution within a crystal therefore represents a simple superposition of the isolated-atom electron densities. In the MO method, as atoms approach one another to form a molecular unit, the isolated-atom wavefunctions, or atomic orbitals (AOs), are assumed to combine to form new wavefunctions, i.e. MOs, characteristic of the molecular unit. These MOs are assumed to be linear combinations of atomic orbitals (LCAOs), and the coefficients of the individual AOs in these linear combinations are determined by HF SCF theory. The electron density within and around the molecular units is therefore not a simple superposition of isolated-atom electron densities, but is determined by the form of the MOs.

The MO method is mathematically more complicated, and therefore is computationally less economical, than is the MEG method. Consequently, generations of entire crystal structures with the MO method are currently intractable for all but the simplest crystal structures. Instead, the MO method is more suitable for modeling gas-phase molecules, which in turn serve as models for the bonding in chemically and geometrically similar structural units in crystals. Gibbs (1982) has reviewed such modelings of the bonding in silicates, and a modeling of the bonding in sulfates in this way is reported in Chapter IV. Oxyanions of several first- and second-row elements have also been modeled with the MO method, and the geometric and dynamic properties of the model oxyanions have been found to be closely correlated with particular features of crystal structures containing these oxyanions (see the references cited in Chapter IV), so that the validity of studying crystal structures in this way has become fairly well established.

The aforementioned limitations of the MO method in generating complete crystal structures provided one of the motivations for developing the MEG method (cf. Gordon and Kim 1972). As noted in Chapter II, this method has been used successfully to generate the structures of noble-gas crystals, of crystals such as the alkali halides where the bonding is believed to be largely ionic, and of monosilicates, where the silicate oxyanions are insular. The MEG method is ideally suited to modeling noble-gas and ionic crystals, due to the way that the method models interatomic interactions. Because no new electronic states are generated as the atoms or ions approach each other, the model does not include covalent effects. For ionic crystals, the binding forces are therefore purely ionic, and for noble-gas crystals, the binding forces are those that obtain between neu-

tral, closed-shell atoms. The MEG method is therefore capable of generating a model crystal structure having purely ionic bonding, and a comparison between such an ionic model structure and that observed for a given material can potentially reveal the features of the observed structure that are due to covalency. This kind of modeling has been undertaken for the crystal structures of $CaCO_3$ in the study described in Chapter II. In Chapter III, the MEG method has been applied to crystal structures where the bonding is believed to be largely ionic, to assess the validity of traditional models of ionic crystals, specifically the well-known radius ratio rule (Pauling 1939) for predicting cation coordination numbers. The structures of the ionic crystals generated with the MEG model are also analyzed in that chapter in an attempt to discover factors other than simple packing considerations that lead to stable atomic arrangements in ionic crystals.

Each of Chapters II through IV represents an individual investigation of the bonding in crystals. Because different materials have been studied in each chapter, this series of studies is not intended to provide an evaluative comparison of the MEG and the MO method. Instead, each chapter provides an illustration of applications of the two methods and demonstrates the kinds of information each can provide about the forces that bind the atoms in crystals and the influences those forces exert on the physico-chemical properties of the crystals.

Chapter II

A MODELING OF OBSERVED AND HYPOTHETICAL STRUCTURE TYPES OF CALCIUM CARBONATE USING MODIFIED ELECTRON GAS METHODS

INTRODUCTION

Theoretical modeling of crystalline materials not only provides the prediction of the behavior of such materials under conditions which are difficult to attain experimentally, but it also allows an exploration of the properties of materials that have neither been found in nature nor synthesized in the laboratory. First-principles models, which require no empirical data, are best suited to these purposes. The modified electron gas (MEG) model (Waldman and Gordon 1979) is a first-principles model which is conceptually simple and computationally economical. It has been successfully used to model the crystal structures of the inert gases and the binary oxides and halides (Gordon and Kim 1972, Cohen and Gordon 1975, 1976, Waldman and Gordon 1979, Jackson 1986, Jackson and Gordon 1988a), and also of certain monosilicate minerals, where the silicate tetrahedra are insular (Jackson 1986, Post and Burnham 1986, Jackson and Gordon 1988a,b). The MEG model has been less successful in its use in modeling monopolysilicate and tectosilicate structures, where oxide ions link silicate tetrahedra into chains and three-dimensional frameworks, respectively (Post and Burnham 1986, Jackson and Gibbs 1988, Jackson and Gordon 1988a). The disiloxy groups in these materials are believed to have significant covalent character, whereas MEG theory is based on a purely ionic bonding model. MEG theory has been extended to model anion polarization (Jackson 1986, Jackson and Gibbs 1988 Jackson and Gordon 1988a), thereby im-

proving the agreement between model and observed structures when applied to the silica polymorphs quartz, cristobalite, and coesite. However, when applied to Mg_2SiO_4 in the forsterite and spinel structure types, use of the polarization model led to poorer agreement between model and observed structures.

Whether or not it accurately reproduces the experimentally observed crystal structures adopted by a given material, the MEG model is useful in that it generates the structure types the material would adopt if the bonding were purely ionic. A comparison of these crystal structures with those observed serves to identify those features of an observed crystal structure that may reflect departures of the bonding from purely ionic character. The $CaCO_3$ polymorphs calcite and aragonite are particularly good candidates for such a study. The CO bonds in these structures are believed to be largely covalent, whereas the CaO bonds are believed to be largely ionic (cf. Lippmann 1973, Reeder 1983, Speer 1983, Klein and Hurlbut 1985). We have therefore undertaken ionic MEG modelings of the structures of calcite and aragonite to gain insight into the ways in which departures from ionic bonding express themselves in the crystal structures. We have also modeled $CaCO_3$ in the diopside and the perovskite structure types to explore their atomic arrangements, elastic properties, and thermodynamic stabilities, with an ionic model.

A REVIEW OF MEG THEORY

Gordon and Kim (1972) formulated the original electron gas (EG) model as a way of calculating the forces between inert-gas atoms. The mathematical details of the model are discussed by those authors and by Clugston (1978). Briefly, the model assumes that the electron density distribution about an isolated atom is that determined from the Hartree-Fock wavefunctions for the atom, and that no rearrangement of the isolated-atom electron densities takes place when the atoms are brought together to form a crystal. The EG model applies specifically to closed-shell atoms and ions, and therefore when applied to species other than inert gases, it is a purely ionic model.

The lattice energy (W) of a crystal is given by

$$W = E_{Cp} + E_{sr} + E_v + E_{v0} \tag{1}$$

where the individual terms in Equation (1) are the point Coulombic, the short-range repulsion, the vibrational (thermal), and the zero-point vibrational energies, respectively. In our calculations, we assume static crystal structures at absolute zero temperature, so $E_v = E_{v0} = 0$. The short-range repulsion energy (E_{sr}) comprises the non-point Coulombic, kinetic, exchange, and correlation energies, respectively:

$$E_{sr} = E_{Cnp} + E_{kin} + E_{exc} + E_{corr}. \tag{2}$$

Each term in Equation (2) is a functional of the electron density, i.e., the energy terms each have the form of a function whose argument is another variable function rather than a set of discrete independent variables (cf. Schlüter and Sham 1982).

The point Coulombic energy, E_{Cp}, is the sum, over all ion pairs in the crystal structure, of the classical Coulombic energy, which treats each ion as a point charge. The non-point Coulombic energy, E_{Cnp}, arises from the overlap of the electron density distributions associated with neighboring ions and, in general, from the effects of non-sphericity of the electron density distributions. In our modelings, each ion has a spherically symmetric electron density distribution, therefore only the overlap effects contribute to E_{Cnp}. In practice, E_{Cp} is calculated using the Ewald method (Ewald 1921, Muhlhausen and Gordon 1981) to expedite convergence, and E_{sr}, which includes E_{Cnp}, is calculated using the pair-potential approximation (Muhlhausen and Gordon 1981); i.e., E_{sr} is calculated initially for each pair of ionic species as a function of distance, resulting in a set of pair potentials for each ion pair, and then the values of E_{sr} at the calculated interionic distances are summed over each ion pair in the structure.

In the MEG model, the electron density functionals are scaled to improve the accuracy of the calculations (cf. Waldman and Gordon 1979). The unscaled density functionals apply to a uniform electron gas comprising an infinite number of electrons, which is not a realistic representation of the electron density in an atomic aggregate. The values of E_{kin}, E_{exc} , and E_{corr} calculated with Hartree-Fock theory for noble-gas atom pairs are assumed to be exact, and the scaling factors for the corresponding functionals to be used in MEG calculations are chosen so that the respective values returned by those functionals match the Hartree-Fock values. The scaling factors thus determined

for noble-gas pairs are assumed to be valid for pairs of ions isoelectronic with the noble-gas atoms. The scaling factors depend only on the number of electrons involved in each functional, and are independent of the crystal structure being modeled. EG calculations of E_{C_p} are intrinsically exact within the additive-density approximation (Waldman and Gordon 1979) and are not scaled.

As we are interested in the thermodynamic stabilities of our model crystal structure types with respect to pressure variations at 0K, we calculate the Gibbs free energy (G):

$$G = W + PV \tag{3}$$

where P and V have their usual thermodynamic meanings. We adopt a reference state consisting of free electrons and gas-phase ions at infinite separation. To calculate wavefunctions for the inherently unstable gas-phase O^{2-} ion, we use a perturbation technique (Watson 1958) in which a Watson sphere, a spherical shell having radius r_0 and charge $+2$, is placed around the ion. The value chosen for r_0 determines the electrostatic potential about the O^{2-} ion. In an MEG model crystal structure, the crystal field stabilizes the O^{2-} ion and determines the electrostatic potential about the ion. Therefore we require that this electrostatic potential at each O^{2-} site (the site potential, $V_{site}(O^{2-})$) in the crystal be equal to $2/r_0$, the electrostatic potential due to the Watson sphere used to stabilize the gas-phase O^{2-} ion. A crystal structure for which this condition is met is said to be electrostatically consistent. To achieve electrostatic consistency in our model structures, we vary the external pressure imposed on the structure in the energy calculation in order to vary the interionic distances, thereby varying $V_{site}(O^{2-})$, until $2/V_{site}(O^{2-})$ is within 10^{-5} a.u. of the initially chosen value of r_0 . This introduces two additional energy terms, the anion self- energy (the energy of the Watson-sphere stabilized O^{2-} ion relative to that of the intrinsically stable O^- ion) and the difference between the correlation energies of O^{2-} and O^-. Self-energy values for O^{2-} have been determined for each r_0 value required for our calculations; the correlation energy difference is assumed to be invariant with r_0. These two terms are added to the minimized G and W values.

COMPUTATIONAL DETAILS

The modeling of the structures and elastic properties of the $CaCO_3$ polymorphs was done in two stages. First, we undertook MEG calculations to obtain the required pair potentials and to generate a series of electrostatically consistent structures over a range of pressures for each structure type. The latter calculations also give G and V for each such structure. We developed a preliminary W-V curve for the structure type at this stage to ensure that the modeling predicted a systematic W-V trend and also to estimate the zero-pressure unit cell volume (V_0) . Next, we fitted our G-V data to a Birch-Murnaghan equation (Birch 1978) to calculate the zero-pressure bulk modulus (K_0) and the G-P curve for each structure type. It is possible in principle to develop G-P relations directly from the results of the MEG calculations, but these usually contain numerical noise which is eliminated by fitting the Birch-Murnaghan equation to these results.

We used the program LEMINPI, written by C. Muhlhausen, for our pair potential calculations and our crystal structure modelings. For Ca^{2+} and C^{4+}, we used the gas phase wavefunctions tabulated by Clementi and Roetti (1974); these are applicable to all of our model structure types. The O^{2-} wavefunctions are also independent of structure type, but different O^{2-} wavefunctions are required for different values of r_0. We used gas-phase O^{2-} wavefunctions calculated by M. D. Jackson with a computer program written by Laws and others (1973). In modeling all structure types, we constrained our energy minimizations to preserve the observed space group symmetry.

The energy minimization routine incorporated into the original version of LEMINPI is based on the Powell algorithm, which locates stationary points without using derivatives. We felt that a potentially more accurate procedure would be to use energy gradients to guide the minimization process. Therefore, after modeling the calcite and aragonite structures using the Powell mimimization routine, we repeated these modelings using a quasi-Newton, double-dogleg minimization routine written by M. B. Boisen, Jr., which does use energy gradients. The results obtained with the quasi-Newton minimizer compare favorably with those obtained with the Powell minimizer; accordingly, we used the quasi-Newton minimizer exclusively for modeling $CaCO_3$ in the diopside and perovskite structure types.

For our fittings of the Birch-Murnaghan equation, we used the program BIRNT, written by R. S. Hemley and modified by M. D. Jackson. The program fits that equation in a form applicable to static crystal structures, neglecting temperature effects, and then calculates W from G and V at each P according to Equation (3). We consider a fitted Birch-Murnaghan equation acceptable when the predicted K_0 and dK_0/dP values and P-V relations are reasonable and when the differences between the Birch-Murnaghan W values and the MEG W values are minimized as nearly as practical.

A MODELING OF THE CRYSTAL STRUCTURE OF CALCITE

The observed calcite structure has $R\bar{3}c$ space group symmetry. As seen in Figure 1, C is 3-coordinate by O in a regular planar triangular configuration. Each O is bonded to one C and two Ca atoms such that no Ca is bonded to more than one O in any one CO_3 group. Figure 2 depicts a CaO_6 group with its adjoining CO_3 groups. In the rhombohedral setting, the unit cell contains only two formula units compared to six formula units in the hexagonal setting, hence we use the former to reduce computational effort. Reeder (1983) gives the transformation relations between these two settings. The asymmetric unit consists of Ca at the origin of the rhombohedral cell, C in special position $x = y = z = 0.25$, and O in special position $y = 0.5 - x, z = 0.25$. With one variable atomic coordinate and two cell constants (a and α) , we had a total of three variable parameters for our energy minimizations.

In the calcite structure generated by the MEG model, a is smaller and α is wider than observed experimentally (see Table 1), but the structure is topologically equivalent to that observed. The non-bonded Ca...C separation distance along [111] is about 9% shorter than observed, and the CO bond lengths and the non-bonded O...O distances are about 6% shorter than observed. Our modeling underestimates the CaO bond lengths by about 1% and the non-bonded O...O distances in the CaO_6 groups by 1-2%.

The MEG model underestimates W for calcite by about 17%, which is quite large compared to the 5-8% underestimate of W for quartz (Jackson 1986, Jackson and Gordon 1988a). The K_0 value calculated for calcite with the MEG model is roughly 50% larger than that determined ex-

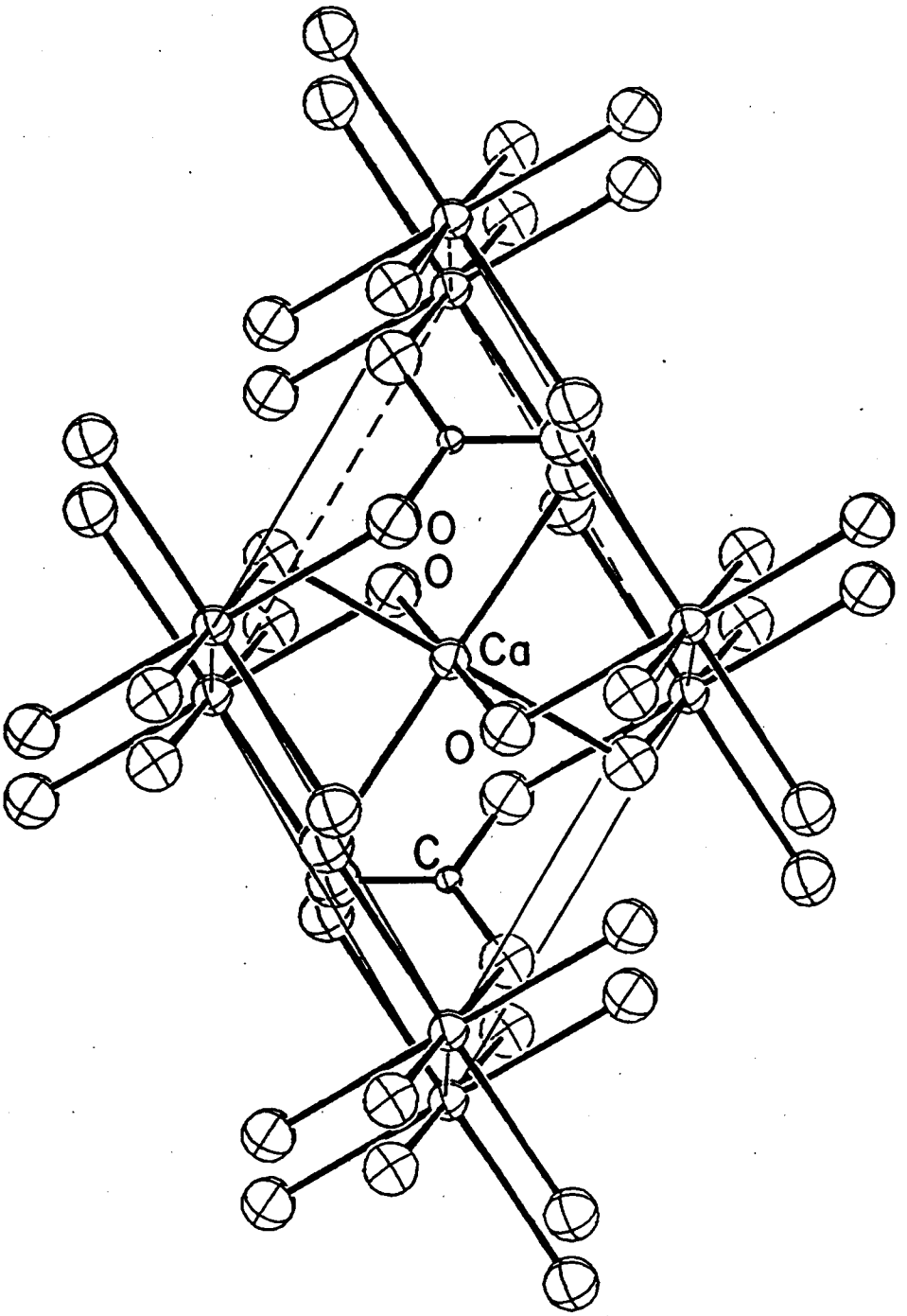

Figure 1. Oblique view of the observed structure of calcite as refined by Effenberger et al. (1981). The viewing direction is about 6° off the *a* axis. Here, as in all subsequent figures depicting $CaCO_3$ structures, the large spheres represent O, the small spheres C, and the intermediate spheres Ca. The rhombohedral unit cell is outlined by the light lines.

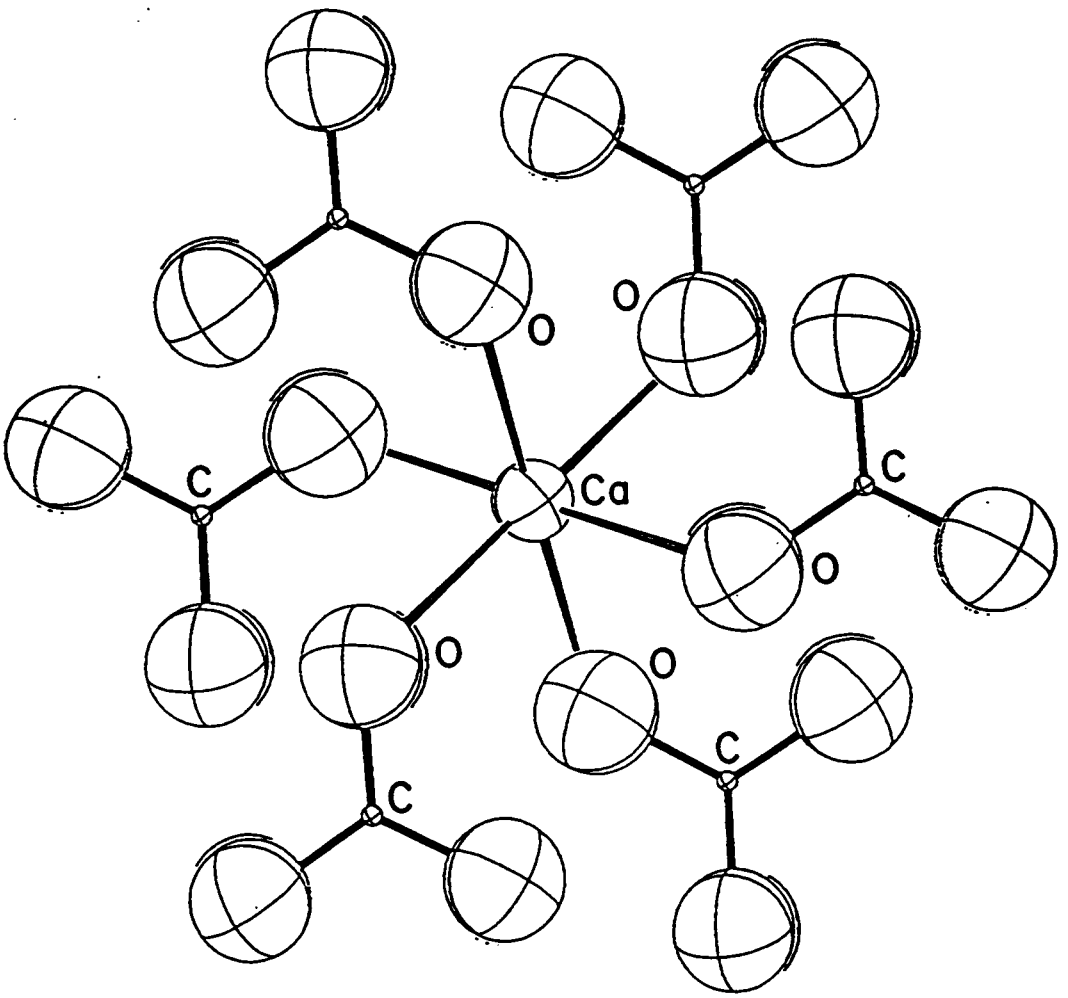

Figure 2. The Ca coordination polyhedron in the observed structure of calcite, with adjoining CO_3 groups.

Table 1. Calcite structures and related data.

	Calculated[a]	Calculated[b]	Observed[c]
Unit cell dimensions			
a (Å)	5.931	5.937	6.375
α (deg)	49.82	49.71	46.08
Interatomic distances (Å) and angles (deg)			
Ca polyhedron			
CaO (6x)	2.327	2.327	2.359
OCaO (2x)	92.01	91.91	92.57
OCaO (2x)	87.99	88.09	87.43
O...O (2x)	3.349	3.345	3.410
O...O (2x)	3.233	3.235	3.260
C polyhedron			
CO	1.211	1.209	1.283
OCO	120[d]	120[d]	120
O...O	2.097	2.095	2.222
Other data			
$\overline{W}$ (kJ mol^{-1})	-15312	-15312	-18430[e]
$\overline{V}$ (Å^3)	56.01	55.99	61.32
K_0 (kb)	1219	1225	826[f]

[a]Powell minimizer.
[b]quasi-Newton minimizer.
[c]cell constants and atomic positional data from Effenberger et al. (1981).
[d]these values were constrained in the energy minimizations.
[e]Wagman et al. (1982).
[f]Dandekar and Ruoff (1968).

perimentally, i.e., the model generates a stiffer structure than that observed experimentally, as it does for the silica polymorphs (Jackson 1986, Jackson and Gibbs 1988, Jackson and Gordon 1988a).

A MODELING OF THE CRYSTAL STRUCTURE OF ARAGONITE

The aragonite structure (Figure 3) has space group symmetry *Pnam*. Dal Negro and Ungaretti (1971) refined the structure in the morphological setting corresponding to the equivalent space group *Pmcn*; we also use this setting in the present study. In the structure, C is 3-coordinate by O in a nearly planar triangular pyramid, and Ca is 9-coordinate by O in a configuration depicted in Figure 4, which also shows the adjoining CO_3 groups. Each Ca is bonded to two of the O atoms in each CO_3 group, and each O is bonded to three Ca atoms in addition to C. There are four formula units per unit cell. The asymmetric unit contains two Ca atoms, one C atom, and one O atom (designated O1), all in special positions $x = 0.25$, and two additional O atoms (designated O2) in general positions, giving nine atomic coordinates not fixed by symmetry. With three independent cell edge lengths, we have a total of 12 variable parameters for the energy minimization.

In the aragonite structure generated by the MEG model (Figure 5), the *a* and *c* cell edges are longer, and the *b* cell edge is shorter, than those observed (see Table 2), and the model unit cell volume is 3% smaller than observed. The model CO bond lengths are 6-7% shorter than observed, but do show approximately the correct lengths relative to one another. The non-bonded O...O distances in the CO_3 groups are underestimated by 6-8%, but the second-nearest-neighbor C...C distance is overestimated by 5%. The largest discrepancy between calculated and observed interatomic distances is in the second- nearest-neighbor Ca...Ca distance, which the model underestimates by 18%.

The model and the observed aragonite structures are not topologically equivalent. The MEG model predicts 8- rather than 9-coordination for Ca (see Figure 6) and 3- rather than 4-coordination for O1 as observed, but it does predict that O2 is 4-coordinate as observed. In the CaO_8 polyhedron, there is one less O1 than in the observed CaO_9 polyhedron, and O1 is bonded to two Ca atoms rather than three as in the observed structure. The dissimilarity between the model and

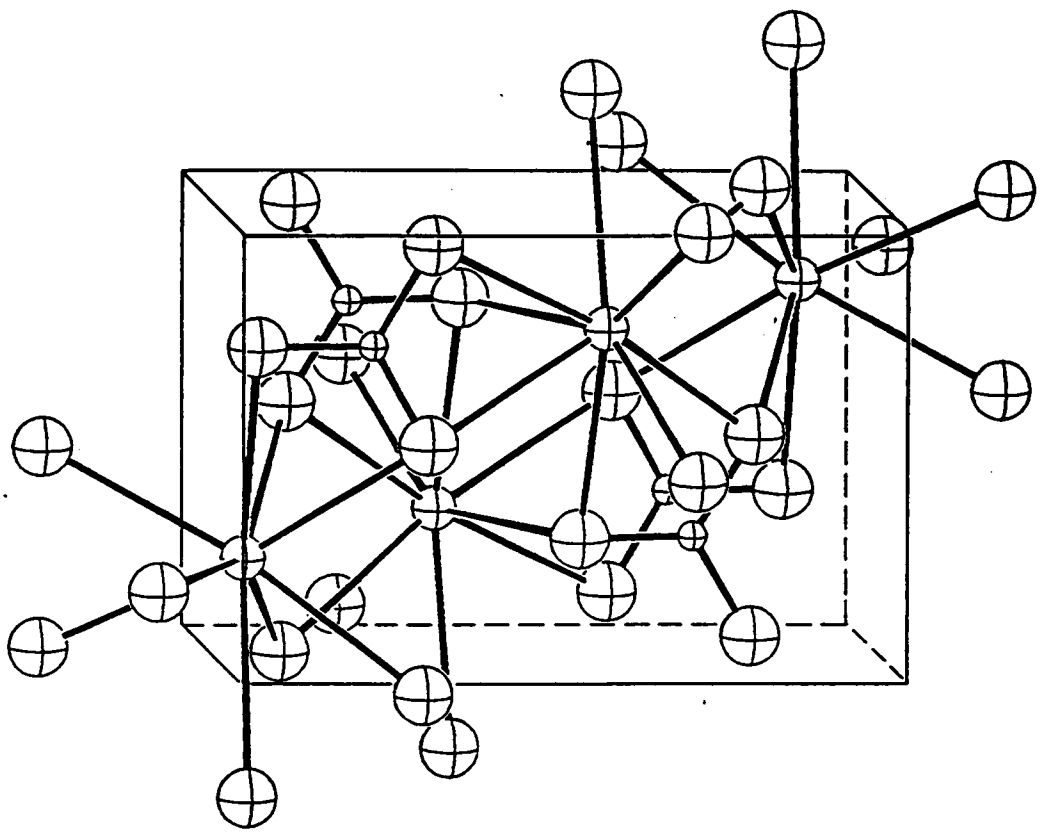

Figure 3. Oblique view of the observed structure of aragonite as refined by Dal Negro and Ungaretti (1971). The viewing direction is about 10° off the *c* axis. The unit cell (space group *Pmcn*) is outlined by the light lines.

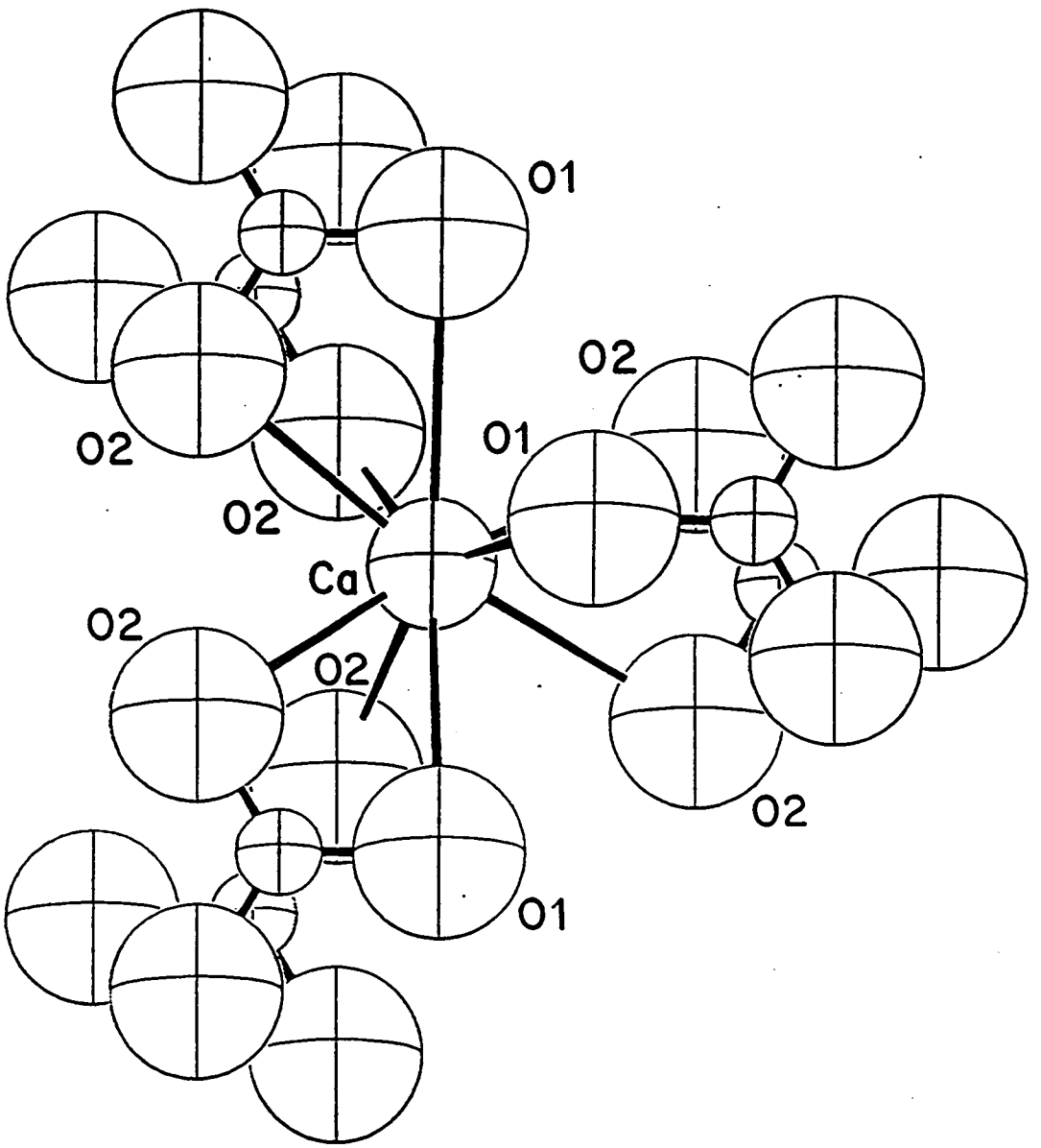

Figure 4. The Ca coordination polyhedron in the observed structure of aragonite (Dal Negro and Ungaretti 1971), with adjoining CO_3 groups.

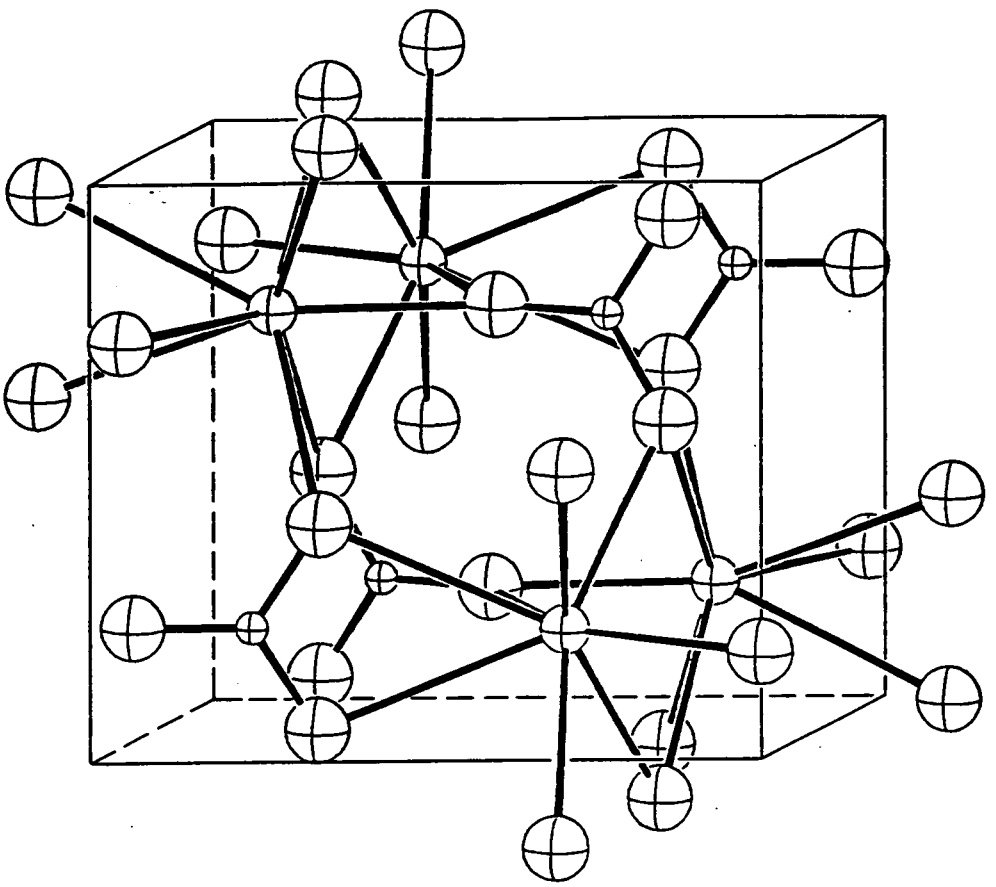

Figure 5. Oblique view of the structure of aragonite found in our MEG modeling. The viewing direction is about 10° off the *c* axis. The *Pmcn* unit cell is outlined by the light lines.

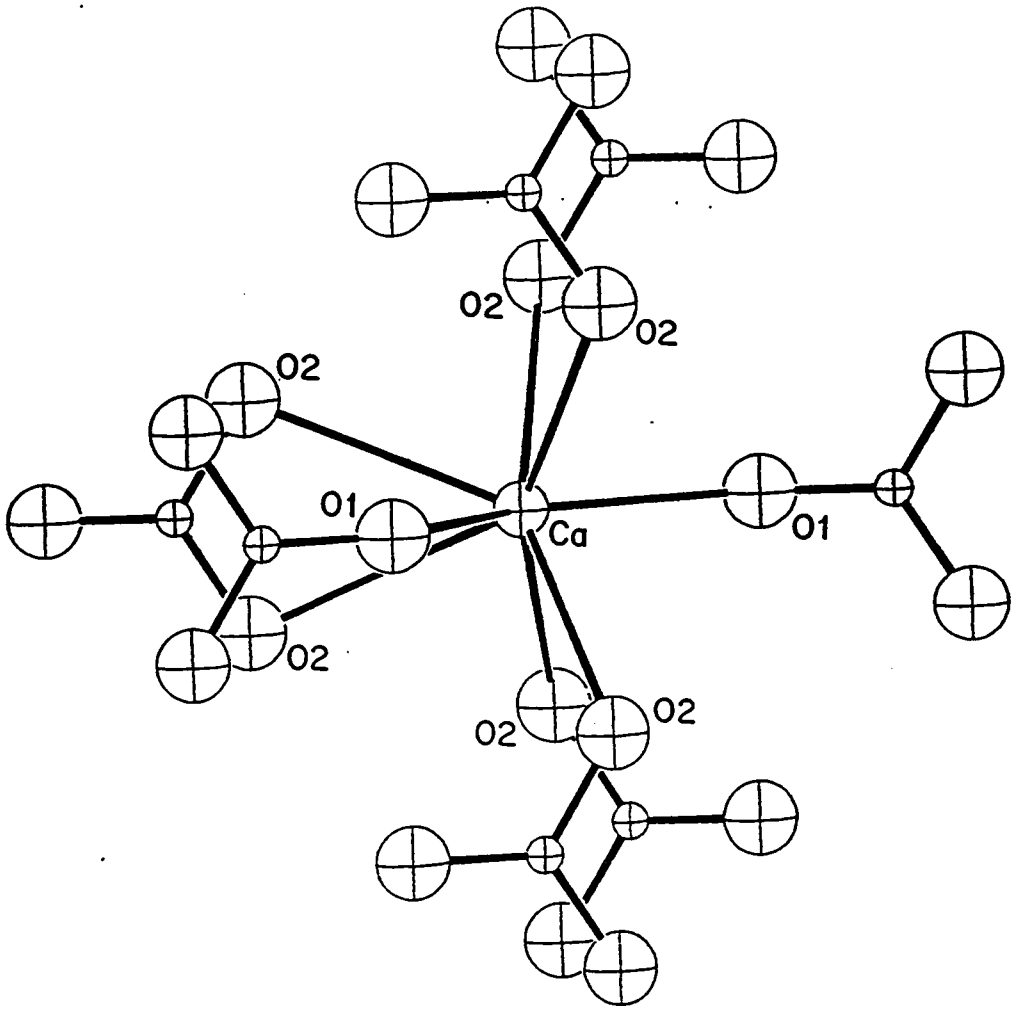

Figure 6. The Ca coordination polyhedron and adjoining CO_3 groups in our model aragonite structure.

Table 2. Aragonite structures and related data.

	Calculated[a]	Calculated[b]	Observed[c]
Unit cell dimensions (Å)			
a	5.821	5.786	4.962
b	6.314	6.327	7.971
c	6.095	6.037	5.739
Interatomic distances (Å) and angles (deg)			
C polyhedron			
CO1	1.188	1.184	1.280
CO2	1.211	1.214	1.287
O1CO2	122.43	122.82	120.70
O2CO2	114.98	114.24	118.46
O1...O2	2.103	2.105	2.231
O2...O2	2.043	2.039	2.212
Ca polyhedron			
CaO1 (max.)	2.446	2.476	2.655
CaO1 (min.)	2.263	2.270	2.411
CaO2 (max.)	2.689	2.652	2.541
CaO2 (intermed.)	2.639	2.531	2.526
CaO2 (min.)	2.358	2.419	2.448
O1CaO1 (max.)	141.10	138.29	138.24
O1CaO1 (min.)	141.10[d]	138.29[d]	71.74
O1CaO2 (max.)	140.12	142.80	144.49
O1CaO2 (min.)	44.65	45.22	72.33
O1CaO2 (avg.)	95.31	95.17	99.51
O2CaO2 (max.)	155.01	155.73	171.48
O2CaO2 (min.)	71.53	72.65	51.59
O2CaO2 (avg.)	100.33	100.91	100.41
O1...O1 (max.)	4.440	4.436	4.962
O1...O1 (min.)	4.440[d]	4.436[d]	2.975
O1...O2 (max.)	4.658	4.666	4.849
O1...O2 (min.)	2.814	2.793	2.231
O1...O2 (avg.)	3.525	3.525	3.731
O2...O2 (max.)	4.879	4.839	5.053
O2...O2 (min.)	2.043	2.039	2.212
O2...O2 (avg.)	3.780	3.780	3.667
Other data			
$\overline{W}$ (kJ mol^{-1})	-15179	-15177	-18430[e]
$\overline{V}$ (Å^3)	56.00	55.25	56.74
K_0 (kb)	1096	1407	505[f]

[a]Powell minimizer.
[b]quasi-Newton minimizer.
[c]cell constants and atomic positional data from Dal Negro and Ungaretti (1971).
[d]There is only one O1CaO1 angle and one O1...O1 distance in the model structures.
[e]Wagman et al. (1982).
[f]Hearmon (1946).

observed Ca polyhedra is probably related to the grossly underestimated Ca...Ca separation distance, coupled with the overestimated C...C separation distance. The differences between the model and observed cell edges are consistent with this view.

Because the observed and the model Ca-containing polyhedra contain different numbers of O atoms, we cannot correlate individual O atoms between the two polyhedra, and so we are limited to summary comparisons between calculated and observed CaO bond lengths and non-bonded O...O distances. Both the maximum and the minimum CaO1 bond lengths are smaller in the model. The variation among the model CaO2 bond lengths is greater than that observed. The maximum non-bonded O...O distances are all shorter in the model structure, as are all of the minimum non-bonded O...O distances except the minimum O1...O2 distance; this exception merely reflects the difference in the O1 positions relative to the O2 positions in the model polyhedron compared to the observed one.

The MEG calculations underestimate W for aragonite by 17-18%, about the same as for calcite. With the Powell minimizer, the MEG calculations overestimate K_0 by 117%; with the quasi-Newton minimizer, the overestimate is about 180%. The calculated K_0 values differ because at V near V_0, W is predicted to vary less with V when the Powell minimizer is used than when the quasi-Newton minimizer is used. These observations provide further evidence that, when applied to crystal structures comprising bonds having significant covalent character, the MEG model generates crystal structures that are notably stiffer than observed.

MODELING OF $CaCO_3$ IN THE DIOPSIDE STRUCTURE

The structure of diopside, $CaMgSi_2O_6$, has been described by Clark et al. (1969) and is depicted in Figure 7. Diopside is a $C2/c$ pyroxene with a monopolysilicate chain. Mg atoms occupy 6-coordinate sites designated $M1$, and Ca atoms occupy 8-coordinate sites designated $M2$, sandwiched in layers between adjacent monopolysilicate chains (Figure 8). We obtain the stoichiometry $CaCO_3$ by replacing Mg with a second Ca and Si with C. To facilitate computation, we adopt a primitive unit cell comprising four formula units (the transformation is described by Jackson and Gibbs 1988). The primitive cell constants obey the relations $a = b$ and $\alpha = \beta$. The

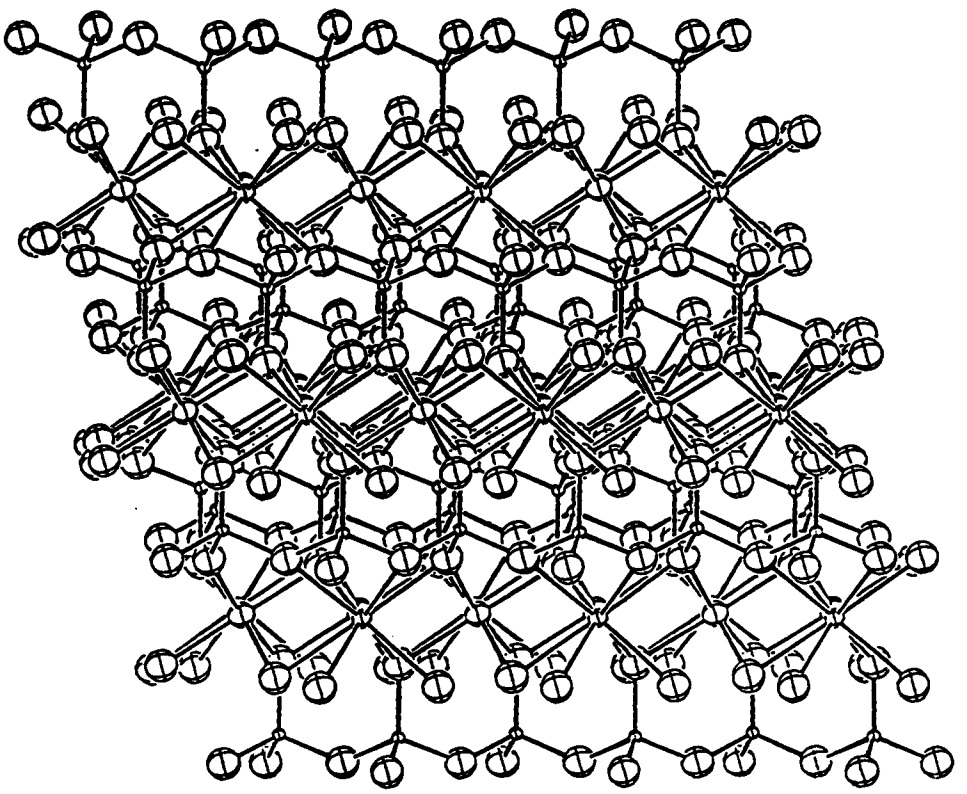

Figure 7. Oblique view of the observed structure of diopside, $CaMgSi_2O_6$ (Clark et al. 1969). The viewing direction is about 3° off the *b* axis of the *C*-centered cell, or 3° off the [110] axis of the primitive cell.

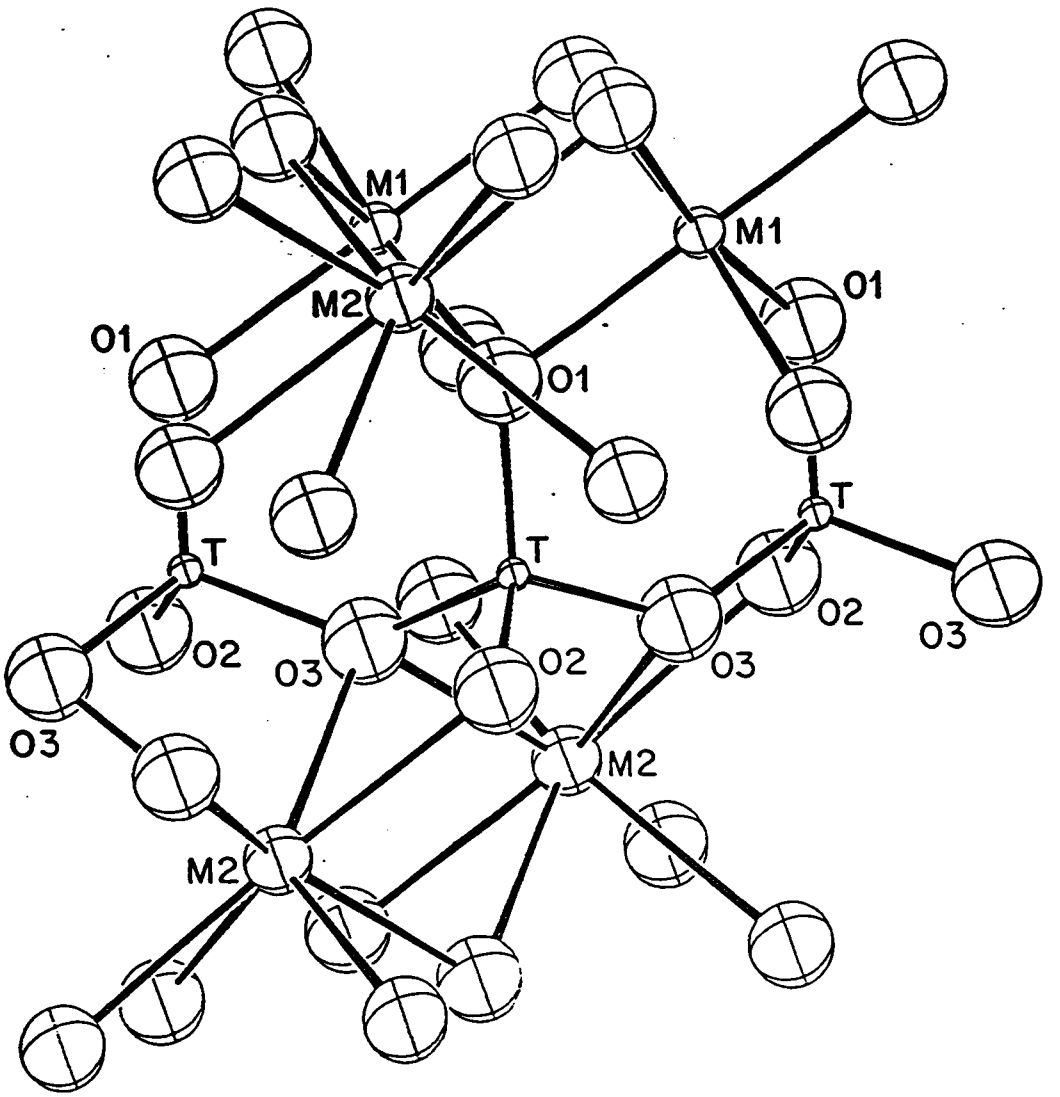

Figure 8. Coordination polyhedra in the observed structure of diopside. The spheres represent, in order of decreasing size, O, Ca, Mg, and Si.

asymmetric unit consists of two Ca atoms in special positions $y = -x$, $z = 0.25$, and one C and three O atoms all in general positions. Thus there are 18 variable parameters for the energy minimization.

Figures 9 and 10 depict the atomic arrangement in the model $CaCO_3$ pyroxene structure, and Table 3 lists the geometric data calculated for that structure. The average CO bond length in this structure is 1.342Å, shorter than the value of 1.368Å that Gibbs et al. (1987) calculated for H_4CO_4 using Hartree-Fock molecular orbital (MO) theory at 6-31G** level. These workers also calculated a bridging CO bond length of 1.391Å in H_6C_2O using the same basis set; a bridging CO bond length of 1.416Å has been observed experimentally (Kimura and Kubo 1959). One of the two bridging CO bond lengths in our diopside structure $CaCO_3$ polymorph (1.403Å) lies between the MO result and the observed one while the other (1.430Å) is signficantly longer than either. The two non-bridging CO bond lengths in our model structure (1.281Å and 1.255Å) are much shorter than expected for 4-coordinate CO bond lengths; in fact they are closer to typical 3-coordinate CO bond lengths. The standard deviation of the CO bond lengths from the mean value in the CO_4 groups in our model structure is about twice the standard deviation of the SiO bond lengths in the SiO_4 groups in diopside. However, the variance of the COC angles from the ideal tetrahedral angle (109.47°) in the model carbonate structure is smaller than the variance of the SiOSi angles from the ideal tetrahedral angle in diopside. Robinson et al. (1971) have found that tetrahedral angle variances are linearly related to mean tetrahedral quadratic elongations, which in turn are convenient measures of polyhedral distortions. Using the relations that these workers obtained, we find that the quadratic elongation of the CO_4 groups in our model carbonate structure is practically equal to that of the SiO_4 groups in diopside. Our results are also in conformity with the observation of Robinson et al. that bond length variances in coordination polyhedra do not show meaningful correlations with bond angle variances or with quadratic elongations.

The OCO angles in the model structure are all within 4° of the corresponding OSiO angles observed in the diopside structure. However, the bridging COC angle in the model structure measures 153.6° , which is more than 15° wider than the SiOSi angle in diopside (135.9°). Using MO theory, Gibbs et al. (1987) calculate a COC angle of 113.8° in H_6C_2O , and Kimura and Kubo

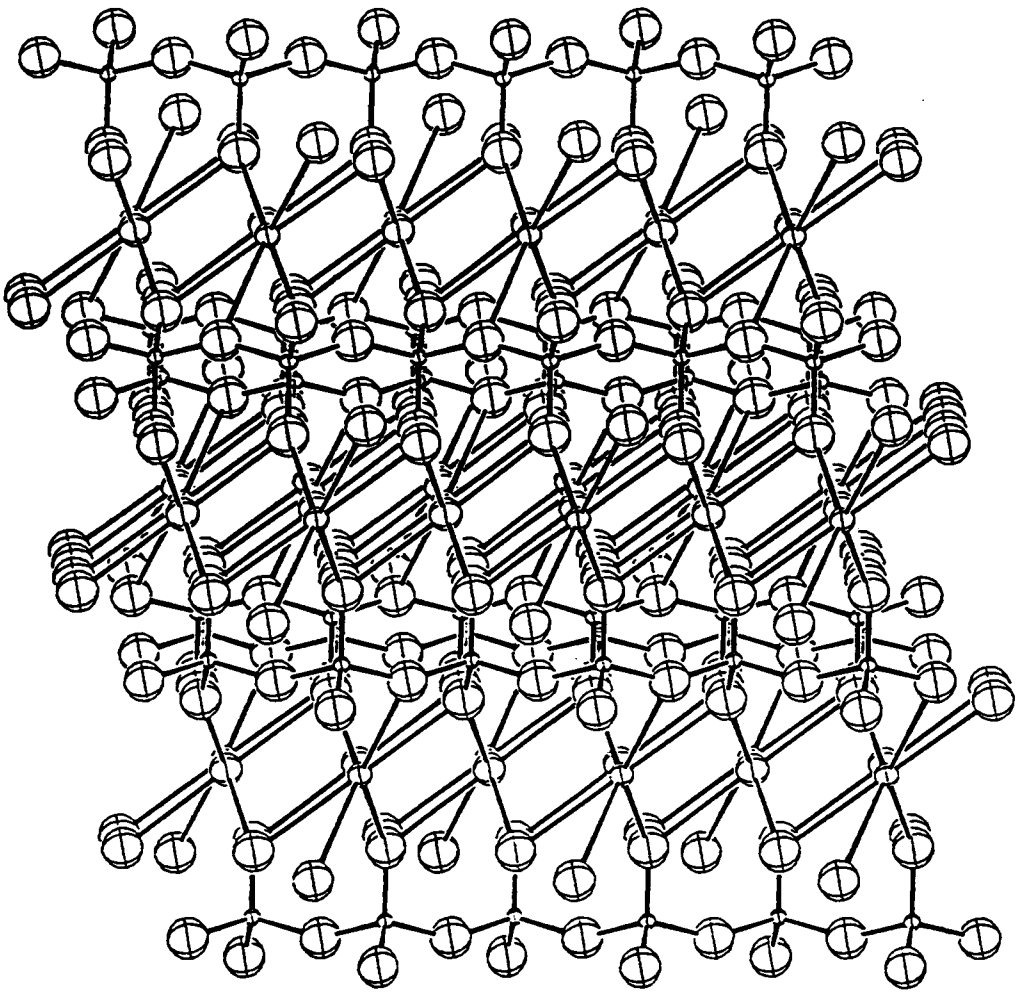

Figure 9. Oblique view of the atomic arrangement in our model of $CaCO_3$ in the diopside structure type. The viewing direction is about 3° off the *b* axis of the *C*-centered cell, or 3° off the [110] axis of the primitive cell.

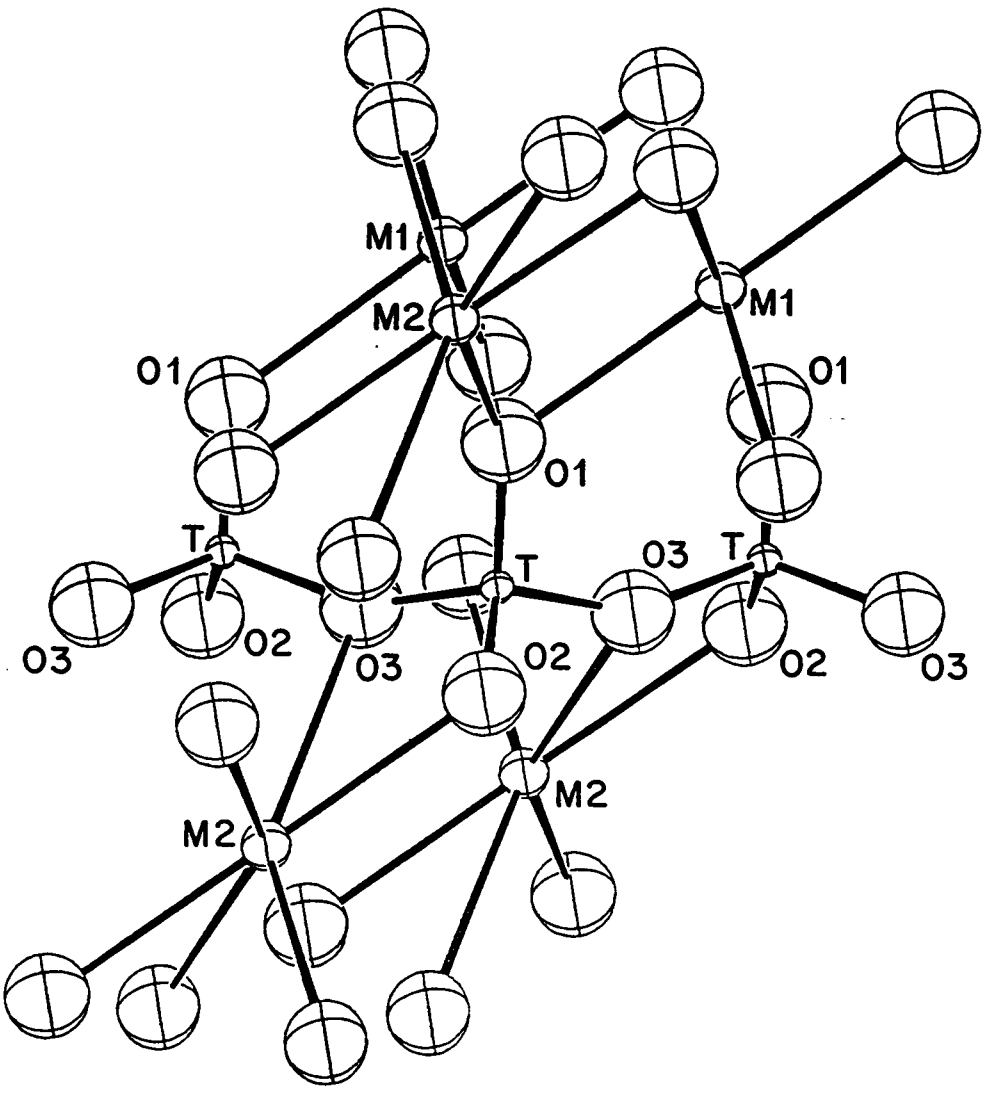

Figure 10. Coordination polyhedra in our model of $CaCO_3$ in the diopside structure type. The spheres represent, in order of decreasing size, O, Ca, and C.

Table 3. Structural and related data for $CaCO_3$ in the diopside structure type.

Unit cell dimensions (primitive cell)			
a (Å)	6.595		
c (Å)	4.586		
α (deg)	97.27		
γ (deg)	88.91		
Interatomic distances (Å) and angles (deg)			
C polyhedron			
CO1	1.281		
CO2	1.256		
CO3	1.436		
CO3	1.407		
O1CO2	118.41	O1...O2	2.179
O1CO3	107.19	O1...O3	2.189
O1CO3	106.24	O1...O3	2.152
O2CO3	105.70	O2...O3	2.148
O2CO3	111.10	O2...O3	2.198
O3CO3	107.73	O3...O3	2.296
Ca1 polyhedron			
CaO1 (2x)	2.243		
CaO1 (2x)	2.416		
CaO2 (2x)	2.272		
O1CaO1	175.33	O1...O1	4.482
O1CaO1 (2x)	97.62	O1...O1 (2x)	3.508
O1CaO1 (2x)	78.56	O1...O1 (2x)	2.953
O1CaO1	72.25	O1...O1	2.849
O1CaO2 (2x)	81.78	O1...O2 (2x)	2.955
O1CaO2 (2x)	101.98	O1...O2 (2x)	3.508
O1CaO2 (2x)	178.63	O1...O2 (2x)	4.688
O1CaO2 (2x)	106.41	O1...O2 (2x)	3.755
O2CaO2	74.94	O1...O2	2.764
Ca2 polyhedron			
CaO1 (2x)	2.343		
CaO2 (2x)	2.240		
CaO3 (2x)	2.675		
O1CaO1	74.89	O1...O1	2.849
O1CaO2 (2x)	81.54	O1...O2 (2x)	2.994
O1CaO2 (2x)	99.87	O1...O2 (2x)	3.508
O1CaO3 (2x)	149.31	O1...O3 (2x)	4.840
O1CaO3 (2x)	105.16	O1...O3 (2x)	3.991
O2CaO2	178.25	O2...O2	4.480
O2CaO3 (2x)	127.54	O2...O3 (2x)	4.413
O2CaO3 (2x)	50.89	O2...O3 (2x)	2.148
O3CaO3	90.14	O3...O3	3.788
Other data			
$\overline{W}$ (kJ mol^{-1})	-15425		
$\overline{V}$ (Å^3)	49.06		
K_0 (kb)	1811		

have observed a COC angle of 111.5° in that molecule. The large departure of the COC angle calculated with the MEG model from the MO and observed values may be due to Coulombic repulsion between the highly-charged C^{4+} ions in the model structure. Such repulsions have been cited as the source of a similar discrepancy between the calculated and observed bridging SiOSi angles in low quartz (Jackson 1986, Jackson and Gordon 1988a).

The average CaO bond lengths (2.298Å for Ca in the M1 site, 2.409Å for Ca in the M2 site) are shorter than the average CaO bond length in natural diopside (2.424Å). In our model zero-pressure structure, Ca1 and Ca2 are both 6-coordinate, which is noteworthy, given that Ca is 8-coordinate in all known Ca-bearing natural pyroxenes. At pressures of 76 kb and higher, the MEG model does predict that Ca2 is 8-coordinate, but Ca1 remains 6-coordinate. Reference to Figures 7 through 10 shows that the CaO polyhedra in the model structure are elongated along [110] relative to the (Mg,Ca)-containing polyhedra in diopside. This may be ascribed to the shorter *T*O bond lengths, and a slightly longer *T*...*T* separation distance along [110], in the model structure than in diopside.

The purely ionic MEG modeling of diopside by Post and Burnham (1986) resulted in a structure which differs from the observed diopside structure even more substantially than does the model of $CaCO_3$ in the diopside structure. Post and Burnham found that the zero-pressure structure for $CaMgSi_2O_6$ was not actually a monopolysilicate structure at all, but a framework structure in which Ca, Mg, and Si are all tetrahedrally coordinated by O. The bridging O in the observed structure is highly overbonded whereas one of the non-bridging O atoms is highly underbonded, but in their model diopside structure, Post and Burnham found that all O atoms exhibited the ideal bond strength sums of 2.0 v.u. They concluded that the discrepancies between the observed diopside structure and their model one indicated substantial covalency in the bonding in natural diopside. In view of this, it is surprising that the diopside structure type of $CaCO_3$ is more similar to that of natural diopside than is the structure generated by Post and Burnham for diopside.

The *W* value for $CaCO_3$ in the diopside structure is markedly lower than that for either the calcite or aragonite structures at all pressures over which we carried out our energy minimizations for the respective structure types. The purely ionic model therefore predicts that $CaCO_3$ is more

stable in the diopside structure than in either the calcite or aragonite structures. It is interesting that an ionic model should predict a stable $CaCO_3$ structure in which all C atoms are 4-coordinate, given that the radius-ratio rule, also developed within the context of an ionic model, predicts that a stable $CaCO_3$ structure should have all C atoms in 3-coordination by O.

MODELING OF $CaCO_3$ IN THE PEROVSKITE STRUCTURE

The ideal perovskite structure (Figure 11) corresponds to the general stoichiometry ABX_3 and is based on a primitive cubic unit cell containing one formula unit (Megaw 1972). The A cations are 12-coordinate and the B cations are 6-coordinate. Natural perovskite, $CaTiO_3$, is believed to possess pseudo-cubic monoclinic symmetry (Zedlitz 1939, Naray-Szabo 1943), and several synthetic materials having the perovskite structure type possess orthorhombic symmetry (cf. Liu et al. 1975, Yagi et al. 1978, O'Keeffe et al. 1979, Sasaki et al. 1983), but all of these structures are topologically equivalent to the ideal one. Departures from the ideal symmetry, particularly among the orthorhombic modifications, commonly result from rigid rotations of the BX_6 groups rather than from distortions of those groups. In our modeling of $CaCO_3$ in the perovskite structure type, we therefore varied all six cell constants and all atomic coordinates, for a total of 21 variable parameters.

We obtained two different structural modifications having the perovskite topology, one tetragonal and one cubic. The atomic coordinates in both modifications are identical with those in the ideal structure, so that these model structures do not display polyhedral rotations of the kind mentioned previously. At any given pressure for which we carried out an MEG calculation, our unit cell volumes and lattice energies calculated for these two structures are virtually identical. We find no systematic W-V relations in either the cubic or the tetragonal structure; therefore, we cannot accurately fit a Birch-Murnaghan equation to the W-V data for either. From the best fit we could make for the cubic modification of this structure type, we estimate the 6-coordinate CO bond length at 1.67Å. We made an MO calculation of the 6-coordinate CO bond length in H_8CO_6 at 6-31G** level and found a value of 1.60Å. The W values we find for both the tetragonal and the cubic modifications are higher at all pressures than those we find for $CaCO_3$ in the calcite, aragonite and

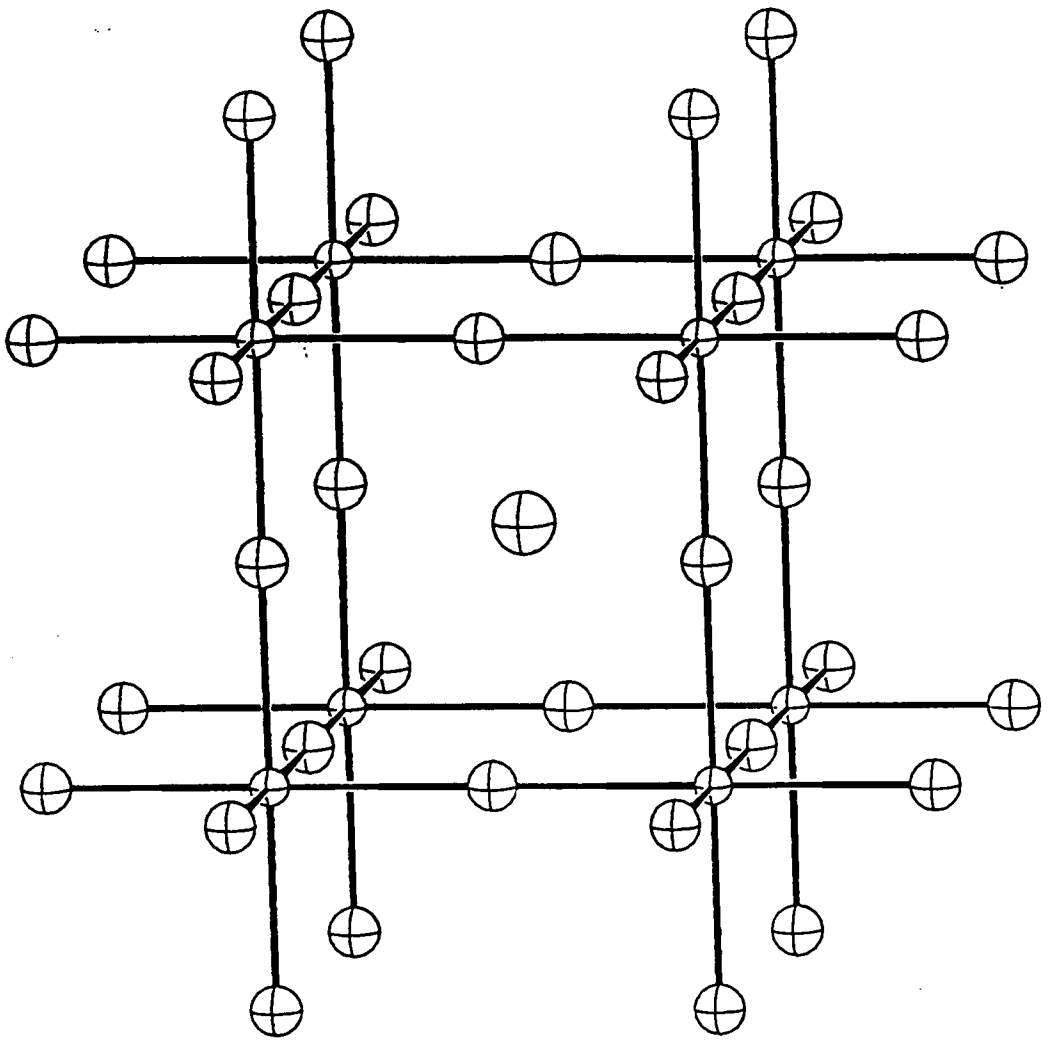

Figure 11. Oblique view of the ideal perovskite structure. The viewing direction is about 10° off the *c* axis. The large sphere represents the 12-coordinate *A* cation; the bonds to this cation have been omitted for clarity. The small spheres represent the *B* cations, and the intermediate-sized spheres represent the anions (*X*).

diopside structure types, hence our MEG modelings do not predict $CaCO_3$ to be more stable in a perovskite structure type than in any of these other structure types.

MODELING OF THE THERMOCHEMISTRY OF $CaCO_3$

As seen in Figure 12, the *G-P* curves generated with the MEG model for calcite and aragonite do not cross within the range of pressures over which we made our calculations. We therefore cannot use the results of our calculation to estimate the calcite-aragonite phase transition pressure. This is a consequence of our MEG calculations predicting nearly equal zero-pressure molar volumes for calcite and aragonite. The experimentally determined zero-pressure molar volume of aragonite is 7.5% smaller than that of calcite. Because the molar volume at a given pressure is the slope of a constant-temperature *G-P* curve at that pressure, and because the isothermal variation of molar volume with pressure is relatively small for solids, the near equality of the molar volumes of calcite and aragonite predicted by our MEG calculations implies that even if the calculated *G-P* curves did intersect at a reasonable *P* value, that value would be very uncertain and highly sensitive to errors in the values of *G* and *P*.

The MEG model ΔW value for the diopside structure type relative to the calcite structure type at zero pressure is -113 kJ mol^{-1} ; for the diopside structure type relative to the aragonite structure types, the difference is -247 kJ mol^{-1} . The diopside structure type is therefore predicted to be almost as stable relative to calcite as calcite is relative to aragonite. The experimentally determined ΔH_f° values of calcite and aragonite differ by less than 1 kJ mol^{-1} at atmospheric pressure and at 298K, so not only does the purely ionic MEG model predict the diopside structure type to be stable by a large margin relative to calcite, it also grossly overestimates the stability of calcite relative to aragonite. This observation and that regarding the calcite-aragonite phase transition pressure indicate that the fully ionic MEG model is deficient in generating the phase relations of $CaCO_3$ with respect to pressure.

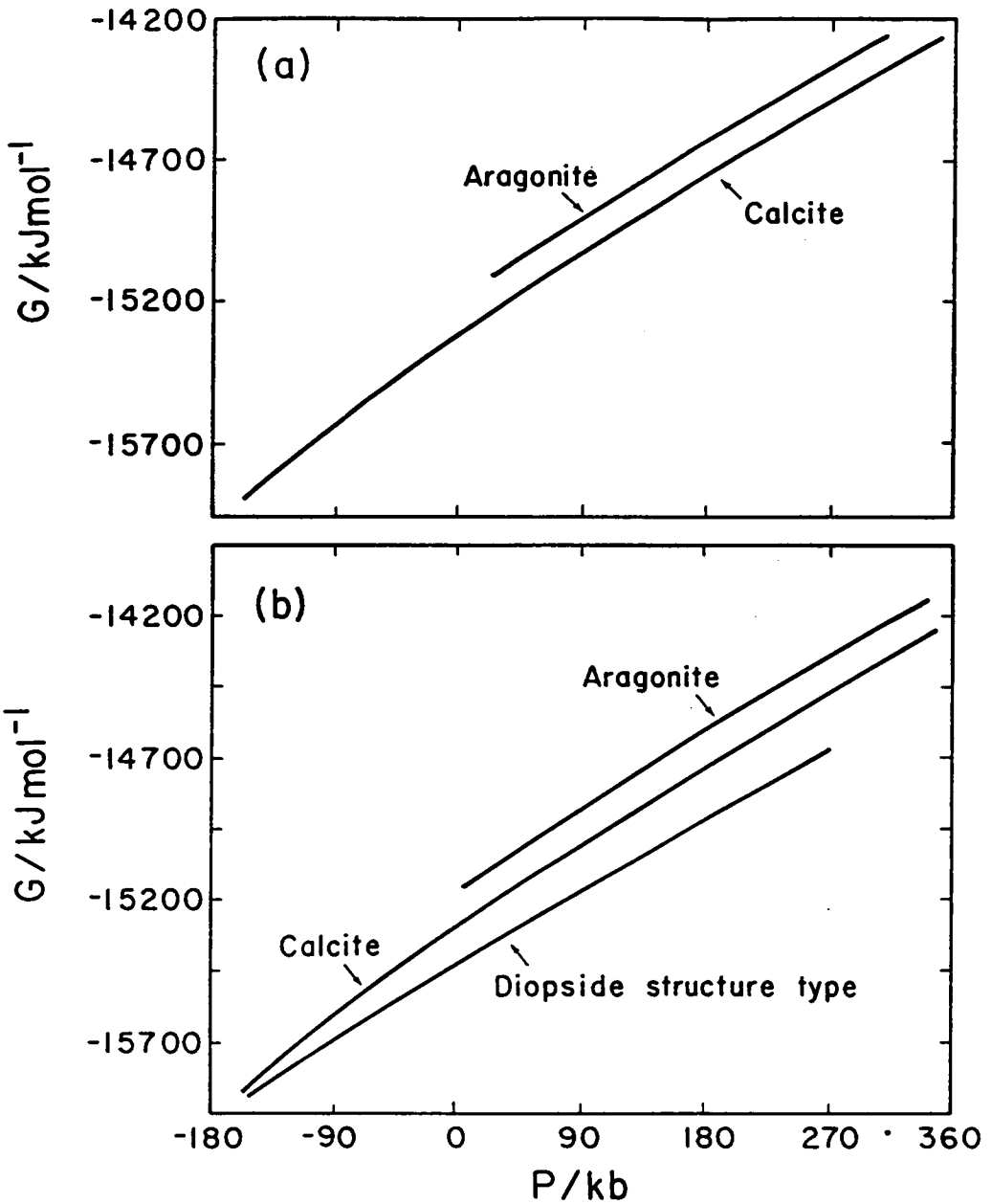

Figure 12. Gibbs free energy (G) as a function of pressure (P) for the $CaCO_3$ structures modeled in this study: (a) results obtained with the Powell minimization routine for the calcite and aragonite structure types (the Powell routine was not used in modeling the diopside structure type); (b) results obtained for the calcite, aragonite, and diopside structure types using the quasi-Newton minimization routine.

DISCUSSION

Our purely ionic modelings of CO_3 units in $CaCO_3$ consistently generate CO bond lengths much shorter than observed. In a previous purely ionic modeling of calcite, Lennard-Jones and Dent (1927) calculated a CO bond length of 1.02Å for the CO_3 group, even shorter than the value found in our modeling of calcite. We suspect that within a purely ionic model, the point Coulombic attractive force between C^{4+} and O^{2-} is so strong that the model short-range repulsive force between these ions does not reach equilibrium with the point Coulombic force at a CO separation distance close to that observed experimentally.

To explore the relative magnitudes of the CO interionic forces in our model structures, we plotted the point Coulombic and the short-range repulsive energies and their sum (Figure 13) for one C^{4+}-O^{2-} ion pair as functions of interionic distance R(CO) over the range of R(CO) values for which pair potentials have been calculated. Because the derivative of the total interionic energy with respect to distance is the net interionic force, the minimum in the interionic energy occurs at the point where the interionic forces are in equilibrium. The minimum in the net energy of the CO ion pair occurs at an R(CO) value shorter than those within the range over which the pair potential calculations were made. We then added the sum of the point Coulombic and short-range repulsive energies for one O^{2-}-O^{2-} ion pair to the sum of these energies for the C^{4+}-O^{2-} pair at each R (CO) value within the stated range, setting $R(\mathrm{OO}) = \sqrt{3}\ R(\mathrm{CO})$ as in an ideal plane- triangular CO_3 group. These two ion pair interactions represent one-third of the pairwise interactions within a CO_3 group and hence the total energy of these two interactions equals one-third of the total energy of the CO_3 group within the purely ionic MEG model. As shown in Figure 14, the minimum in this total energy occurs at $R(\mathrm{CO}) \approx 1.22$Å , which is quite close to the R(CO) values found for calcite and aragonite in our modelings. It therefore appears that in our model calcite and aragonite structures, the second-nearest-neighbor OO repulsions (point Coulombic and short-range), and not the nearest-neighbor CO short-range repulsions, play the dominant role in balancing the attractive force between the C and O ions. The observation that these non-bonded O...O distances are also shorter than in the observed calcite and aragonite structures, not only in our model CO_3 groups but

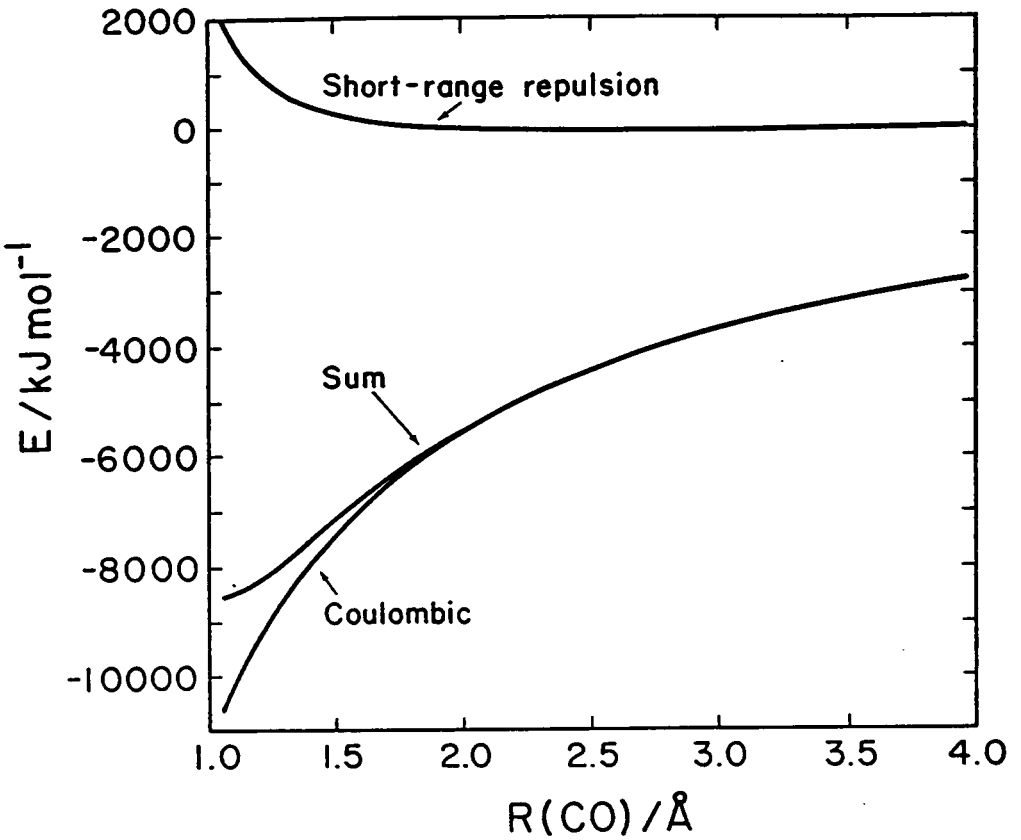

Figure 13. Point coulombic energy and short-range repulsive energy, and the net interionic energy (point coulombic plus short range repulsive) as functions of interionic distance R(CO) for a single C^{4+}-O^{2-} ion pair.

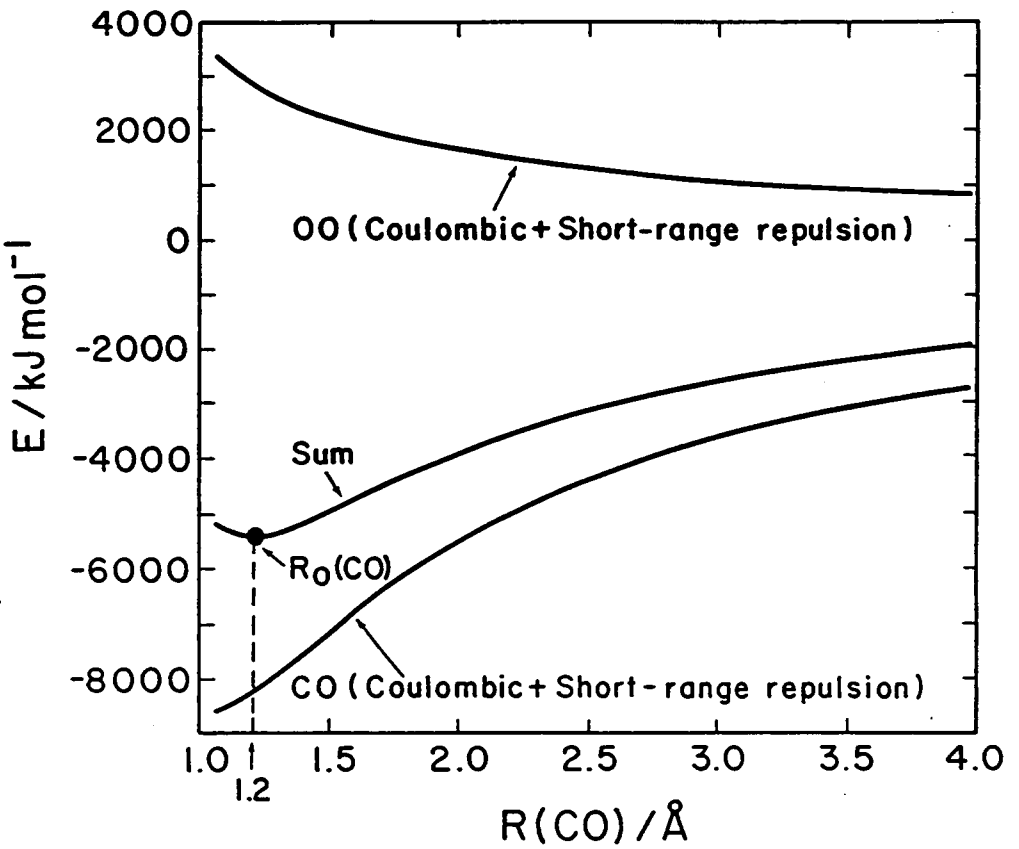

Figure 14. Net interionic energies (point coulombic plus short- range repulsive) for the ion pairs C^{4+}-O^{2-} and O^{2-}-O^{2-} , and the sum of these energies, as functions of R(CO).

almost generally in our model structures, suggests that the purely ionic MEG model predicts weaker OO repulsion forces than those which exist in actual crystals of these materials.

In contrast to the results for 3-coordinate C, our MEG modelings predict an average 4-coordinate CO bond length (1.35Å) quite close to the 4-coordinate CO bond length calculated with MO theory (1.32Å). Our estimate of 1.67Å for the 6-coordinate CO bond length is somewhat longer than the MO value (1.60Å). In comparing the CO bond length--bond order relationship predicted with the MEG model to that predicted with MO theory, we find that these two theoretical models predict the same qualitative trend (see Figure 15). Both curves show a decrease in slope with increasing bond order. This is also observed in the SiO bond length--bond order curve, but the decrease in slope is less pronounced than in the CO curves. This may also reflect the influence of OO repulsions, which would be more significant for the CO bonds than for the SiO bonds, due to the shorter CO bond lengths and the concomitantly shorter non-bonded O...O distances.

We initially expected closer agreement between the geometric features of our model Ca coordination polyhedra and those observed experimentally, given that the CaO bond is believed to be mainly ionic. For calcite, the agreement is close, although this is partially forced by symmetry constraints. The CaO bond lengths in that model structure are somewhat short, as are the non-bonded O...O distances, again suggesting that the model repulsion forces are weaker than those in actual crystals. For aragonite, the model Ca coordination geometry appears to be perturbed by errors in predicting cation-cation distances, so the discrepancies between the model and observed Ca polyhedra do not clearly reflect non-ionic character in the CaO bonds. Factors external to the Ca coordination polyhedra probably also lead to the prediction of 6- rather than 8-coordination for Ca in the model diopside structure type, as discussed previously, so it is difficult to say that our prediction of 6-coordinate Ca in this structure is due to the largely ionic character of the CaO bond.

That our MEG calculations of the lattice energies of calcite and aragonite account for only about 83% of the experimental lattice energies of both at zero pressure is probably also due mainly to assuming that the charges on C and O are equal to their respective valences. In particular, the assumption that C is actually ionized to C^{4+} is unreasonable considering that the fourth ionization potential for C is larger than the third ionization potential for Ar. The charge distribution studies

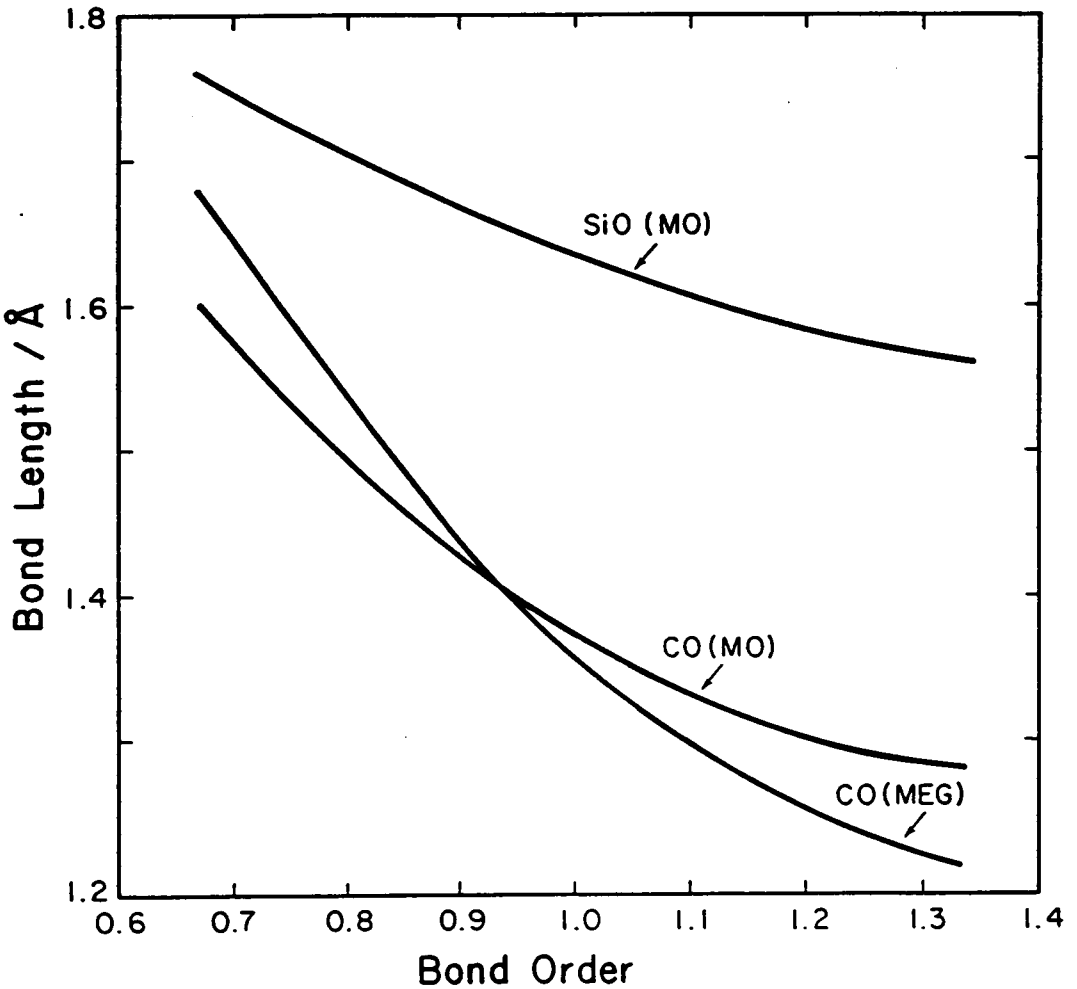

Figure 15. Bond length vs. bond order for SiO and CO bonds. The curves were generated by spline interpolation and do not represent regression relations.

of Yuen et al. (1978) and Effenberger et al. (1981) suggest that the charge on C is about +1 and that on O is about -1. In determining the experimental value of W for $CaCO_3$ using a Born-Haber cycle, we find that the ionization potential for C makes by far the largest contribution to W, which further supports the view that the disagreement between the calculated and experimental W values arises mainly from the assumption of purely ionic bonding. In contrast to our results for $CaCO_3$, a purely ionic MEG model accounts for about 98% of the zero-pressure lattice energy of periclase, a substance in which the bonding is believed to be predominantly ionic (Jackson 1986, Jackson and Gordon 1988a). For low quartz (SiO_2), in which the bonding is believed to be about half ionic and half covalent, a purely ionic MEG calculation accounts for about 95% of the lattice energy (Jackson 1986, Jackson and Gordon 1988a).

The bulk moduli of both calcite and aragonite calculated with the purely ionic MEG model are much larger than observed, indicating that the purely ionic model predicts both polymorphs to be too rigid. Jackson and Gibbs (1988) also found that a purely ionic MEG modeling of the structure of coesite (SiO_2) predicted a structure that was too rigid, but that an MEG calculation in which allowance was made for O^{2-} polarization resulted in improved agreement between the calculated and observed bulk moduli of coesite. Interestingly, the purely ionic MEG modeling of periclase (Jackson 1986, Jackson and Gordon 1988a) predicted a bulk modulus lower than that observed experimentally.

In all our modelings except for calcite, we noted that the program LEMINPI tended to generate some structures that were electrostatically consistent but that did not fit into the systematic W-V relation described by the other electrostatically consistent structures for the same polymorph. This was observed with the quasi-Newton minimizer as well as with the Powell minimizer; furthermore, both minimizers generated essentially the same "outlier" structures for each polymorph. We suspect that the energy surfaces contain a large number of local minima that serve as traps for these minimization algorithms, as they would for any minimization algorithm devised to date. That we did not generate any "outlier" structures in our modeling of calcite is probably due to the geometric constraints imposed by the small number of variable parameters.

CONCLUSIONS

The purely ionic MEG model generates 3-coordinate CO bond lengths in calcite and aragonite to be shorter than observed experimentally in such crystals. The model also indicates that in the CO_3 groups in these crystal structures, the lower limit to the CO bond length is fixed by second-nearest-neighbor OO repulsions rather than by nearest-neighbor short-range CO repulsions. From the relatively short non-bonded O...O distances in these model crystal structures, particularly in the CO_3 groups, we infer that the MEG model may be underestimating the OO repulsion forces.

The thermochemistry of $CaCO_3$ is not even qualitatively modeled with the purely ionic MEG model. The calcite-aragonite phase transformation pressure cannot be generated because the relevant thermochemical data calculated with the model deviate too much from the experimental values. Furthermore, the model predicts that a polymorph of $CaCO_3$ having the diopside structure with 4-coordinate C is more stable than either calcite or aragonite at zero pressure, contrary to observation. These results are consistent with the belief that the CO bonds in carbonates are largely covalent; we should not expect a purely ionic model to reproduce observed thermochemical properties of materials where the bonding is not purely ionic. However, we can take these results as providing a baseline for refinements of the model.

From our experience in the present study, and from that related by Post and Burnham (1986) in their purely ionic modeling of diopside, we recommend that purely ionic MEG modelings of crystal structures comprising dominantly covalent bonds, or of crystal structures whose symmetry imposes relatively few constraints on atomic positions, be used more as a means of investigating the implications of an ionic bonding model than as a means of predicting the observed physicochemical properties of those crystal structures.

Results of ionic modelings such as those we have obtained, which deviate markedly from observation, should also be used to motivate and guide the development of more suitable models. The MEG method is economical and its results are not biased by experimental data. The scientific value of results showing poor agreement with observation depends on how we use the results: we can take them as indicating a poor model and stop using that model, or we can develop more rigorous models which correct the deficiencies of the initial model.

Chapter III

AN EXPLORATION OF THE RELIABILITY OF THE RADIUS RATIO RULE USING PURELY IONIC MODEL CRYSTAL STRUCTURES

INTRODUCTION

Shannon and Prewitt (1969) assert that crystal structure types and cation coordination numbers are determined principally by cation-anion radius ratios, as originally proposed by Goldschmidt (cf. Goldschmidt 1954), and that the possibility of one cation substituting for another on a given site in a crystal structure is largely dependent on the two cations having nearly the same radius. These assertions motivated Shannon and Prewitt to generate a set of ionic radii to add to a collection of such sets which had already become rather large (e.g. Landé 1920, Wasastjerna 1923, Goldschmidt et al. 1926, Pauling 1927, Zachariasen 1931, Ahrens 1952, Fumi and Tosi 1964, Slater 1964). Zoltai and Stout (1984) state that the concept of ionic radii is one of the most important principles of mineralogy in that it is the basis of the radius ratio rule (Pauling 1939), and that that rule determines the coordination of cations by anions in the crystal structures of rock-forming minerals. Elementary mineralogy texts in general stress the importance of ionic radii and the radius ratio rule for understanding such phenomena as cation site preferences and solid solution behavior (cf. Ernst 1969, Frye 1974, Zoltai and Stout 1984, Klein and Hurlbut 1985).

Pauling (1939) formulated the radius ratio rule in a discussion of ionic crystal structures. These are commonly described by extension of the notions used to describe noble-gas crystal structures (cf. Pauling 1939, 1960, Coulson 1961, Kittel 1976, McWeeny 1979). The atoms in both

of these types of crystals are assumed to be hard spheres that fill space with maximum packing efficiency. The principal difference between these two types of crystals is considered to be in the nature of the binding forces: Coulomb forces bind ionic crystals together whereas van der Waals forces bind noble-gas crystals together. Cations are assumed to be smaller than anions, and to fill interstices in a closest-packed anion array in an ionic crystal so that the cation-anion distance is determined by the sum of the cation and anion radii and the coordination number (or ligancy) of the cation is determined by the radius ratio.

Although considerable success has been claimed in using the radius ratio rule to predict cation coordination numbers in crystals (cf. Shannon and Prewitt 1969), there are some fairly common crystals where cation coordination numbers are incorrectly determined by the radius ratio rule. Among these are some of the alkali halides, as we shall demonstrate; this is particularly noteworthy in that the bonding in these substances is believed to be largely ionic.

We have generated the structures of purely ionic alkali halide crystals in each of three common binary structure types using the modified electron gas (MEG) model (Waldman and Gordon 1979). We have determined the structure type among these three that is most stable for each alkali halide within this model, and we now compare the cation coordinations in the most stable structures to those determined by the radius ratio rule. We also have examined the factors that determine the atomic arrangements in these purely ionic crystal structures. We have determined the bulk moduli of our model crystal structures and the transition pressures between different polymorphs of several of the alkali halides, and we compare these to the values found in other MEG modelings and to those found by experiment.

COMPUTATIONAL METHODS

The theory underlying the MEG model has been discussed previously (Gordon and Kim 1972, Waldman and Gordon 1979), but two fundamental assumptions of the model are worth reiterating: (1) the electron density about a given isolated atom or ion is as determined by Hartree-Fock theory; (2) as atoms or ions are brought together to form a crystal, the electron densities about the individual atoms or ions superpose without rearrangement. In addition, we assume that all

interionic interactions are pairwise additive, i.e., many-body effects can be neglected. In this study, we modeled the alkali halides AX (A = Li, Na, K, Rb; X = F, Cl, Br, I) in each of the ideal sphalerite, rocksalt, and CsCl structure types. The coordination numbers of A by X in these structures are 4, 6, and 8 respectively. We used the same computer programs and the same computational techniques in this study as in our study of carbonate crystal structures (Chapter II), except that: (1) in the present study, no ions require Watson sphere stabilization; and (2) we used the quasi-Newton double-dogleg minimization routine written by M.B. Boisen, Jr., for all our energy minimizations. Also as in that study, we used the gas-phase ionic wavefunctions tabulated by Clementi and Roetti (1974). These tables include atoms and ions with atomic numbers equal to or less than 54 (Xe), so we cannot model the Cs halides. For each structure type, we maintained the ideal space group symmetry ($Fm3m$ for the sphalerite and rocksalt types, $Pm3m$ for the CsCl type), varying only the unit cell edge length. We adopted primitive unit cells for the two fcc structures to reduce computational effort; this also increases the precision of numerical integrations (Muhlhausen and Gordon 1981).

Cohen and Gordon (1975) have previously modeled the same 16 alkali halides as have we, but they did not model any of them in a structure type in which A is 4-coordinate by X. Furthermore, these workers apparently used MEG theory only to generate the interionic repulsive potentials, whereas we have also used MEG theory to calculate the lattice energy of our model crystals. Muhlhausen and Gordon (1981) generated LiF and NaF in the sphalerite structure type using the MEG model and found LiF to be more stable in that structure type than in the rocksalt structure type as observed. Our study of carbonates (Chapter II) shows that within an ionic model, $CaCO_3$ is more stable when C is in 4-coordination than in 3- or 6-coordination by O, and Jackson and Gibbs (unpublished data) found that $MgSiO_4$ is more stable with Mg in 4-coordination than in the observed 6-coordination by O. We therefore feel it may be useful to model each of the alkali halides in structures with 4-coordinate alkali metal atoms.

RESULTS

Table 4 lists our calculated bond lengths and lattice energies for the alkali halides modeled in the rocksalt structure type, together with those calculated by Cohen and Gordon (1975) and those observed. Our bond lengths agree with those of Cohen and Gordon and with those observed within 0.01 Å on average, and almost half of our bond lengths are equal to those of Cohen and Gordon. Our lattice energies are on average within 3.1 kJ mol^{-1} of those of Cohen and Gordon and within 19.2 kJ mol^{-1} of those observed. The largest deviations of our bond lengths and lattice energies from those of Cohen and Gordon occur for LiCl: our bond length is 0.07 Å longer and our lattice energy is 28 kJ mol^{-1} higher than theirs. The largest deviations of our bond lengths and lattice energies from those observed occur for NaCl: our bond length is 0.14 Å longer and our lattice energy is 32 kJ mol^{-1} higher than those observed.

The results of our modelings of the alkali halides in the CsCl structure type, together with those of Cohen and Gordon, are shown in Table 5. Comparison of the data in that table to the corresponding entries in Table 4 shows that within an ionic model, RbI is slightly more stable in the CsCl structure type than in the rocksalt structure type as observed. It is also evident that our bond lengths and lattice energies again show the largest deviations from those of Cohen and Gordon in the case of LiCl: our bond length is 0.1 Å longer and our lattice energy is 35 kJ mol^{-1} higher than theirs. On average, our bond lengths deviate from those of Cohen and Gordon by less than 0.01 Å and our lattice energies deviate from theirs by 3.7 kJ mol^{-1}.

For the most part, our bond lengths for the chlorides of each alkali metal show larger deviations from the values of Cohen and Gordon and from those observed than do our bond lengths for the other halides of any given alkali metal. This is also true of the lattice energies. The cause of this anomalous behavior among the chlorides is uncertain, but could lie in a deficiency in the gas phase Cl^- wavefunction.

The results of our modelings of the alkali halides in the sphalerite structure type are listed in Table 6. Comparison of our calculated lattice energies for the sphalerite and the rocksalt structure types shows that LiF and LiCl are both more stable in the former. However, the lattice energy differences between structure types for both LiF and LiCl are small compared to the differences

Table 4. Bond lengths and lattice energies, rocksalt structure type.

	This study		Cohen and Gordon (1975)		Observed	
	$R(AX)$/Å	W/kJ mol^{-1}	$R(AX)$/Å	W/kJ mol^{-1}	$R(AX)$/Å	W/kJ mol^{-1}
LiF	2.13	-1008	2.13	-1006	2.014	-1032
LiCl	2.67	-817	2.60	-845	2.570	-844
LiBr	2.71	-821	2.73	-816	2.751	
LiI	2.93	-785	2.90	-785	3.000	
NaF	2.44	-887	2.44	-887	2.317	-912
NaCl	2.96	-743	2.93	-753	2.820	-775
NaBr	3.05	-729	3.05	-730	2.989	-729
NaI	3.25	-692	3.25	-690	3.237	-679
KF	2.71	-815	2.71	-813	2.674	-814
KCl	3.17	-706	3.14	-712	3.147	-709
KBr	3.25	-693	3.25	-692	3.298	-667
KI	3.42	-662	3.44	-661	3.533	-632
RbF	2.83	-788	2.83	-787	2.815	
RbCl	3.27	-687	3.26	-690	3.291	
RbBr	3.37	-670	3.39	-667	3.445	
RbI	3.56	-640	3.58	-639	3.671	

Observed data: bond lengths: compiled by Tosi (1964); lattice energies: Chase et al. (1985)

Table 5. Bond lengths and lattice energies, CsCl structure type.

	This study		Cohen and Gordon (1975)	
	$R(AX)$/Å	W/kJ mol^{-1}	$R(AX)$/Å	W/kJ mol^{-1}
LiF	2.31	-940	2.31	-937
LiCl	2.90	-762	2.80	-797
LiBr	2.93	-774	2.94	-772
LiI	3.08	-758	3.09	-758
NaF	2.59	-850	2.59	-850
NaCl	3.14	-711	3.09	-850
NaBr	3.22	-707	3.22	-706
NaI	3.37	-680	3.40	-680
KF	2.83	-793	2.83	-793
KCl	3.31	-686	3.27	-697
KBr	3.39	-682	3.39	-681
KI	3.55	-658	3.57	-659
RbF	2.97	-770	2.96	-769
RbCl	3.40	-672	3.38	-681
RbBr	3.51	-663	3.51	-662
RbI	3.67	-640	3.69	-640

between our calculated lattice energy and that observed for these substances. We note also that Cohen and Gordon (1975) calculated a lattice energy for LiCl in the rocksalt structure type which is within 1 kJ mol^{-1} of the observed lattice energy. These observations suggest that the difference between our calculated lattice energies in the rocksalt and in the sphalerite structure types may not be significant for LiF and probably are not significant for LiCl.

We determined bulk moduli and phase transition pressures by fitting our calculated pressures, unit cell volumes, and Gibbs free energies to second-order Birch-Murnaghan equations (Birch 1978). Our results, together with those of Cohen and Gordon and those observed, are presented in Tables 7 and 8; we report no results for LiI in the rocksalt and CsCl structure types as we could not accurately fit Birch-Murnaghan equations in these cases. In Table 8, we do not list explicit phase transition pressures less than zero as such values are not physically meaningful. We also do not list explicit phase transition pressures greater than 100 kb because such pressures are outside the range of pressures used in the Birch-Murnaghan fittings. Such pressures are also above the working limit of 65 kb for reliable high-pressure crystal structure determinations using a diamond-anvil cell (Hazen and Finger 1982). Our bulk moduli agree with those calculated by Cohen and Gordon (1975) within 1 kb on average, but are about 15 kb lower on average than those observed. This is in contrast to MEG results for many silicates (Jackson 1986, Jackson and Gibbs 1988, Jackson and Gordon 1988) and to those for the carbonates (Chapter II), where the bulk moduli calculated with MEG methods are higher than observed. Our phase transition pressures agree with those of Cohen and Gordon (1975) within 5 kb, and with the observed phase transition pressures within 10 kb, on average for those substances for which explicit transition pressures are listed. The largest disagreements tend to occur for the lowest transition pressures.

To explore the role of non-bonded XX repulsions in determining the AX bond lengths in our model crystal structures, we calculated the equilibrium AX bond lengths in a model diatomic AX molecule, using the classical Coulombic energy as the attractive potential and using the MEG pair potentials for the AX bond to model the AX repulsive potential. The resulting bond lengths are listed in Table 9. The AX bond length in each diatomic molecule is shorter than the AX bond length in the model AX crystal structures for all coordinations of A by X, indicating that in each

Table 6. Bond lengths and lattice energies, sphalerite structure type.

	$R(AX)$/Å	W/kJ mol^{-1}
LiF	1.95	-1019
LiCl	2.46	-819
LiBr	2.52	-808
LiI	2.70	-760
NaF	2.30	-874
NaCl	2.79	-729
NaBr	2.89	-704
NaI	3.12	-659
KF	2.59	-792
KCl	3.02	-685
KBr	3.11	-665
KI	3.32	-628
RbF	2.71	-762
RbCl	3.14	-662
RbBr	3.26	-640
RbI	3.46	-606

Table 7. Bulk moduli (in kb).

	Rocksalt structure			CsCl structure	Sphalerite structure
	LG[a]	CG[a]	Obs.[a]	LG	LG
LiF	727	706	867	690	576
LiCl	322	366	354	293	153
LiBr	340	325	---[b]	269	222
LiI	---[c]	187	211	---[c]	215
NaF	458	455	514	505	345
NaCl	238	246	285	251	164
NaBr	224	221	229	252	145
NaI	187	185	171	224	102
KF	345	343	342	426	233
KCl	218	205	202	226	127
KBr	185	186	180	172	130
KI	154	158	129	170	80
RbF	315	310	---[b]	264	200
RbCl	179	185	185	215	120
RbBr	170	162	159	151	110
RbI	141	140	127	246	82

[a]LG = Lindsay and Gibbs (this study), CG = Cohen and Gordon (1975); Observed data compiled by Cohen and Gordon (1975).
[b]Extrapolation to 0K not possible (Simmons and Wang 1971).
[c]Birch-Murnaghan equation could not be fitted accurately (see text).

Table 8. Phase transition pressures (in kb).

	Sphalerite type to rocksalt type	Rocksalt type to CsCl type		
	LG[a]	LG	CG	Obs.
LiF	57	(> 100)	2900	(> 100)
LiCl	5	(> 100)	980	(> 100)
LiBr	(< 0)	(> 100)	924	(> 100)
LiI	---[b]	---[b]	184	(> 100)
NaF	(< 0)	(> 100)	326	(> 100)
NaCl	(< 0)	(> 100)	107	(> 100)
NaBr	(< 0)	81	79	(> 100)
NaI	(< 0)	24	23	(> 100)
KF	(< 0)	88	85	(> 100)
KCl	(< 0)	51	34	20
KBr	(< 0)	25	23	19
KI	(< 0)	7	4	18
RbF	(< 0)	68	65	(> 100)
RbCl	(< 0)	29	17	6
RbBr	(< 0)	12	10	5
RbI	(< 0)	(< 0)	---[c]	3

[a]The symbols "LG", "CG", and "Obs." have the same meanings as in Table 7.
[b]Birch-Murnaghan equations could not be fitted accurately (see text).
[c]Cohen and Gordon (1975) do not list a value for RbI.

of these crystal structures, the value of $R(AX)$ is influenced to some degree by the non-bonded XX interactions. Figure 16a shows the bond-length--bond-order relations in four representative model crystal structures; the bond order is defined as the ratio of cation valence to cation coordination number. Figure 16b shows the bond-length--bond-order relations that would be found for the same crystal structures if the XX distance, $R(XX)$, were invariant with the cation coordination number and if $R(AX)$ were determined from $R(XX)$ by the interatomic geometry. To calculate the $R(AX)$ values plotted in Figure 16b, we arbitrarily chose the constant $R(XX)$ values to be those calculated for the rocksalt structure types. The variation in $R(AX)$ with bond order at constant $R(XX)$ is larger than for the $R(XX)$ values actually found in the model structures, because in the model structures, $R(XX)$ increases as the cation coordination number decreases. This suggests that the nature of the XX interactions would not be accurately modeled by closest packing of hard spheres whose radii are invariant with cation coordination number.

We attempted to determine a set of ionic radii from the AX bond lengths in our model crystal structures. Because the majority of our most stable structures are of the rocksalt type, we determined 6-coordinate radii for all of the alkali metal and halide ions. Noting that the lattice energies of RbI in the rocksalt and CsCl structure types are within 1 kJ mol^{-1} of each other, we assumed that if the radius ratio rule could be used to determine coordination numbers, then $r(Rb^+)/r(I^-) = \sqrt{3} - 1$ for both structures, as this is the upper limit to the radius ratio for 6-coordination and the lower limit for 8-coordination according to the rule. Assuming further that $R(RbI) = r(Rb^+) + r(I^-) = 3.56$Å in the rocksalt structure type, we determined that $r(Rb^+) = 1.50$Å and $r(I^-) = 2.05$Å. Using these values and the AX bond lengths for the other rocksalt-structure alkali halides, we determined the ionic radii listed in Table 10, where we compare them to the Pauling crystal radii, the Shannon-Prewitt crystal radii, and the Shannon-Prewitt effective ionic radii. One of our radii agrees with the corresponding Shannon-Prewitt effective ionic radius, and two more of our radii are within 0.01Å of the corresponding Shannon-Prewitt effective ionic radii, but most of our radii deviate markedly from those of Pauling and from those of Shannon and Prewitt. Furthermore, our radii are not consistent, as demonstrated by our attempt to use them to estimate the 6-coordinate LiX bond lengths. These estimates are also listed in Table

Table 9. Lengths of alkali halide bonds in absence of non-bonded repulsions.

Bond	Bond length /Å
LiF	1.56
LiCl	2.02
LiBr	2.13
LiI	2.43
NaF	1.98
NaCl	2.42
NaBr	2.55
NaI	2.78
KF	2.27
KCl	2.65
KBr	2.77
KI	2.98
RbF	2.40
RbCl	2.79
RbBr	2.92
RbI	3.12

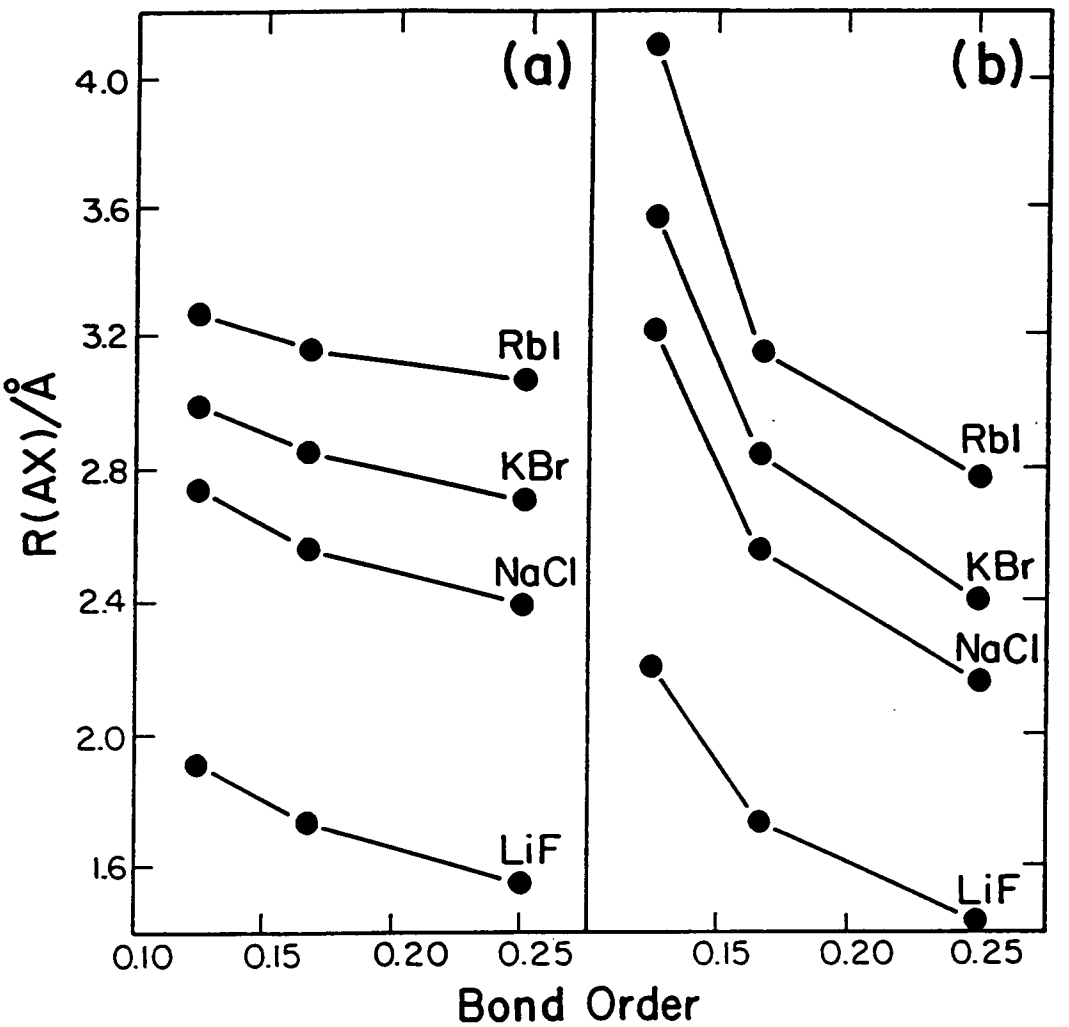

Figure 16. Variation in AX bond length with bond order (defined in text) in alkali halide crystals, (a) as found with the MEG model, and (b) as would be found with the MEG model if all non-bonded XX distances were fixed at their values in the rocksalt structure type.

Table 10. Ionic radii for the alkali metal and halide ions (in Å).

	This study	Pauling (1927)	Shannon and Prewitt (1969) (crystal)	(effective)
Li^+	0.39	0.60	0.88	0.74
Na^+	1.19	0.95	1.16	1.02
K^+	1.37	1.33	1.52	1.38
Rb^+	1.50	1.48	1.63	1.49
F^-	1.33	1.36	1.19	1.33
Cl^-	1.77	1.81	1.81*	1.81*
Br^-	1.87	1.95	1.96*	1.96*
I^-	2.05	2.20	2.20*	2.20*

*Shannon and Prewitt list only the Ahrens radii for these anions.

10 and compared to the bond lengths calculated with the MEG model for the rocksalt-structure Li halides.

DISCUSSION

As we noted earlier, the radius ratio rule predicts incorrect coordination numbers in some alkali halides. In Figure 17, we have plotted points corresponding to each of the observed alkali halide crystal structures (except those of Cs) in the $r(X)$-$r(A)$ plane for each of the three published sets of radii listed in Table 10. On each plot, we have also shown fields corresponding to the cation coordination numbers determined by the radius ratio rule. The observed structure type for each of these materials is the rocksalt type, therefore none of the field boundaries in any of the plots in Figure 17 would appear if the radius ratio rule determined the correct cation coordination numbers. Instead, the radius ratio rule determines the correct coordination numbers for only eight of the alkali halides when the Pauling radii are used, for only seven to nine of the alkali halides when the Shannon-Prewitt effective ionic radii are used, and for only five to seven of the alkali halides when the Shannon-Prewitt crystal radii are used. In each plot in Figure 17, there are points that lie close to coordination field boundaries. Due allowance for error in the values of $r(A)$ and $r(X)$ renders ambiguous the coordination numbers determined with the radius ratio rule for the corresponding structures. Use of the Shannon-Prewitt radii apparently does not improve the reliability of the radius ratio rule compared to what the rule exhibits with the Pauling radii. However, Shannon and Prewitt make no claim that their radii should necessarily yield accurate determinations of coordination numbers; their stated purpose for generating these radii was to provide a means of estimating interatomic distances in oxide and fluoride crystal structures. We consider the incorrect determinations of coordination numbers to be indicative more of deficiencies in the radius ratio rule itself than of deficiencies in the work of Shannon and Prewitt (1969). The coordination numbers determined in our MEG modelings are in closer agreement with experiment than are those found with the radius ratio rule using the Pauling or the Shannon-Prewitt ionic radii. The only discrepancies between our coordination numbers and those observed are for the two lightest alkali halides and the heaviest one, and for these, the differences between the lattice energy calculated for the most

stable structure type within the MEG model and that calculated for the rocksalt structure type are smaller than the differences between the calculated and observed lattice energies, so by our modeling, these substances are close to being stable in the rocksalt structure type as well. It should be noted that in our modeling of these crystal structures, we made no prior assumptions as to the radii of any of the ions, and that the ionic radii we did attempt to determine were not generally suitable for predicting the bond lengths in our crystal structures. We therefore feel that the radius ratio rule is not suitable for determining coordination numbers in crystals, even where the bonding is believed to be largely ionic.

Muhlhausen and Gordon (1981) have suggested a possible reason for the disagreement between the coordination number of Li in LiF determined with the MEG model and that observed. These workers noted that the electron densities from neighboring anions overlap considerably in LiF, and consequently the neglect of many-body interactions can lead to errors in calculating the lattice energy and the bond length. They also modeled LiF using a shell-stabilized F^- wavefunction which concentrates the anion electron density close to the nucleus. With the shell-stabilized wavefunction, Muhlhausen and Gordon found that LiF is more stable in the rocksalt structure type as observed than in the sphalerite structure type; with the free-ion F^- wavefunction, they found the opposite order of stability. Other possible sources of error in the MEG model include neglect of anion polarization, van der Waals interactions, and zero-point vibrational energy, all of which are expected to make rather small contributions (cf. McWeeny 1979, Muhlhausen and Gordon 1981).

The results Muhlhausen and Gordon (1981) obtained with the shell-stabilized F^- wavefunction appear to illustrate again the role of non-bonded repulsions between neighboring anions in determining the lattice energy and equilibrium geometry of an ionic crystal. We note that Muhlhausen and Gordon likened the contraction of the anion electron densities resulting from shell stabilization to an effective increase in the cation-anion radius ratio; thereby providing another indication of how deeply entrenched the radius ratio concept is in the solid-state sciences. Considering the deficiencies of the radius ratio rule as a means of determining coordination numbers, we prefer to view the effect of shell stablilization in terms of its effect on the anion-anion repulsion energies within the MEG model. Concentrating the electron density close to the nucleus reduces

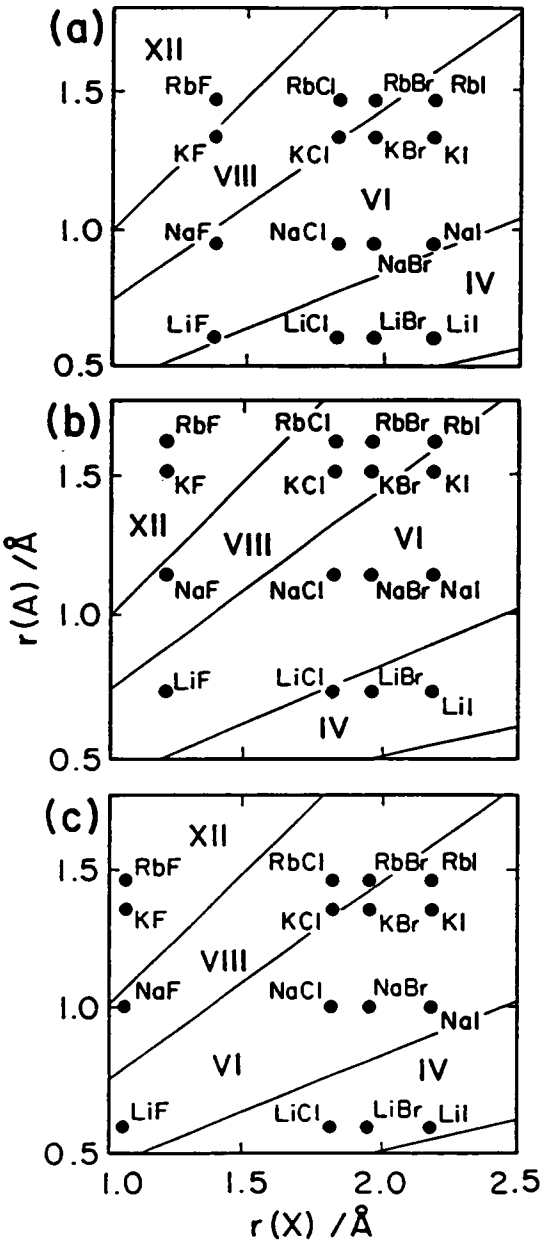

Figure 17. Alkali halide crystals plotted according to $r(A)$ and $r(X)$ using (a) Pauling (1927) radii, (b) crystal radii of Shannon and Prewitt (1969), and (c) effective ionic radii of Shannon and Prewitt (1969).

the electron density at nearest-neighbor and next-nearest neighbor ion sites in a crystal structure. The total electron density between nearest-neighbor and next-nearest-neighbor ions, resulting from superposition of the isolated ion densities, is thereby reduced, and the interaction energy between the anions, being a functional of the electron density, is also reduced. This in turn reduces the magnitude of a positive contribution to the lattice energy and so makes the lattice energy more negative, i.e., the crystal structure becomes more stable when there is less superposition of electron density from neighboring anions. In crystals with higher cation coordination numbers, the anion-anion distances are shorter, relative to the cation-cation distances than in crystals with lower cation coordination numbers (see Figure 16 and the accompanying discussion). The electron density overlap from neighboring anions would be significantly larger at a shorter anion-anion distance due to the exponential form of the radial wavefunction. It is therefore reasonable to expect that anion shell stabilization would effect a larger reduction of the anion-anion repulsion energy in crystals having larger cation coordination numbers, thereby stabilizing crystal structures with high cation coordination numbers relative to crystal structures with low cation coordination numbers.

Our analysis of bond lengths and bond orders in the preceding section illustrates another way of reducing the positive contributions and increasing the negative contributions to the lattice energies of ionic crystals. We noted that the bond length decreases, and the non-bonded anion-anion distance increases, as bond order increases (i.e., as coordination number decreases). We also noted that in all of our MEG model crystal structures, the bond length is longer than in a diatomic molecule generated with the MEG model and composed of the same atoms, which implies that there is an attractive force between the cation and the anion along the bond axis in the crystals. This means that any shortening of the bond in the crystal increases the negative contribution to the lattice energy made by the Coulombic attraction, provided that the bond length in the crystal remains longer than that calculated for the isochemical diatomic molecule. Increasing the distance between neighboring anions reduces the positive contributions to the lattice energy arising from the Coulombic forces between the anions. Although the anion-anion pair potentials tend to be negative at large anion-anion distances, they are not large enough in absolute value to offset the positive Coulombic potential. Again, the radii of individual atoms is immaterial; the interatomic distances

appear to be those corresponding to a minimum in the lattice energy and not necessarily those corresponding to a maximum in the atomic packing efficiency. We find no simple rule for determining coordination numbers from a single quantitative property of the individual atomic or ionic species that make up a crystal.

O'Keeffe (1977) noted that for a given coordination number of A by X in ionic crystals, the AX distances are nearly equal, as previously observed by Shannon and Prewitt (1969), and that the XX distances tend to be as large as possible within the constraint of fixed AX distances. This means that the structures of such crystals have close to the maximum volume attainable with fixed AX distances. O'Keeffe concluded that when the atomic arrangement in such a crystal corresponds to a close-packed geometry, such an arrangement is a consequence of the tendency of the crystal to attain a maximum volume. These observations are consistent with our hypothesis concerning XX distances in ionic crystals.

We emphasize that our results and interpretations apply strictly to crystals having purely ionic bonds. The nature and effects of the binding forces are more complex and more difficult to model mathematically for bonds having more covalent character. However, Phillips (1970) appears to have found a relatively simple rule for determining cation coordination numbers in certain types of crystals having partial covalent bonding. Phillips showed that the bandgap, E_g, can be partitioned into a homopolar (covalent) part, E_h, and an ionic part, C, according to

$$E_g^2 = E_h^2 + C^2. \tag{4}$$

Using values of E_g and C determined by optical spectroscopy for over 60 binary crystals, Phillips showed that the cations in these crystals are 4-coordinate when $C^2/E_g^2 < 0.785$ and are 6-coordinate when $C^2/E_g^2 > 0.785$. For two crystals, $C^2/E_g^2 \approx 0.785$; these each have one polymorph with 4-coordinate cations and one polymorph with 6-coordinate cations. All cation coordination numbers were determined correctly with this method. These results seem to imply that the ionic or covalent character of the bonding in a crystal is a major factor in determining the crystal structure. Once again, the radii of individual atoms or ions have no direct bearing on cation coordination numbers.

CONCLUSIONS

The radius ratio rule is not reliable for predicting coordination numbers of cations in crystals. It was derived within the context of ionic bonding in crystals by assuming that the ions in crystals behave as though they have well defined radii and fill space so as to maximize packing efficiency. The rule should therefore be most accurate in determining the coordination numbers in crystals having largely ionic bonding. Alkali halide crystals are believed to be largely ionically bonded, yet the radius ratio rule determines the correct coordination numbers for only about half of these at best, and leads to large errors in the coordination numbers of several of the alkali halides.

Analyses of crystal structures generated with the purely ionic MEG model suggest that the most stable structure type for a given alkali halide crystal is one where the energy due to attractive forces between cations and anions is a maximum while the energy due to repulsive forces between neighboring anions is a minimum, so that the lattice energy is minimized. Lattice energies and geometries are determined within this model without prior knowledge of ionic radii, and the cation coordination numbers so determined agree with those observed in all but three of the alkali halides, and for these the difference in the lattice energy calculated for the most stable model structure and the lattice energy calculated for the observed structure is within the error of the model. An attempt to determine ionic radii from the MEG model crystal structures, following the procedures used to determine such radii from observed crystal structures, resulted in a set of ionic radii that did not accurately reproduce the bond lengths even in model alkali halide crystals having the structure type from which the radii were estimated. These observations cast sufficient doubt on the validity of the radius ratio rule as a means of predicting coordination numbers to warrant relegating the rule to the history of the solid-state sciences and not retaining it as a fundamental principle of those sciences.

Chapter IV

A MOLECULAR ORBITAL STUDY OF BONDING IN SULFATE MOLECULES: IMPLICATIONS FOR SULFATE CRYSTAL STRUCTURES

INTRODUCTION

Sulfates show less variability in their crystal structures and are less abundant in the earth's crust than silicates, even though both of these materials contain tetrahedral oxyanions. Sulfate minerals with polymerized sulfate tetrahedra have yet to be reported, in contrast with the silicates, for which a large variety of polymerized structures are known. Klein and Hurlbut (1985) claim that the SO bond is so strong that the sharing of a common O atom between two sulfate groups would destabilize the resulting S_2O_7 group relative to the monomeric SO_4 groups, rendering minerals with sulfate polymers energetically unfavorable. However, a number of sulfates containing polymerized sulfate anions have been synthesized in the laboratory. These observations attracted our attention to studying the bonding in sulfates and to comparing it to the bonding in tetrahedrally-coordinated oxyanions of other second-row atoms, particularly Si and P.

It is now fairly well established that our understanding of bonding in oxide crystals can be improved by studying the bonding mechanisms in hydroxyacid molecules that are chemically and structurally similar to polyhedral units of interest in crystals (Almenningen et al. 1963, Barrow et al. 1979, Gibbs et al. 1981, Gibbs 1982). Furthermore, molecular orbital (MO) calculations on a variety of such molecules have yielded minimum-energy bond lengths and angles that match those reported for chemically similar molecules and crystals. They have also yielded deformation electron

density maps that are similar to those observed for the silica polymorphs and selected borate crystals (cf. Gibbs et al. 1972, Tossell and Gibbs 1977, 1978, Newton 1981, Gibbs et al. 1981, Gibbs 1982, Hill et al. 1983, O'Keeffe et al. 1985, Zhang et al. 1985, Spackman et al. 1987, Geisinger et al. 1987).

MO studies on a variety of other TO_4 tetrahedral oxyanions containing first- and second-period atoms have also been completed (Downs and Gibbs 1981, Geisinger and Gibbs 1981, Geisinger 1983, Dytrych 1983, O'Keeffe et al. 1985, Gibbs et al. 1987,1988). In addition, Louisnathan et al. (1977) have used semi-empirical Extended Hückel calculations to study bond overlap population vs. bond length variation in sulfates. When the SO bonds in the sulfate anions in crystals were clamped at a constant length, the resulting overlap populations served to rank the SO bond lengths, with shorter bonds involving wider OSO angles. However, these workers were unable to explain the narrow range of SOS angles observed between corner-sharing sulfate groups. Geisinger and Gibbs (1981) and, more recently, Geisinger et al. (1985) have completed MO calculations on thiosilicate, silicate, borosilicate, and aluminosilicate corner-sharing tetrahedra, using STO-3G basis sets, with emphasis on the variations of observed bond lengths and bridging TOT bond angles and on the energetics involved in varying these parameters. Their results were shown to provide qualitative insight into bond length and angle variations in thiosilicate, framework silicate, and aluminosilicate structures, and to reproduce correlations between bond strength sums and SiO and AlO bond length variations.

The bridging SiSSi angles in thiosilicate crystals show a narrow range of values (105°-115°), and calculations on the molecule H_6Si_2S show a large barrier to linearity ($\Delta E_T = E_T(\theta) - E_T(180°)$), where $\theta = TOT = 103.9°$ (Gibbs et al. 1988). In contrast, bridging SiOSi angles in silicate crystals show a wide range of values (120°-180°), and a small ΔE_T value is found for $H_6Si_2O_7$. It appears from these observations that the ΔE_T values calculated for appropriate molecules may be transferrable and can be used to mimic ΔE_T values for comparable units in crystals, which in turn may provide insight into the range of bridging angles and the structures of polymerized tetrahedral groups that can form stable units. Furthermore, ΔE_T may play a role in the glass-forming properties of materials comprising corner-sharing tetrahedra, given that the structures of silicate glasses are believed to consist of corner-sharing SiO_4 tetrahedra linked together

with a wide range of bridging angles (cf. Warren 1972, Böttger 1974, Newton and Gibbs 1980, Gibbs et al. 1981, Dean 1982, Navrotsky et al. 1985).

In this study, we optimize the geometries of SO_3, H_2SO_4, $H_2S_2O_7$, and H_6SO_6, using robust 6-31G** bases and present comparisons with earlier work. Total charge and deformation densities of these molecules are also calculated and examined. In addition, the vibrational spectrum for H_2SO_4, the energy of the reaction forming sulfuric acid from water and sulfur trioxide, and the variation in the total energy of H_2SO_4 as a function of the torsional angles are calculated. Also a comparison is made of the deformation densities for $H_6Si_2O_7$, $H_4P_2O_7$, and $H_2S_2O_7$, and bonded radii of S and O are obtained from total charge density maps.

GEOMETRY AND BONDING IN SULFATE ANIONS

Optimized Geometries of H_2SO_4 and $H_2S_2O_7$

The geometries of H_2SO_4 and $H_2S_2O_7$ were both optimized using the GAUSSIAN 82 program (Binkley et al. 1982, Hehre et al. 1986). Both of these molecules were constrained in the calculations to have C_2 point symmetry (Figure 18). The H_2SO_4 molecule has two types of SO bonds: a single SO[H] bond, where the O atom is bonded to both S and H, and a double S = O bond where the O is bonded only to S (Table 11). The lengths of these bonds fall within the range of SO bond lengths reported for crystals and molecules. The SO[H] bond is, as expected, significantly longer (1.569Å) than that (1.411Å) calculated for the S = O bond. The bond angles calculated for the molecule show wide variations but match those reported for the gas-phase molecule (Kuczkowsky et al. 1981). They also compare favorably with those (Table 11) observed in a crystal (Yu and Mak 1978). The two bond lengths calculated for the molecule are within 0.01Å of the experimental gas-phase bond lengths and within 0.05Å of those in the crystal.

The geometry of the $H_2S_2O_7$ molecule shows the expected trends (see Table 12). The SO[S] bridging bond is the longest (1.623Å), the SO[H] bond is intermediate (1.553Å), and the S = O bond is the shortest (1.405Å). The OSO angles in $H_2S_2O_7$ vary in a regular way (O = S = O (123.3°) > O = SO[H] (109.1°) > O = SO[S] (108.1°) > [H]OSO[S] (95.8°)), with the wider angles involving the shorter bonds with larger fractional s-character and small bond strength sums (see below). This

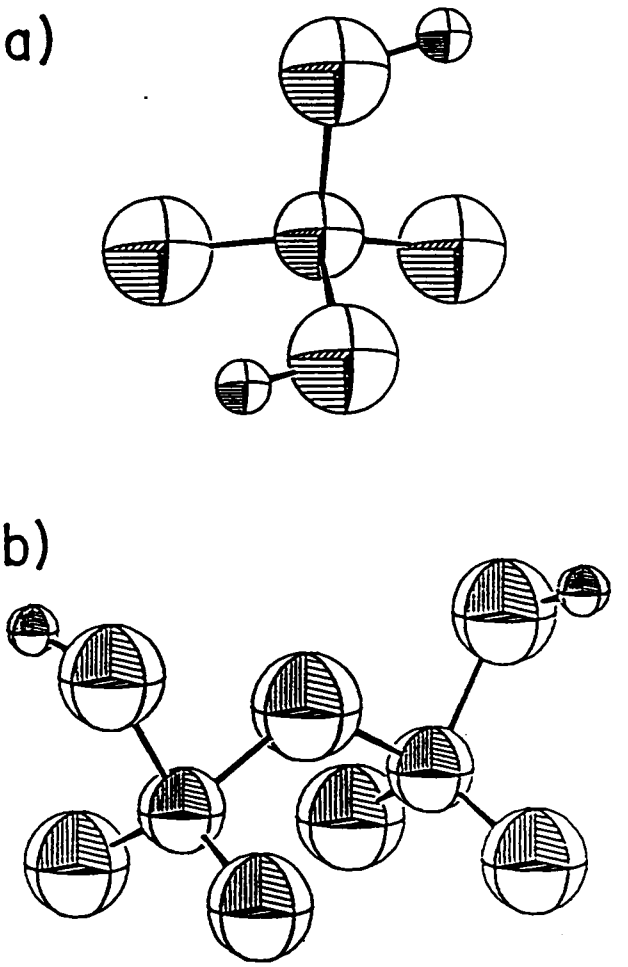

Figure 18. Optimized geometries of (a) H_2SO_4 and (b) $H_2S_2O_7$ calculated with a 6-31G** basis set.

Table 11. Geometric parameters for H_2SO_4

Parameter	MO (this study)	Gas-phase (Kuczkowsky et al. 1981)	Crystal (Yu and Mak 1978)
SO[H]	1.569Å	1.574Å	1.528(5)Å
S=O	1.411	1.422	1.419(5)
OH	0.950	(not given)	(not given)
[H]OSO[H]	101.8°	101.3°	103.7(4)°
[H]OSO	107.4	108.5	106.3(3), 101.6(3)
O=S=O	123.5	123.3	118.3(4)
SOH	110.5	(not given)	(not given)
[H]O...O[H]	2.435Å	(not given)	(not given)
[H]O...O	2.403	(not given)	2.624Å
O...O	2.486	(not given)	(not given)

Two different values of [H]OSO were found in crystalline H_2SO_4 because the OSO plane is not perpendicular to the [H]OSO[H] plane in the reported structure.

result also conforms with the predictions of the VSEPR model (cf. Gillespie 1972) where shorter bonds of higher bond strength and greater bond density require more space in the valence shell and wider valence angles than longer ones of lower bond strength. The bond lengths calculated for $H_2S_2O_7$ are similar to those observed in disulfate units in crystals (cf. Douglade and Mercier 1979, Einstein and Willis 1981). Also, the SOS bond angle calculated for the molecule (125.6°) , compares well with the average SOS angle (122.4°) observed in polysulfate crystals.

In a re-examination of the structure of melilite, Smith (1953) discovered that the SiO bond lengths in the mineral increase in a regular way with the sum of the Pauling bond strengths reaching each atom bonded to Si. Baur (1970) has since shown that such a correlation holds for a large variety of bond types, including that displayed in Figure 19 for the SO bonds in sulfate crystals. When the SO bond lengths calculated for H_2SO_4 and $H_2S_2O_7$ are plotted against bond strength sum, we find that these points fall along the general trend of the sulfate data set established for crystals (Figure 19), indicating that the properties of an SO bond in a sulfate group in a molecule are not all that different from those in a sulfate group in a crystal.

Correlation Between SO Bond Length and Fractional s-Character

As indicated above, the OSO angles calculated for H_2SO_4 and $H_2S_2O_7$ correlate with the SO bond lengths, with wider angles involving shorter bonds. The theory of sp^3 hybridization as discussed by Coulson (1961, see also Bingel and Luttke 1981) provides an estimate of the fractional s-character, f_i, for the ith SO bond in an SO_4 group from the OSO angles where

$$f_i = \frac{1}{\sqrt{1+\lambda_i^2}}. \tag{5}$$

and where λ_i is the hybridization parameter. Following the method described by Zhang et al. (1985) and applied by Boisen and Gibbs (1987) to a variety of tetrahedral oxyanions, the hybridization parameter is given by

$$\lambda_i^2 = -\frac{\cos\theta_{jk}}{\cos\theta_{ij}\cos\theta_{ik}} \tag{6}$$

Table 12. Optimized geometry of $H_2S_2O_7$

Parameter	Value
SO[S]	1.623Å
SO[H]	1.553
S=O	1.405
OH	0.951
SOS	125.6°
[S]OSO[H]	95.8
[S]OS=O	108.1
[H]OS=O	109.1
O=S=O	123.3
SOH	111.2
[H]O...O[S]	2.357Å
[H]O...O	2.410
[S]O...O	2.454
O...O	2.436

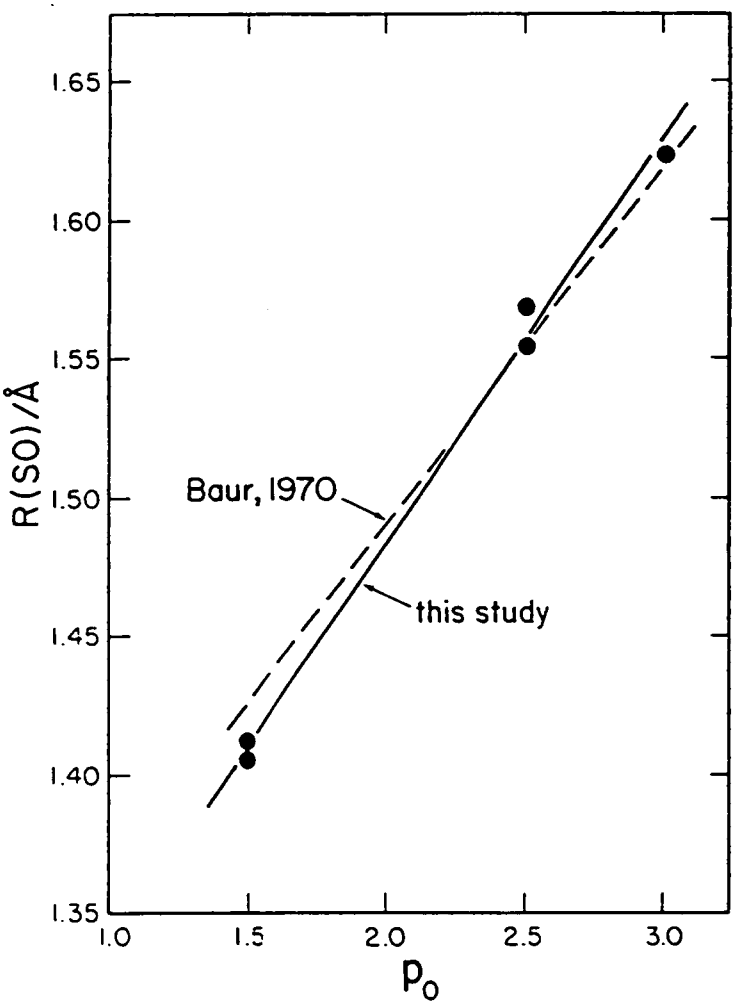

Figure 19. SO bond lengths vs. p_O, the sum of the Pauling bond strengths reaching the O atom from the S and H atoms to which the O is bonded.

where θ_{ij} is the valence angle (not necessarily the bond angle) between the ith and jth bonds; θ_{ik} and θ_{jk} are defined analogously. Klahn (1983) has warned against using the actual bond angles as the θ values in this equation, and so an ideal tetrahedron was fitted to SO_4 groups using a FORTRAN 77 program prepared by Boisen and Gibbs (1987). The correlations between f_i and SO bond lengths for the molecules H_2SO_4 and $H_2S_2O_7$ and for sulfate tetrahedra in crystals are shown in Figure 20. The two regression lines are nearly parallel, providing additional grounds for believing that the bonding in sulfate molecules is not all that different from that in a sulfate crystal.

Deformation Energetics of the Bridging SOS Angle in $H_2S_2O_7$

After optimizing the geometry of $H_2S_2O_7$, single-point energy calculations were made as a function of the SOS angle at 20° intervals from 100° to 180°. In each of these calculations, all other geometric parameters of the molecule were held fixed. A plot of the energy variation of the dimer as a function of the TOT angle is compared with those reported for $H_4P_2O_7$ and $H_6Si_2O_7$ in Figure 21 (O'Keeffe et al. 1985). The ΔE_T value is much greater for the sulfate dimer than that calculated for the silicate and phosphate dimers (see Table 13). The energy curves for the three dimers are displayed in Figure 22 with a histogram showing the frequency distribution of the TOT angles reported for crystals. The mode in each histogram corresponds to the interval containing the average bond angles for crystals. An examination of the figure suggests that the greatest standard deviation, $s(\theta)$, of the angles observed about the mean is exhibited by the silicates, as expected because $H_6Si_2O_7$ has the smallest ΔE_T value. On the other hand, the sulfates show the smallest $s(\theta)$ value, as expected because of the larger ΔE_T calculated for $H_2S_2O_7$. Both ΔE_T and the $s(\theta)$ value of the observed bridging angles are intermediate for the phosphates.

Geisinger et al. (1985) have shown that ΔE_T for several molecules with SiOT units correlates with the range of SiOT angles observed in a variety of silicate crystals. The range is a valid small-sample estimate of the standard deviation, but it can be unreliable in certain cases. Therefore, we have chosen to plot the more stable statistic $s(\theta)$ vs. ΔE_T. Figure 23a shows a systematic decrease in $s(\theta)$ with increasing ΔE_T. It is expected that $s(\theta)$ should also depend on the bending force constant,

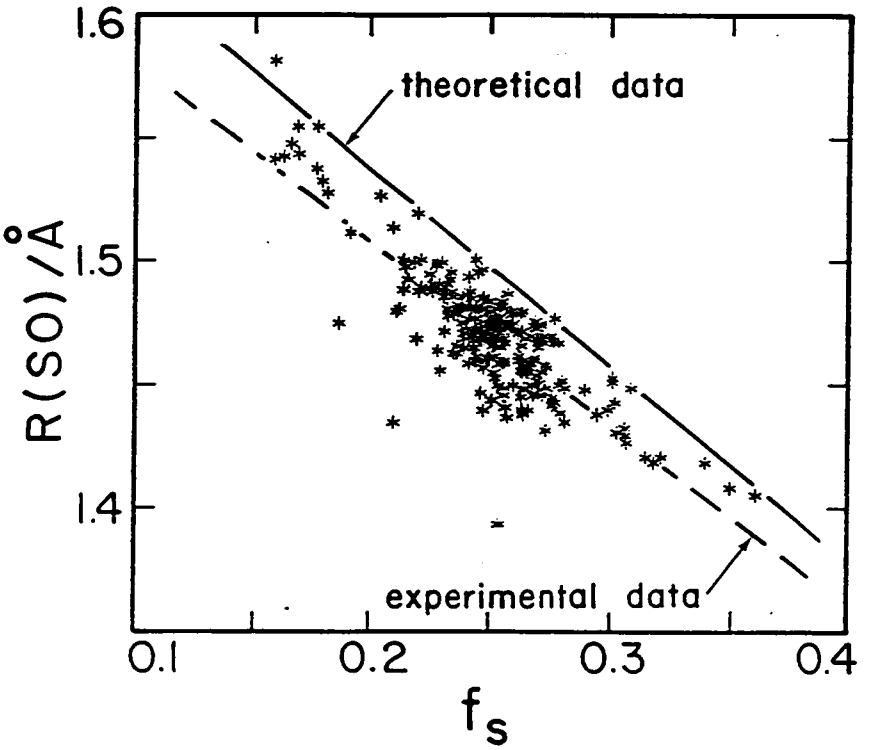

Figure 20. SO bond length vs. fractional s-character (f_s) of the bond.

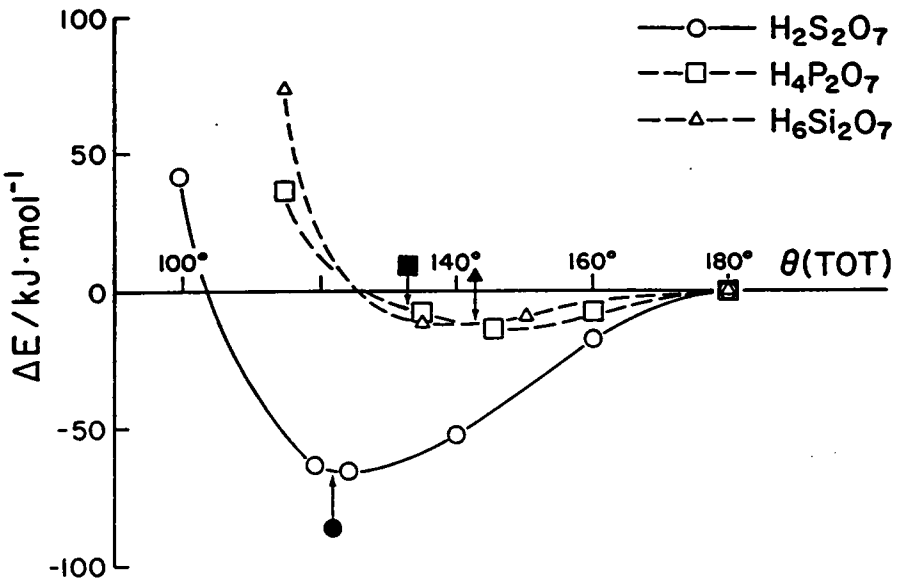

Figure 21. Total energy vs. bridging *TOT* bond angle. Solid symbols with arrows mark the average observed bridging angle in crystals.

Table 13. Barriers to linearity and optimized bridging angles for three tetrahedral dimers.

TOT groups	ΔE_T/kJ-mol^{-1}	θ_{equil}	Reference
SOS	-64.500	125.6°	(1)
POP	-13.600	145.0	(2)
SiOSi	-9.373	141.0	(2)

References: (1) This study. (2) O'Keeffe et al. 1985.

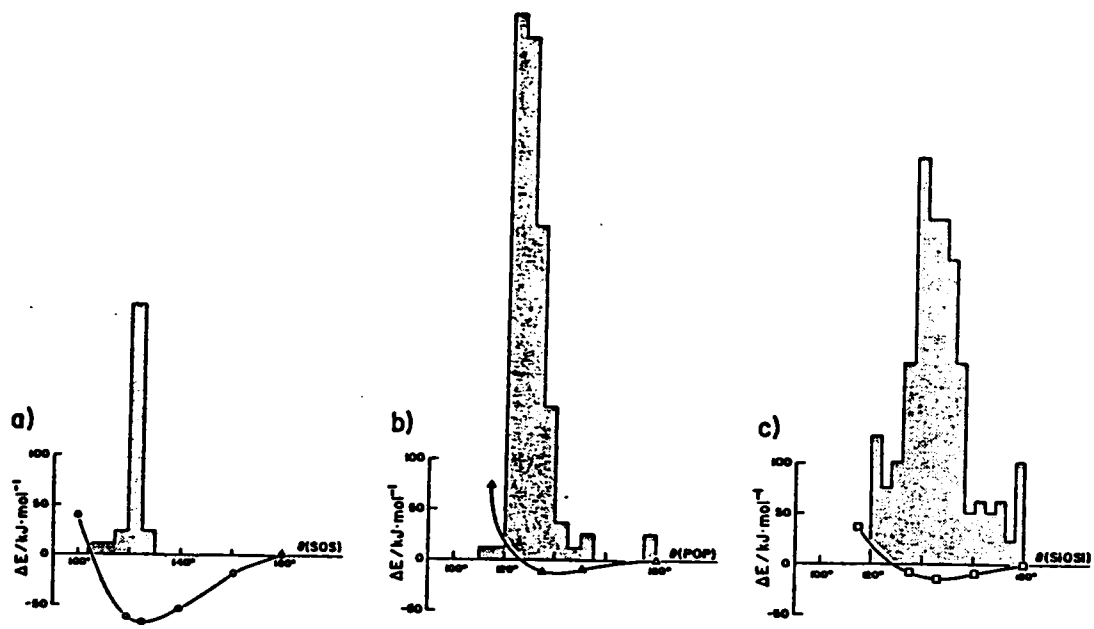

Figure 22. Energy curves from Figure 21, with histograms of observed bridging *TOT* angles in crystalline substances: (a) polysulfates (curve: this study; histogram: Dytrych 1983); (b) polyphosphates (curve: O'Keeffe et al. 1985; histogram: Dytrych 1983); (c) polysilicates (curve: O'Keeffe et al. 1985; histogram: Geisinger et al. 1983).

$$K_{\theta\theta} = \frac{1}{r_o^2}\left(\frac{\partial^2 E}{\partial \theta^2}\right), \tag{7}$$

of the bridging angle θ. Figure 23b shows $s(\theta)$ plotted against $K_{\theta\theta}$ values calculated with MO theory. As expected, the smallest $s(\theta)$ values reported for crystals correspond to the largest $K_{\theta\theta}$ values calculated for the molecules. In other words, the variability of a TOT angle in a crystal should be a function of the compliance of the angle, the greater the bending force constant of the angle, the smaller the variability of the angle.

The narrow range of bridging SOS angles could also be ascribed to a paucity of data for polysulfate crystal structures. The present results do not permit an unequivocal decision as to whether energetics or sample size imposes the more severe restriction on the range of bridging angles. However, the success of previous comparisons between barriers to linearity and ranges of bridging bond angles (Downs and Gibbs 1981, Dytrych 1983, Geisinger 1983, Geisinger et al. 1985) suggests that a relatively narrow range of bridging angles is expected for polysulfates even if these had as large a number of representatives as do the silicates.

All reports of sulfate glasses which we have found in the literature state that the structures of these glasses involve monomeric rather than polymerized SO_4 tetrahedra (cf. Narasimham and Rao 1978, Sundar and Rao 1980). Sulfate oxyanions can occur in silicate glasses such that SO_4 tetrahedra may share corners with one or two SiO_4 tetrahedra (Holmquist 1978), but we have found no reports of glass structures in which SO_4 tetrahedra share corners with other SO_4 tetrahedra. This observation may be ascribed in part to the large ΔE_T value for $H_2S_2O_7$ and to the weak SO[S] bond. As we conjecture that the stiffness of the bridging SOS angle limits the ability of an S_2O_7 group to adapt to a wide variety of crystal structures, we can also conjecture that the stiffness of the SOS angle would preclude a wide range of randomly-distributed values for the bridging SOS angle in a glass structure. This observation is consistent with that made by Geisinger and Gibbs (1981) with respect to thiosilicates, and suggests that neither class of materials is likely to readily form glasses of the random-network type hypothesized for vitreous silicates.

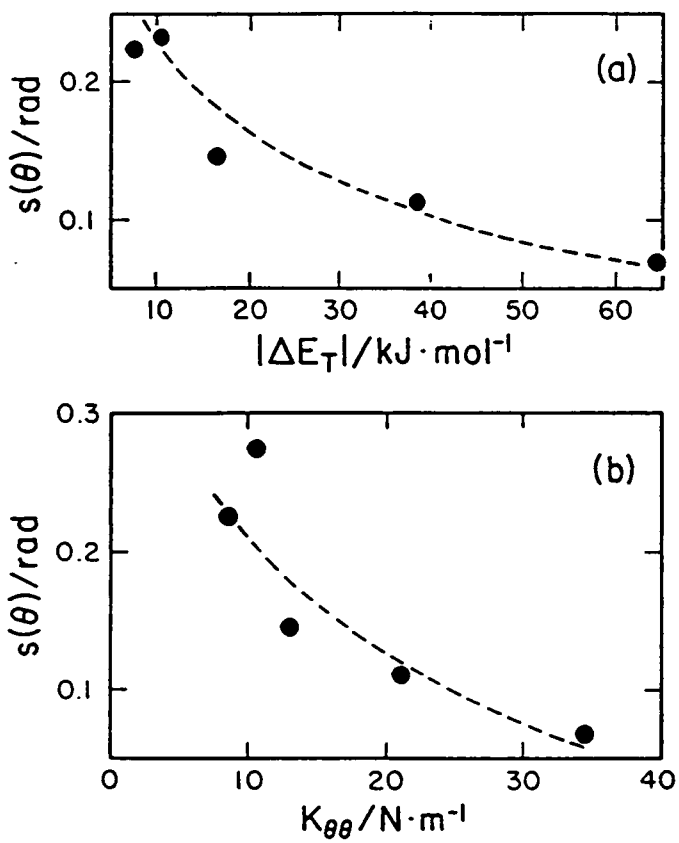

Figure 23. Standard deviations ($s(\theta)$) of bridging *TOT* angles in various T_2O_7 groups in crystals as a function of (**a**) barrier to bending (ΔE_T) of the *TOT* angle; (**b**) bending force constant ($K_{\theta\theta}$) of the *TOT* angle. The dashed curve in each diagram represents the least-squares function fitted to the data.

DYNAMIC PROPERTIES OF H_2SO_4

Vibrational Spectra

The frequencies and atomic displacements associated with each of the vibrational modes of H_2SO_4 were calculated using GAUSSIAN 82. In Table 14, the calculated frequencies are compared with those observed by Giguere and Savoie (1963). The calculated Raman activities and the IR intensities are also listed. A linear regression analysis of the observed and calculated frequencies shows that the calculated frequencies serve to rank the observed ones with a coefficient of determination of 0.99. The scatter diagram of ν(obs) vs. ν(calc) and the regression line corresponding to the equation

$$\nu(\text{obs}) = 0.551 + 0.914\nu(\text{calc}) \tag{8}$$

are shown in Figure 24. The two highest frequencies measured for H_2SO_4 correspond to OH stretches, which are typically troublesome to measure and assign. In fact, the assignments (symmetric vs. asymmetric) for these two modes, as interpreted from the GAUSSIAN 82 output, are calculated to be opposite those made by Giguere and Savoie (note that these two modes were not used in the regression analysis). The observation that the ν(calc) values are about 10% larger, in general, than the corresponding ν(obs) values can be ascribed to the neglect of anharmonicity, vibrational-rotational coupling, and centrifugal distortion in the model used to calculate the frequencies.

The mode assignments made by Giguere and Savoie are, with a few exceptions, in agreement with those calculated in this study. Four of the calculated modes are displayed in Figure 25. One of these corresponds to the largest discrepancy between calculated and observed frequency (Figure 25a). Giguere and Savoie assigned this as an asymmetric OH wagging mode, an assignment that conforms to the present study. Figure 25b shows the mode assigned as the $S(OH)_2$ rocking mode by Giguere and Savoie, an assignment that is supported by the calculations. Two modes for which our calculations do not support their assignments are illustrated in Figures 8c and 8d. The former was assigned as an $S(OH)_2$ symmetric stretch, and the latter an SO_2 asymmetric stretch. The cal-

Table 14. Vibrational spectra of H_2SO_4

Calculated (this study)					Observed (Giguere and Savoie, 1963)		
ν/cm^{-1}	symmetry	assignment	IR Int.	Raman Act.	ν/cm^{-1}	symmetry	assignment
254.7	a	OH wag sym	36	4	265(?)	a_2	OH wag sym
326.9	b	OH wag asym	21	2	265(?)	b_2	OH wag asym
398.9	a	$S(OH)_2$ bend sym	0	2	380	a_1	$S(OH)_2$ bend sym
466.3	a	torsion	3	1	390	a_2	torsion
537.7	b	$S(OH)_2$ rock	12	2	400	b_2	$S(OH)_2$ rock
605.6	a	$S(OH)_2$ bond sym + SO_2 bond sym	21	4	560	a_1	SO_2 bend sym
608.9	b	SO_2 rock + $S(OH)_2$ bend or rock	18	4	625	b_2	SO_2 rock
938.9	a	"composite": see Figure 25(c)	27	19	900	a_1	$S(OH)_2$ stretch sym
1002.4	b	$S(OH)_2$ rock	100	4	960	b_1	$S(OH)_2$ stretch asym
1261.0	a	OH wag sym	25	2	1150	b_1	SOH bend asym
1279.3	b	OH way sym	29	3	1160	a_1	SO_2 stretch sym
1317.2	a	SO_2 stretch sym + $S(OH)_2$ bend + SOH bend	66	9	1200	b_1	SOH bend asym
1573.7	b	"composite"; see Figure 25(d)	99	1	1410	b_2	SO_2 stretch asym
4109.9	b	OH stretch asym	90	27	3500	a_1	OH stretch sym
4114.9	a	OH stretch sym	13	100	3600	b_1	OH stretch asym

IR and Raman intensities are reported as percentages of the intensity of the strongest line in each spectrum (1002.4 cm^{-1} for IR, 4114.9 cm^{-1} for Raman).

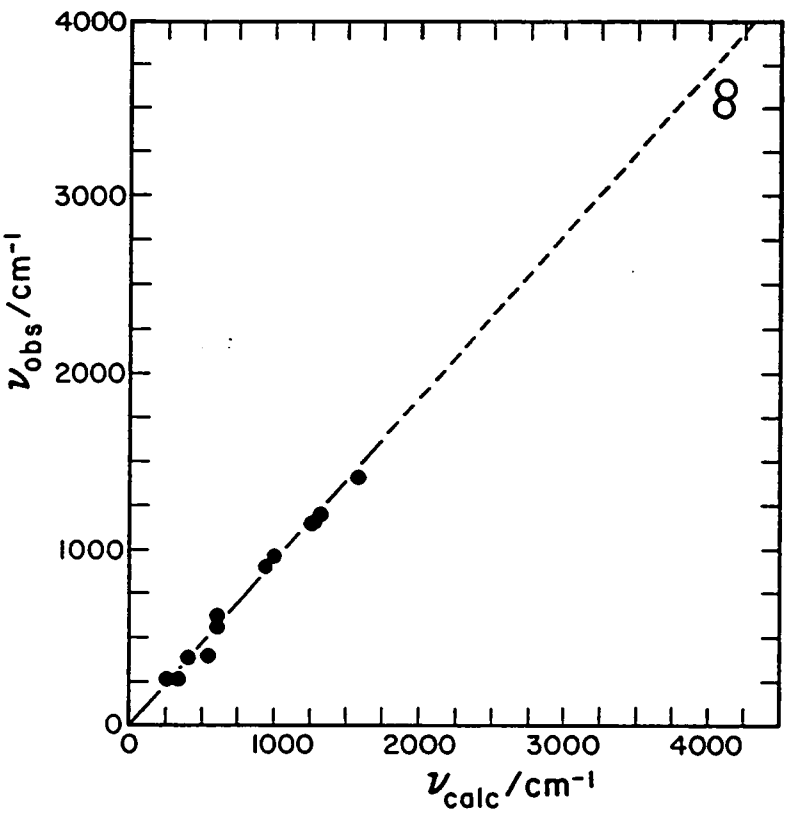

Figure 24. Observed vs. calculated vibrational frequencies for H_2SO_4. The two high-frequency modes, indicated by open circles, were excluded from the regression analysis. The dashed portion of the regression line is extrapolated from the relation fitted to the lower-frequency data (solid circles).

culated atomic displacements are difficult to describe as any particular stretching or bending, but appear to be composites of several motions involving both stretching and bending. The vibration depicted in Figure 25c does appear to be primarily stretching in character, as Giguere and Savoie concluded, but the one shown in Figure 25d seems to involve more bending than stretching, contrary to their assignment. It should be noted that the point symmetry of the optimized molecule is C_2; Giguere and Savoie assumed a point symmetry of C_{2v}, which could have affected their assignments of the various modes.

The infrared intensities and Raman activities were determined using a coupled perturbed Hartree-Fock (CPHF) procedure (cf. Schaefer and Yamaguchi 1986, Yamaguchi et al. 1986) to evaluate analytically the derivatives of the dipole moment and the dipole polarizability with respect to the normal coordinates. The GAUSSIAN 82 output reports absolute infrared intensities and Raman activities, but we have chosen to report relative values in Table 14. Vibrational intensity calculations in previous studies (Frisch et al. 1985, Frisch et al. 1986, Yamaguchi et al. 1986) indicate that qualitatively correct trends in both infrared intensities and Raman activities are predicted theoretically but that the absolute magnitudes of these quantities are not accurate. Giguere and Savoie (1963) did not report intensities in their experimental spectrum of H_2SO_4, so we cannot compare our calculated infrared intensities to experimental values. We expect that if absolute intensities had been reported in the experimental spectrum, we should have found that our calculated absolute intensities overestimated the experimental ones, primarily due to our use of the harmonic approximation (Yamaguchi et al. 1986).

Energetics of Formation

An MP2 calculation was made using the 6-31G** optimized geometry of H_2SO_4 to obtain a more accurate value for the total energy. Similar MP2 calculations were made for SO_3 and H_2O. The energy values obtained from these calculations were used to calculate the energy of reaction for $H_2O + SO_3 \rightarrow H_2SO_4$ at 0K and 298K (Table 15). Also listed are the results of earlier 3-21G* calculations (Chen and Plummer 1985) and experimental reaction enthalpies at 0K and 298K determined from JANAF data. The agreement between the theoretical and experimental energies is good. The difference between the MP2-level reaction energy and the restricted Hartree-Fock

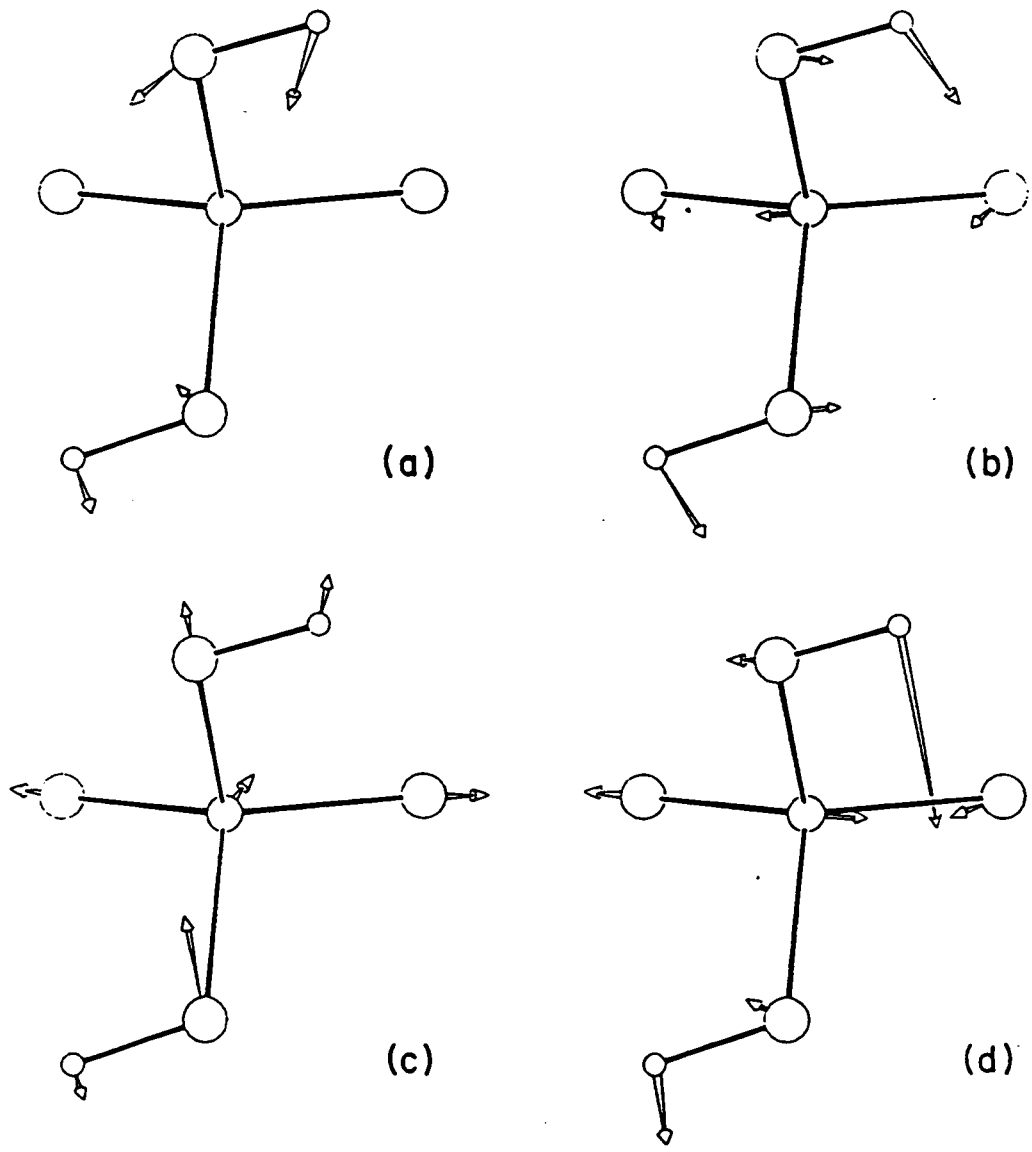

Figure 25. Selected vibrational modes of H_2SO_4 (indicated frequencies are calculated values from this study): **(a)** 326.9 cm^{-1}, asymmetric OH wag, which shows the largest disagreement with the observed value of 265 cm^{-1}; **(b)** 537.7 cm^{-1}, $S(OH)_2$ rock; **(c)** 938.9 cm^{-1}, assigned as $S(OH)_2$ symmetric stretch but appears to be a composite of several stretching and bending motions; **(d)** 1573.7 cm^{-1}, assigned as SO_2 asymmetric stretch, but also appears to be a composite mode.

Table 15. Calculated and experimental reaction energies.

Reaction: $H_2O + SO_3 \rightarrow H_2SO_4$; ΔE_{rxn} values in kJ mol^{-1}		
Source	RHF only	RHF + MP2
This study, MP2/6-31G**, 0K	-124.8	-88.7
298K	-126.0	-90.0
Chen and Plummer (1985), 3-21G*	-205.0	-124.1

Experiment: $\Delta H°_{rxn}(0K) = -92.3$ kJ mol^{-1}
$\Delta H°_{rxn}(298K) = -94.3$ kJ mol^{-1}

The experimental reaction enthalpies were determined from JANAF $\Delta H°_f$ data for H_2O, SO_3 (Stull and Prophet 1971), and H_2SO_4 (Chase et al. 1982).

(RHF) value determined without the MP2 correction is rather large. This serves to emphasize the need for modeling beyond the RHF level when dealing with reactions which are not isodesmic.

Another reaction of interest is $H_2S_2O_7 + H_2O \rightarrow 2H_2SO_4$, which can be used to assess the stability of $H_2S_2O_7$ relative to H_2SO_4 in the presence of water. At the RHF level, the energy of this reaction is -94 kJ mol^{-1} , indicating that H_2SO_4 is favored. Although an MP2 correction is needed to obtain a more accurate value, the magnitude of this energy is enough greater than zero that this qualitative observation of relative stabilities is probably reliable, particularly since the reaction is isodesmic. By comparison, the RHF-level reaction energy for $H_2SO_4 + SO_3 \rightarrow H_2S_2O_7$ is -31 kJ mol^{-1}, about one third the value of the other reaction. The correlation energy in this non-isodesmic reaction may be large enough even to preclude a qualitative conclusion that $H_2S_2O_7$ is stable relative to H_2SO_4 in the presence of SO_3. The relative magnitudes of these energy values, and the abundance of water in nature (which makes the first reaction more likely in a natural setting even before the energies are considered), may provide an explanation of the destabilization of the S_2O_7 dimer and the predominance of monomeric SO_4 units in sulfate minerals.

Energy as a Function of Torsional Angle

Geometry optimizations of gas-phase H_4TO_4 molecules (T = C, Si, Ge, Sn) within the constraints of C_1 symmetry show that these molecules have S_4 symmetry within the error of the calculation (Gibbs et al. 1988). They also show that such a molecule with S_4 symmetry is stabilized relative to one having D_{2d} symmetry, and that the stabilization increases as the TO bond length increases. Previous studies suggest that the gas-phase molecule H_2SO_4 has C_{2v} symmetry. As C_{2v} is a subgroup of D_{2d} rather than of S_4, we optimized the geometry within the constraints of C_2 point symmetry to learn whether the resulting symmetry is C_2 or C_{2v}. An examination of the resulting geometry of the molecule (Figure 18) shows that the OH bonds project out of the OSO plane, in conformity with C_2 symmetry. As a final test that the molecule has C_2 symmetry, we calculated the gradients of all variable parameters within the constraints of C_1 symmetry. Since the maximum gradient was less than 3×10^{-4}, and since all the eigenvalues of the Hessian matrix were positive, we concluded that the molecule has C_2 symmetry within the computational error.

In an exploration of the effect of rotating the OH bonds of H_2SO_4 about the SO bond vectors, we completed single-point calculations on the molecule at torsional angles $\tau = 0°$, $\tau = 45°$, 135°, and 180°. The $\tau = 0°$ structure is also called the U-conformation, and the $\tau = 180°$ structure is also called the W-conformation. The torsional angle is defined as the dihedral angle between the HOS and the OSO planes, illustrated by the inset in Figure 26. An additional calculation was made for the S-conformation, where the torsional angle is 0° for one OH bond and 180° for the other. These geometric variations were made in a way that preserved at least C_2 symmetry (the actual symmetry of the U- and W-conformations is C_{2v}); the other geometric parameters were allowed to vary within this symmetry constraint. The energy of the optimized molecule was taken as that at the 90° torsional angle. The resulting relation of energy change as a function of τ is displayed in Figure 26, where the energy change at each angle is defined relative to that at $\tau = 0°$. The curve in Figure 26 represents the truncated Fourier series

$$\Delta E_T = -49.00 + 19.01 \cos(\tau) + 20.50 \cos(2\tau) + 6.99 \cos(3\tau) + 2.50 \cos(4\tau) \qquad (9)$$

which was fitted by least squares to the calculated energies. The largest energy change, 67 kJ mol^{-1}, is between the torsional angles of 0° and 90°. A local maximum in the curve is at 180°, where the energy differs from the global minimum by only 15 kJ mol^{-1}. The energy of the S-conformer is 20 kJ mol^{-1} above that of the W-conformer. This suggests that if rotation of the OH bonds about the SO vectors would occur so as to pass through a C_{2v} structure, it would be more likely to occur through the W-conformation than through the U-conformation.

Chen and Plummer (1985) obtained two conformations of H_2SO_4, one with C_{2v} and one with C_2 symmetry, in calculations at the 3-21G* level. They note that the former is 3-4 kcal mol^{-1} (12.6-16.7 kJ mol^{-1}) higher in energy than the latter. They also note that the two structures can be transformed into one another by simultaneous rotation of the OH bonds about the SO[H] bond vectors. The rotational barrier through the W-conformation, determined in the present study, falls within this range and the W-conformation does have C_{2v} symmetry. However, Chen and Plummer do not give a detailed description of their C_{2v} conformer, so it is not certain that it has the

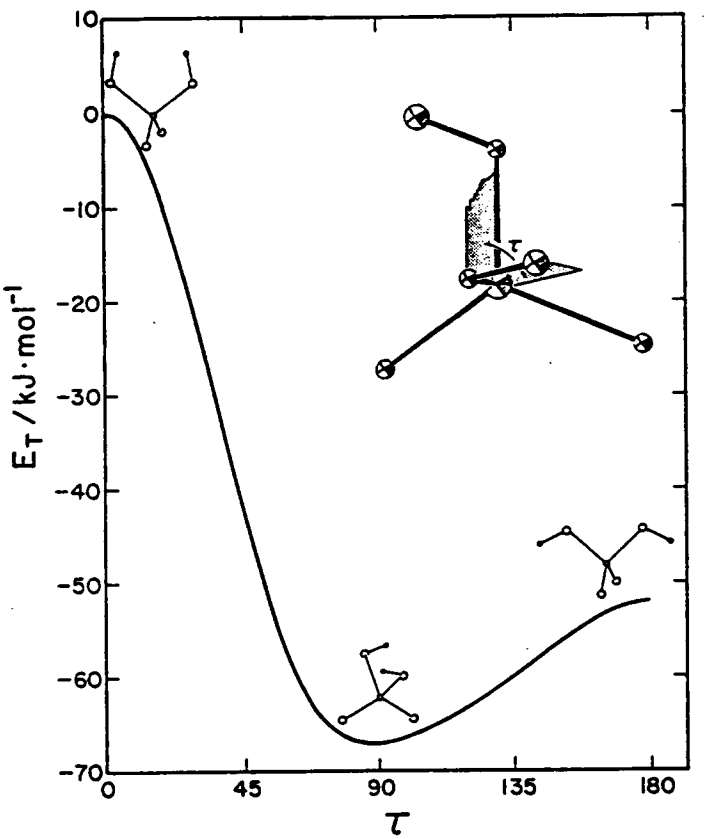

Figure 26. Total energy of H_2SO_4 as a function of the dihedral angle τ (see inset) between the HOS and OSO planes. The curve was generated by a truncated Fourier series fitted to the data (see text).

W-conformation. They do report a torsional angle of 93.1° for their C_2 structure, compared to 90.8° obtained by us.

CHARGE DENSITY ANALYSES

In an exploration of the deformation of the electron density and the bonded radii of S and O, we calculated total charge and deformation density maps for SO_3, H_2SO_4, H_6SO_6, and $H_2S_2O_7$. The geometry of H_6SO_6 was optimized at the 6-31G** level, assuming C_s symmetry. The maps reported in this study were calculated with DENMAP (written by R. Stevens, modified by J. A. Tossell and L. W. Finger) using the density matrices provided by the GAUSSIAN 82 calculations. The optimized geometries of SO_3 and H_6SO_6 are shown in Figure 27.

Deformation Densities of the TOT Groups in Tetrahedral Dimers

Using the results of semi-empirical MO calculations, Tossell (1983) was able to relate the magnitude of the *TOT* angle in molecules and crystals to electronegativity considerations, with wider angles being associated with the more electronegative *T* cations. From quantitative MO calculations, O'Keeffe and Gibbs (1985), and more recently Gibbs et al. (1988), have shown that the size of the angle also appears to be related to the electron density distribution of the *TOT* group (T=C,Si,Ge,Sn) of a H_6T_2O molecule. When the angle is narrow, as in H_6C_2O, the electron density is concentrated as bonding peaks in the CO bonds. On the other hand, the deformation maps for the other three molecules, which have wider *TOT* angles, show a continuum of charge density buildup in the interior region of the *TOT* angle between the bonding peaks. It seems that the wider angles in these molecules serve to reduce the repulsion between the electron density build-up in the bonds and that delocalized in the interior of the angle.

Deformation maps were calculated in this study for $H_6Si_2O_7$, $H_4P_2O_7$, and $H_2S_2O_7$ to see whether the narrower angle in $H_2S_2O_7$, relative to those in $H_6Si_2O_7$ and $H_4P_2O_7$ can be related in a similar way to the electron density distribution of the *TOT* group. An examination of the deformation maps displayed in Figure 28 shows a systematic decrease in the charge density build-up on the interior side of the angle as the angle decreases in the sequence $H_6Si_2O_7$, $H_4P_2O_7$,

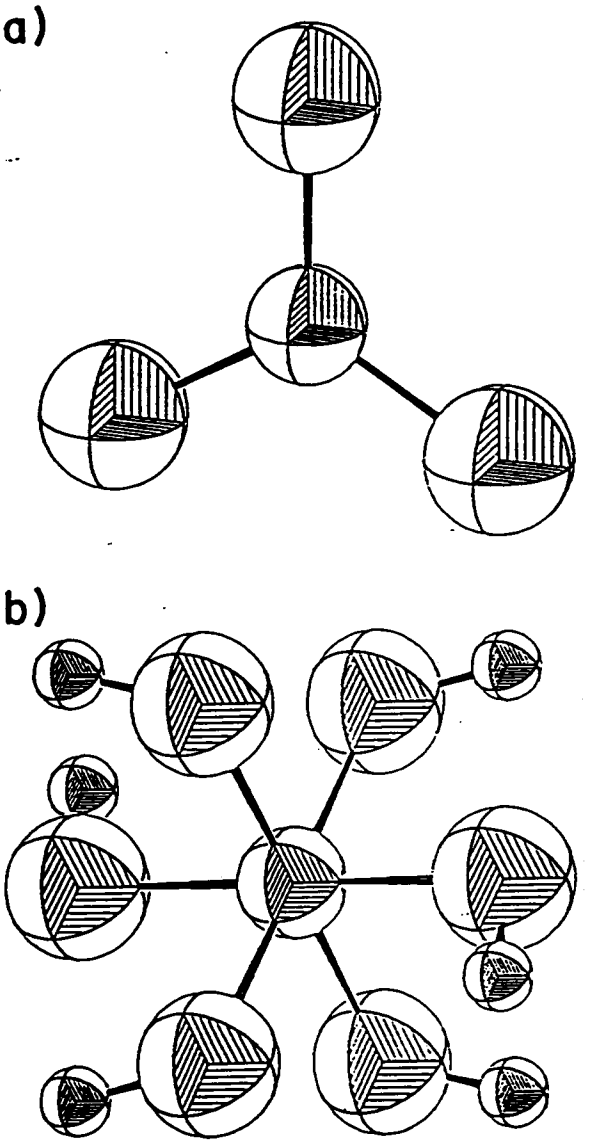

Figure 27. Optimized 6-31G** geometries of (a) SO_3 and (b) H_6SO_6. The large spheres represent O, the intermediate ones S, and the small ones H.

$H_2S_2O_7$. The sulfate dimer exhibits the smallest density on the interior side of the angle ($0.05 - 0.10$ e Å^{-3}), the phosphate dimer exhibits an intermediate density ($0.10 - 0.15$ e Å^{-3}), and the silicate dimer exhibits the largest density ($0.15 - 0.20$ e Å^{-3}). This suggests that the trend in observed equilibrium bridging angles for these dimers is related to the electron density build-up in the interior of the angles. In the case where there is a large build-up of negative charge in the interior of the angle, one expects repulsion between this region and the bonding peaks. This repulsion is reduced, as suggested above, when the angle widens. This view is consistent with the observed bridging angles in crystals, which decrease in the order SiOSi, POP, SOS. It is also consistent with the angle variations calculated for the H_6T_2O molecules studied by Gibbs et al. (1988) and those predicted by electronegativity considerations (Tossell 1983).

Bonded Radii of Sulfur and Oxygen

Studies by Shannon and Prewitt (1969) and Shannon (1981) indicate that the effective ionic radius of a cation in a crystal increases in a regular way with coordination number. In a determination of the bonded radius of sulfur for increasing coordination number, total charge density maps were calculated for the molecules SO_3, H_2SO_4 and $H_2S_2O_7$, and H_6SO_6, where the sulfur coordination is 3, 4, and 6, respectively (Figure 29). The bonded radius of S, r(S) and that of O, r(O), were estimated from these maps by measuring the distance from the center of each of these atoms to the point of minimum density along the SO bond and then scaling these distances to the optimized bond length. These radii are plotted as a function of the optimized bond length R(SO), in Figure 30. A linear regression analysis of r(S) and r(O) vs. the calculated SO bond length, $R(SO)_i$, shows that the slopes of these two lines are statistically identical. This implies that as the bond length increases, the bonded radii of both S and O atoms increase at about the same rate. Because bond strengths decrease (and therefore bond lengths increase) with increasing coordination, these trends also imply that the radii of the two atoms participating in the SO bond increase at the same rate as the coordination number increases and the s-character of the SO bond decreases. Finger and Gibbs (1985) and Gibbs and Boisen (1986) have shown in a study of $H_{8-m}T^{m+}O_4$ hydroxyacid molecules that the bonded radii of the T cations and the oxide ion also increases linearly and at the same rate for T = Li, Be, B, C and T = Na,Mg,...,S. This result implies, for a given

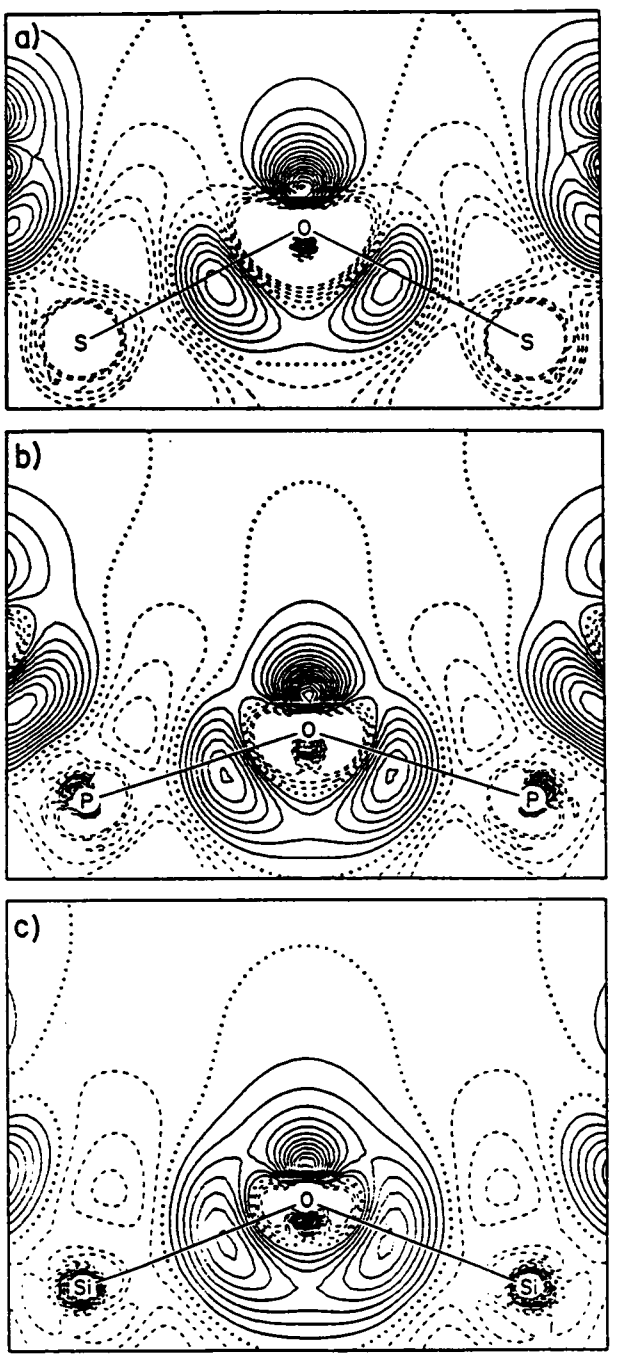

Figure 28. Calculated deformation density maps for (a) $H_2S_2O_7$ (this study); (b) $H_4P_2O_7$ (O'Keeffe et al. 1985); (c) $H_6Si_2O_7$ (O'Keeffe et al. 1985). Broken lines indicate negative contours, dotted line is the zero contour, and solid lines indicate positive contours. Contour interval is 0.05 e $Å^{-3}$.

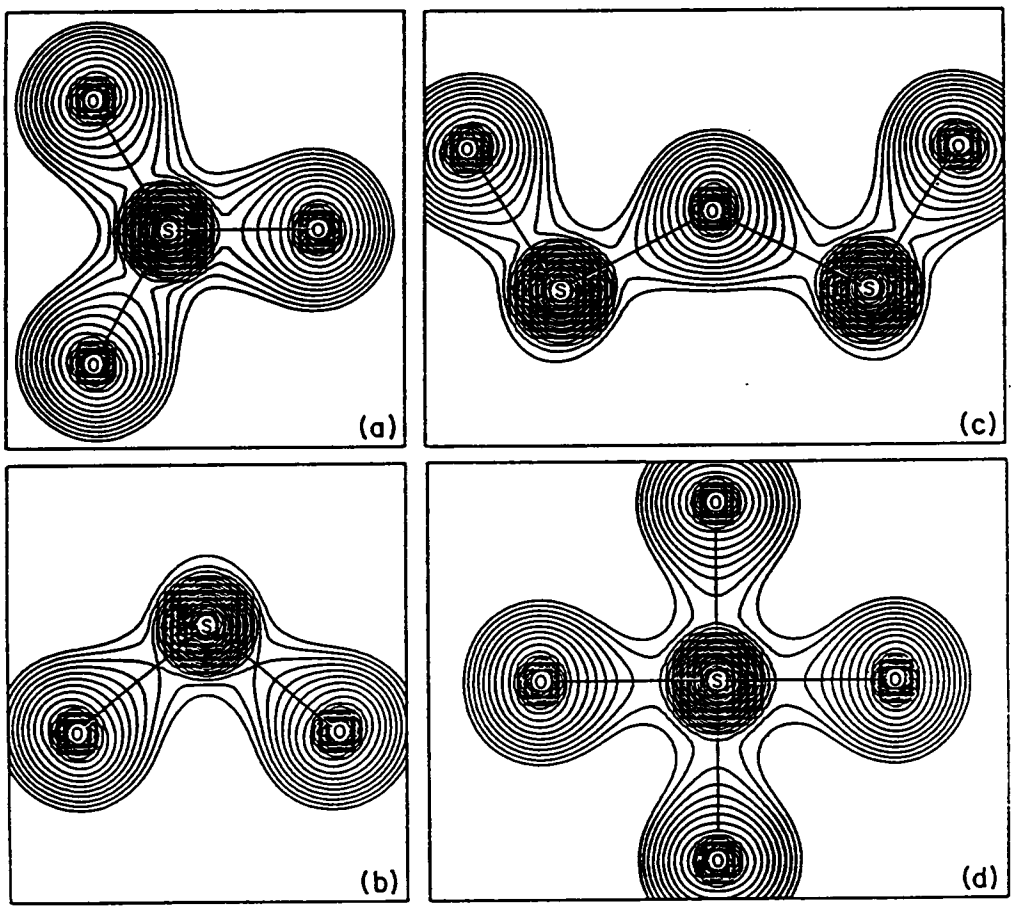

Figure 29. Calculated total density maps for **(a)** SO_3; **(b)** H_2SO_4; **(c)** $H_2S_2O_7$; **(d)** H_6SO_6. Lowest level is 1.0 e Å^{-3}; contour interval is $10^{0.1\rho'}$ where $\rho' = \rho$ / (1 e Å^{-3}) and ρ is total density.

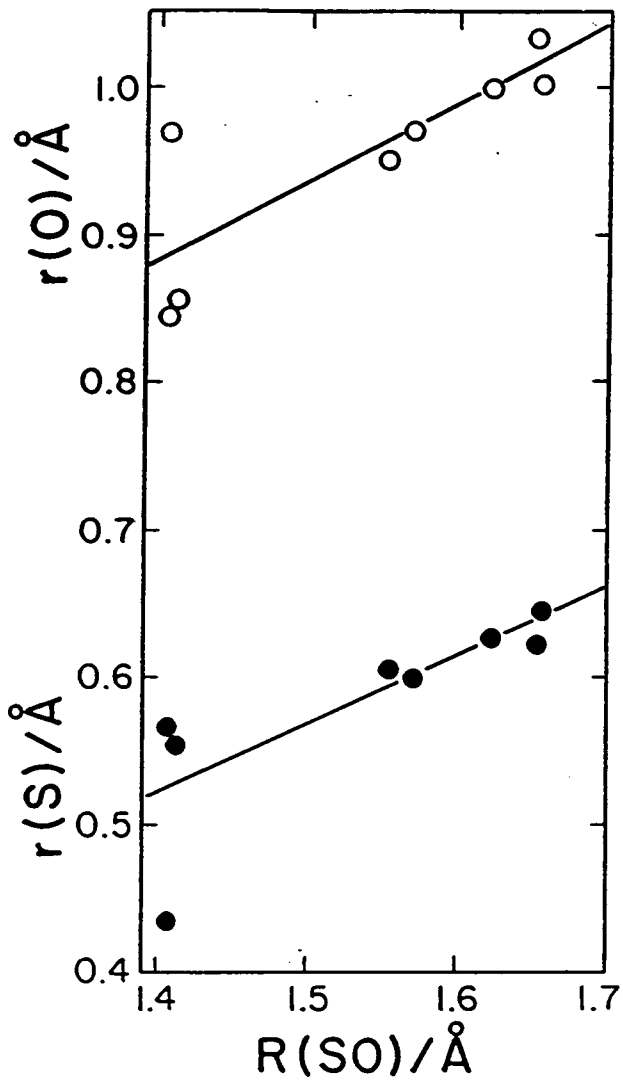

Figure 30. Bonded radii r(S) and r(O) vs. SO bond length estimated from the maps shown in Figure 29. The solid circles represent sulfur radii; the open circles represent oxygen radii.

row, that an increase in TO bond length is shared equally between the bonded radii of both the cation and the anion as one *T* cation is replaced by another.

The deviation from sphericity shown by the total charge density contours about the oxygens as compared with sulfur (Figure 29) is a reflection of the greater polarizability of the oxygen atom and of the covalency of the SO bond, particularly in those molecules where the sulfur is 3- and 4-coordinate. Lattice energy calculations employing the modified electron-gas model have been recently used to model the polarization of the O^{2-} ion by means of two shells of negative charge. Application of this model to the silica polymorphs has resulted in structures that mimic observed structures much better than those generated by the fully ionic model (Jackson and Gordon 1988, Jackson and Gibbs 1988). The form of the total density distributions determined in this study supports the ad hoc correction for the covalency of a bond using optimized shells of negative charge.

SUMMARY

(1) MO calculations have produced mathematical models of the molecules H_2SO_4 and $H_2S_2O_7$ which accurately reproduce several properties of monomeric and dimeric sulfate tetrahedral oxyanions. The calculated geometry of H_2SO_4 matches that in the gas-phase and the crystalline state. The calculations show that wider bond angles are associated with shorter bonds, with SO bond length decreasing linearly with increasing fractional s-character and increasing bond strength sum, p(O), in conformity with observations made on monomeric and dimeric groups in sulfate and polysulfate crystals.

(2) The reaction energy calculated for $SO_3 + H_2O \rightarrow H_2SO_4$ at 6-31G**/MP2 level agrees closely with the experimental enthalpies for this reaction at both 0K and 298K. The reaction energy calculated at 6-31G** level (without the MP2 correction) for $H_2S_2O_7 + H_2O \rightarrow 2H_2SO_4$ allows a qualitative observation that $H_2S_2O_7$ is destabilized relative to H_2SO_4 in the presence of water. This may explain the absence of sulfate dimers in minerals.

(3) Vibrational frequencies calculated for H_2SO_4 are in reasonable agreement with those observed in the gas-phase molecule (Giguere and Savoie 1963). The atomic displacements associated

with each vibrational mode are for the most part in agreement with the assignments made by those workers.

(4) The barriers to bending and the bending force constants of the *TOT* angles increase, and the *TOT* angles themselves decrease, in the series SiOSi, POP, SOS. Deformation density maps show an increasing buildup of charge density in the interior region of the *TOT* angle in the series SOS, POP, SiOSi. It is plausible that a buildup of charge density between the bridging bonds would repel the negative charge density in the bonding peaks along the bond vectors, widening the bridging angle. The large barrier to linearity is likely to limit the adaptability of the S_2O_7 group to different crystal structures, and may explain the narrow deviation of the SOS angles in polysulfate crystals from the observed average value. It also suggests that sulfate glasses are unlikely to adopt structures based on polymerized sulfate tetrahedra, in contrast to silicate glassses, where the SiOSi angle shows a wider range of values.

(5) From total density maps calculated for SO_3, H_2SO_4, $H_2S_2O_7$, and H_6SO_6, we have estimated the bonded radii of S and O in various coordinations of S by O. We find that as the SO bond length increases in response to increasing coordination number and increasing s-character of the SO bond, the bonded radii of S and O increasing at the same rate. Furthermore, the polarization of O by S along the SO bond is clearly evident in the total density maps, indicating that a purely ionic treatment of sulfate crystal structures is not appropriate, and that some means of modeling this polarization would be needed.

Chapter V

CONCLUDING COMMENTS

A major difference between the MEG and the MO methods, other than those differences already mentioned, is that the MO method provides a more detailed modeling of bonds themselves. The LCAO approximation used in the MO method makes bonds explicit features of the model; in the MEG method, where AOs associated with neighboring atoms remain unaltered at all interatomic distances, bonds are implicit features of the model. Charge density mappings are therefore inherently more meaningful in the context of an MO model, where rearrangements of electron density are assumed to occur as atoms are brought together to form bonds. We did not undertake charge density mappings in our MEG studies mainly because the computational resources available to us do not lend themselves to such mappings, but also because the features of such maps can probably be envisioned intuitively from the implications of the additive-density assumption. The charge and deformation density distributions generated with the MO method are apparently quite realistic, as evidenced by the close agreement between our maps and those determined from x-ray diffraction experiments reported in Chapter IV. There is no reason to expect that charge and deformation density distributions would be modeled realistically with the MEG method. Consequently, we should not expect the MEG method to be as useful as the MO method appears to be for determining barriers to linearity or for forming hypotheses related to bridging angle variations. On the other hand, we should expect the MEG method to be more useful than the MO method would be for testing hypotheses related to ionic crystal structures, because covalency effects are

eliminated with the purely ionic MEG method, and because the MEG method provides models of entire crystal structures.

The variations in charge and deformation density distributions found in Chapter IV may provide an explanation of the observations made in comparing the CO_3 groups in calcite and aragonite modeled with the MEG method to those observed. In Figure 28 (Chapter IV), we see that the deformation density in the bridging *TOT* groups is more concentrated near the axes of those bonds believed to have larger covalent character. We have already noted that the CO bond is expected to have a large covalent character, and the deformation density in bridging COC units modeled with the MO method is concentrated along the bond axis (Gibbs et al. 1987). This means that there is a higher electron density near these bond axes in the molecule than in the promolecule, a hypothetical aggregate of atoms chemically and geometrically identical with the molecule, but composed of spherically symmetric, non-interacting atoms. It is therefore likely that the buildup of electron density along the bond axis would screen a pendant atom from the core charge of the central atom in a molecule to a greater extent than in the corresponding promolecule. If the buildup of electron density along a bond axis does increase with increasing covalency, we should expect the resulting screening of pendant atoms from the core charge of the central atom in a molecule to increase with increasing covalency. In the corresponding promolecule, there would be no increase in the buildup of electron density with increasing covalency, because by hypothesis the atoms in the promolecule retain spherically symmetric charge densities and do not interact. The electron density distribution generated with the MEG method is expected to be more nearly that of a promolecule than that of a molecule, due to the additive-density approximation. Consequently, the pendant atoms in a molecule modeled with the MEG method would not be expected to be as completely screened from the core charge of the central atom as would the pendant atoms in a molecule modeled with the MO method. This would result in a stronger attractive force between the central atom and the pendant atoms in a CO_3 group modeled with the MEG method than in one modeled with the MO method. This in turn would result in a shorter CO bond length in a CO_3 group modeled with the MEG method than in one modeled with the MO method. As we noted, the electron density distribution modeled with the MO method is probably fairly close

to that observed, therefore we should expect that the CO bond lengths determined with the MEG method would be shorter than observed. Anion polarization effects may contribute to the buildup of deformation density near a bond axis. As we noted in Chapter IV, inclusion of a shell model for anion polarization in the MEG method results in closer agreement between model and observed structures where the bonding in those structures is believed to have significant covalent character (Jackson 1988, Jackson and Gibbs 1988, Jackson and Gordon 1988).

Both the MEG method and the MO method have provided information that allows us to comment on atomic and ionic radii in relation to crystal structures. In Chapter III, we found that the MEG method determined correct cation coordination numbers in all but three of 16 alkali halide crystals whereas the radius ratio rule determined correct cation coordination numbers in no more than nine of the same 16 crystals. The results of those MEG modelings suggest that energy minimization is more important than packing efficiency in determining the stability of an ionic crystal structure, a suggestion which is physically reasonable. In Chapter IV, using the MO method, we found that as SO bond lengths increase in response to decreasing SO bond strengths with increasing coordination of S by O, the bonded radii of S and O increase at about the same rate. This result is consistent with those found previously for other hydroxyacid molecules (Finger and Gibbs 1985, Gibbs and Boisen 1986), and is at variance with the assumption of Shannon and Prewitt (1969) and of Shannon (1981) that cation radii increase at a greater rate than anion radii with increasing cation coordination number.

The methods described and demonstrated in Chapters II through IV represent two of several tools available for theoretical studies of the bonding in crystals. Each has its strengths and each has its limitations. Like the tools in a workshop, the tools for modeling bonding in crystals must be applied to the tasks for which they are designed. The MO method is obviously the better choice of the two methods just described if detailed modeling of bonds is desired or if localized phenomena are to be modeled. The MEG method is the better choice for modeling a crystal structure on a larger scale, especially if a hypothetical purely ionic crystal structure is to be generated. With continued refinement and improvement, the MEG model may find applicability even to modeling crystal structures having more covalent character.

References

Ahrens LH (1952) The use of ionization potentials. Part 1. Ionic radii of the elements. Geochim Cosmochim Acta 2:155-169

Almenningen A, Bastiansen O, Ewing V, Hedberg K, Traetteberg M (1963) The molecular structure of disiloxane, $(SiH_3)_2O$. Acta Chim Scand 17:2455-2460

Barrow MJ, Ebsworth EAV, Harding MM (1979) The crystal and molecular structures of disiloxane (at 108K) and hexamethyldisiloxane (at 148K). Acta Cryst B35:2093-2099

Baur WH (1970) Bond-length variation and distorted coordination polyhedra in inorganic crystals. Trans Am Crystallogr Assoc 6:125-155

Bingel WA, Luttke W (1981) Hybrid orbitals and their applications in structural chemistry. Angew Chemie 20:899-911

Binkley JS, Frisch MJ, DeFrees DJ, Raghavachari K, Whiteside RA, Schlegel HB, Fluder EM, Pople JA (1982) GAUSSIAN 82. Department of Chemistry, Carnegie-Mellon University, Pittsburgh, PA

Birch F (1978) Finite strain isotherm and velocities for single-crystal and polycrystalline NaCl at high pressures and 300°K . J Geophys Res 83:1257-1267

Boisen Jr MB, Gibbs GV (1987) A method for calculating fractional s-character for bonds of tetrahedral oxyanions in crystals. Phys Chem Minerals 14:373-376

Böttger, H (1974) Vibrational properties of non-crystalline solids. Phys Stat Solidi B64:9-43

Cameron M, Papike JJ (1980) Crystal chemistry of silicate pyroxenes. In: Prewitt, C.T. (ed.), Reviews in Mineralogy, vol. 7, pp. 5-92. Mineralogical Society of America, Washington DC

Cameron M, Papike JJ (1981) Structural and chemical variations in pyroxenes. Am Mineral 65:1-50

Chase MW, Curnutt JL, Downey JR, McDonald RA, Syverud AN, Valenzuela EA (1982) JANAF thermochemical tables, 1982 supplement. J Phys Chem Ref Data 11:695-940

Chase Jr MW, Davies CA, Downey Jr JR, Frurip DJ, McDonald RA, Syverud AN (1985) JANAF thermochemical tables, 3rd ed. J Phys Chem Ref Data 14 (supp 1)

Chen TS, Plummer PLM (1985) Ab initio MO investigation of the gas-phase reacton $SO_3 + H_2O \rightarrow H_2SO_4$. J Phys Chem 89:3689-3693

Clark JR, Appleman DE, Papike JJ (1969) Crystal- chemical characterization of clinopyroxenes based on eight new structure refinements. In: Papike, J.J. (ed.), Pyroxenes and Amphiboles: Crystal Chemistry and Phase Petrology. Mineralogical Society of America Special Paper 2, pp. 31-50. Mineralogical Society of America, Washington DC

Clementi E, Roetti C (1974) Roothaan-Hartree-Fock atomic wavefunctions. Basis functions and their coefficients for ground and certain excited states of neutral and ionized atoms, $Z \leq 54$. Atom Data Nuc Data Tables 14:177-478

Clugston MJ (1978) The calculation of intermolecular forces. A critical examination of the Gordon-Kim model. Adv Phys 27:893-912

Cohen AJ, Gordon RG (1975) Theory of the lattice energy, equilibrium structure, elastic constants, and pressure-induced phase transitions in alkali-halide crystals. Phys Rev B12:3228-3241

Cohen AJ, Gordon RG (1976) Modified electron-gas study of the stability, elastic properties, and high-pressure behavior of MgO and CaO crystals. Phys Rev B14:4593-4705

Coulson CA (1961) Valence. Oxford University Press, Oxford UK

Dal Negro A, Ungaretti L (1971) Refinement of the crystal structure of aragonite. Am Mineral 56:768-772

Dandekar DP, Ruoff AL (1968) Variation in the elastic constants of calcite with temperature. J Appl Phys 39:3694-3699

Dean P (1972) The vibrational properties of disordered systems: numerical studies. Rev Mod Phys 44:127-168

Douglade J, Mercier R (1979) Structure crystalline du disulfate d'antimoine (III) $Sb_2(S_2O_7)_3$. Acta Cryst B35:1062-1067

Downs JW, Gibbs GV (1981) The role of the BeOSi bond in the structures of beryllosilicate minerals. Am Mineral 66:819-826

Dytrych WJ (1983) A comparison of theoretical and observed bridging bond lengths and angles in condensed phosphates and sulfates. M.S. thesis, Virginia Polytechnic Institute and State University, Blacksburg, VA

Effenberger H, Mereiter K, Zemann J (1981) Crystal structure refinements of magnesite, calcite, rhodochrosite, siderite, smithsonite and dolomite, with discussion of some aspects of the stereochemistry of calcite-type carbonates. Z Krist 156:233-243

Einstein FW, Willis AC (1981) Structure of tellurium (IV) pyrosulfate. Acta Cryst B37:218-220

Ernst WG (1969) Earth Materials. Prentice-Hall, Englewood Cliffs, NJ

Ewald PP (1921) The calculation of optical and electrostatic latice potentials. Ann Phys 64:253-287

Finger LW, Gibbs GV (1985) A derivation of bonded radii from theoretical molecular charge distributions (abstr). EOS 66(18):356

Frisch MJ, Schaefer III HF, Binkley JS (1985) Theoretical study of the structure and spectroscopic characteristics of protonated carbon dioxide. J Phys Chem 89:2192-2194

Frisch MJ, Yamaguchi Y, Gaw JF, Schaefer III HF, Binkley JS (1986) Analytic Raman intensities from molecular electronic wave functions. J Chem Phys 84:531-532

Frye K (1974) Modern Mineralogy. Prentice-Hall, Englewood Cliffs, NJ

Fumi FG, Tosi MP (1964) Ionic sizes and Born repulsive parameters in the NaCl-type alkali halides. I. Huggins-Mayer and Pauling forms. J Phys Chem Solids 25:31-43

Geisinger KL (1983) A theoretical and experimental study of bonding in silicates and related materials. Ph. D. Dissertation, Virginia Polytechnic Institute and State University, Blacksburg, VA

Geisinger KL, Gibbs GV (1981) SiSSi and SiOSi bonds in molecules and solids: a comparison. Phys Chem Minerals 7:204-210

Geisinger KL, Gibbs GV, Navrotsky A (1985) A molecular orbital study of bond length and angle variations in framework structures. Phys Chem Minerals 11:266-283

Geisinger KL, Spackman MA, Gibbs GV (1987) Exploration of structure, electron density distribution and bonding in coesite with Fourier and pseudoatom refinement methods using single crystal x-ray diffraction data. J Phys Chem 91:3237-3244

Gibbs GV (1982) Molecules as models for bonding in silicates. Am Mineral 67:421-450

Gibbs GV, Boisen Jr MB (1986) Molecular mimicry of structure and electron density distributions in minerals. Mat Res Soc Symp Proc 73:515-527

Gibbs GV, D'Arco P, Boisen Jr MB (1988) Molecular mimicry of bond length and angle variations in germanate and thiogermanate crystals: A comparison with variations calculated for C-, Si- and Sn-containing oxide and sulfide molecules. J Phys Chem 91:5347-5354

Gibbs GV, Finger LW, Boisen Jr MB (1987) Molecular mimicry of the bond-length--bond-strength variations in oxide crystals. Phys Chem Minerals 14:327-331

Gibbs GV, Meagher EP, Newton MD, Swanson DK (1981) A comparison of experimental and theoretical bond length and angle variations for minerals, inorganic solids, and molecules. In: O'Keeffe M, Navrotsky A (eds) Structure and Bonding in Crystals, Vol 1, pp 195-225. Academic Press, New York

Gibbs GV, Hamil MM, Lousinathan SJ, Bartell LS, Yow H (1972) Correlations between SiO bond length, SiOSi angle, and bond overlap populations calculated using extended Huckel molecular orbital theory. Am Mineral 57:1578-1613

Giguere PA, Savoie R (1963) The normal vibrational frequencies and the thermodynamic functions of H_2SO_4 and D_2SO_4. J Am Chem Soc 85:287-289

Gillespie RJ (1972) Molecular Geometry. Van Nostrand Reinhold, London

Goldschmidt VM (1954) Geochemistry (Alex Muir, ed). Oxford University Press, London

Goldschmidt VM, Barth T, Lunde G, Zachariasen WH (1926) Geochemical distribution law of the elements. VI. Crystal structure of the rutile type with remarks on the geochemistry of the bivalent and quadrivalent elements. Skrifter Norske Videnskaps Akad. Oslo, Mat-Nat Kl 1

Gordon RG, Kim YS (1972) Theory for the forces between closed-shell atoms and molecules. J Chem Phys 56:3122-3133

Hazen RM, Finger LW (1982) Comparative Crystal Chemistry. Wiley, New York, NY

Hearmon RFS (1946) Elastic constants of anisotropic materials. Rev Mod Phys 18:409-440

Hehre WJ, Radom L, Schleyer R, Pople JA (1986) Ab initio Molecular Orbital Theory. Wiley, New York.

Hill RJ, Newton MD, Gibbs GV (1983) A crystal chemical study of stishovite. J Solid State Chem 47:185-200

Holmquist S (1978) Reaction models for sulphate in glass. Phys Chem Glasses 18:76-77

Jackson MD (1986) Theoretical Investigations of Chemical Bonding in Minerals. Ph.D. thesis, Harvard University, Cambridge, MA

Jackson MD, Gibbs GV (1988) A modeling of the coesite and feldspar framework structure types of silica as a function of pressure using modified electron gas methods. J Phys Chem 92:540-545

Jackson MD, Gordon RG (1988a) A MEG study of the olivine and spinel forms of Mg_2SiO_4. Phys Chem Minerals 15:514-520

Jackson MD, Gordon RG (1988b) MEG investigation of low- pressure silica--shell model for polarization. Phys Chem Minerals (In press)

Kim YS, Gordon RG (1974) Theory of binding of ionic crystals: application to alkali-halide and alkaline-earth- dihalide crystals. Phys Rev B9:3548-3554

Kimura K, Kubo M (1959) Structures of dimethyl ether and methyl alcohol. J Chem Phys 30:151-158

Kittel C (1976) Introduction to Solid State Physics, 5th edn. Wiley, New York, NY

Klahn B (1983) The relations between the valence angles of sp^3-hybridized central atoms for all possible local symmetries. J Molec Struc 104:49-77

Klein C, Hurlburt CS (1985) Manual of Mineralogy, 20th edn. (after J. D. Dana). Wiley, New York, NY

Kuczkowsky RL, Suenram RD, Lovas FD (1981) Microwave spectrum, structure, and dipole moment of sulfuric acid. J Am Chem Soc 103:2561-2566

Landé A (1920) The size of atoms. Z Physik 2:87-89

Laws E, Walpole Computer Programmers (1971) Atomic SCF Program. Department of Chemistry, Harvard University, Cambridge, MA, and Massachusetts Department of Corrections, Walpole, MA

Lennard-Jones JE, Dent BM (1927) Some theoretical determinations of the structure of carbonate crystals.--I. Proc Royal Soc London A113:673-689

Lippmann F (1973) Sedimentary Carbonate Minerals. Springer-Verlag, Berlin

Liu L, Ringwood AE (1975) Synthesis of a perovskite-type polymorph of calcium silicate ($CaSiO_3$). Earth Planet Sci Lett 28:209-211

Louisnathan SJ, Hill RF, Gibbs GV (1977) Tetrahedral bond length variations in sulfates. Phys Chem Minerals 1:53-69

McWeeny R (1979) Coulson's Valence, 3rd edn. Oxford University Press, Oxford, UK

Megaw HD (1972) Structure and transitions in perovskites (abstr). J Phys 33:C2.1-C2.5

Muhlhausen C, Gordon RG (1981) Electron-gas theory of ionic crystals, including many-body effects. Phys Rev B23:900-923

Narasimham PSL, Rao KJ (1978) Phase diagram and glass formation in the K_2SO_4-$ZnSO_4$ system. J Non-Cryst Solids 27:225-246

Naray-Szabo SV (1943) The structural type of perovskite. Naturwissensch 31:202-203

Navrotsky A, Geisinger KL, McMillan P, Gibbs GV (1985) The tetrahedral framework in glasses and melts--Inferences from molecular orbital calculations and implications for structure, thermodynamics, and physical properties. Phys Chem Minerals 11:284-298

Newton MD (1981) Theoretical probes of bonding in the siloxyl group. In: O'Keeffe M, Navrotsky A (eds) Structure and Bonding in Crystals, Vol 1. Academic Press, New York

Newton MD, Gibbs GV (1980) Ab initio calculated geometries and charge distributions for H_4SiO_4 and $H_6Si_2O_7$ compared with experimental values for silicates and silioxanes. Phys Chem Minerals 6:221-246

O'Keeffe M (1977) On the arrangements of ions in crystals. Acta Cryst A33:924-927

O'Keeffe M, Gibbs GV (1985) Ab initio MO calculations on cyclodisiloxanes and other Si-X-Si-X rings and the problem of "silica-*w*". J Phys Chem 89:4574-4577

O'Keeffe M, Hyde BG, Bovin JO (1979) Contribution to the crystal chemistry of orthorhombic perovskites: $MgSiO_3$ and $NaMgF_3$. Phys Chem Minerals 4:299-305

O'Keeffe M, Domenges B, and Gibbs GV (1985) Ab initio molecular orbital calculations on phosphates: comparison with silicates. Jour Phys Chem 89:2304-2309

Pauling L (1927) Sizes of ions and structure of ionic crystals. J Am Chem Soc 49:765-792

Pauling L (1939) The Nature of the Chemical Bond. Cornell University Press, Ithaca, NY

Pauling L (1960) The Nature of the Chemical Bond, 3rd ed. Cornell University Press, Ithaca, NY

Phillips JC (1970) Ionicity of the chemical bond in crystals. Rev Mod Phys 42:317-356

Post JE, Burnham CW (1986) Ionic modeling of mineral structures and energies in the electron gas approximation: TiO_2 polymorphs, quartz, forsterite, diopside. Am Mineral 71:142-150

Reeder RJ (1983) Crystal chemistry of the rhombohedral carbonates. In: Reeder, R.J. (ed.), Reviews in Mineralogy, vol. 11, pp. 1-48. Mineralogical Society of America, Washington DC

Robinson K, Gibbs GV, Ribbe PH (1971) Quadratic elongation: a quantitative measure of distortion in coordination polyhedra. Science 172:567-570

Schlüter M, Sham LJ (1982) Density functional theory. Phys Today 35:36-43.

Shannon RD (1981) Bond distances in sulfides and a preliminary table of sulfide crystal radii. In: O'Keeffe M, Navrotsky A (eds) Structure and Bonding in Crystals, Vol. 2. Academic Press, New York

Shannon RD, Prewitt CT (1969) Effective ionic radii in oxides and fluorides. Acta Cryst B25:925-946

Simmons G, Wang H (1971) Elastic Constants: Single Crystal Elastic Constants and Calculated Aggregate Properties. MIT Press, Cambridge, MA

Slater JC (1964) Atomic radii in crystals. J Chem Phys 41:3199-3204

Smith JV (1953) Reexamination of the crystal structure of melilite. Am Mineral 38:643-661

Spackman MA, Hill RJ, Gibbs GV (1987) Exploration of structure and bonding in stishovite with Fourier and pseudoatom refinement methods using single crystal and powder x-ray diffraction data. Phys Chem Minerals 14:139-150

Speer JA (1983) Crystal chemistry and phase relations of orthorhombic carbonates. In: Reeder, R.J. (ed.), Reviews in Mineralogy, vol. 11, pp. 145-190. Mineralogical Society of America, Washington DC

Stull DR, Prophet H (eds) (1971) JANAF Thermochemical Tables, 2nd ed. National Bureau of Standards, Washington, DC

Sundar HGK, Rao KJ (1980) Glass formation in the ternary sulphate system K_2SO_4-Na_2SO_4-$ZnSO_4$. J Chem Soc Faraday I 76:1617-1626

Tossell JA (1983) A qualitative molecular orbital study of the stability of polyanions in mineral structures. Phys Chem Minerals 9:115-123

Tossell JA, Gibbs GV (1977) Molecular orbital studies of geometries and spectra of minerals and inorganic compounds. Phys Chem Minerals 2:21-57

Tossell JA, Gibbs GV (1978) The use of molecular orbital calculations on model systems for the prediction of bridging-bond-angle variations in siloxanes, silicates, silicon nitrides, and silicon sulfides. Acta Cryst A34:463-472

Wagman DD, Evans WH, Parker VB, Schumm RH, Halow I, Bailey SM, Churney KL, Nutall RL (1982) The NBS tables of chemical thermodynamic properties. Selected values for inorganic and C_1 and C_2 organic substances in SI units. J Phys Chem Ref Data 11 (supp 2)

Waldman M, Gordon RG (1979) Scaled electron gas approximation for intermolecular forces. J Chem Phys 71:1325-1329

Warren BE (1972) X-ray studies of the structure of glass. Soviet Phys--Crystallogr 16:1106-1113

Wasastjerna JA (1923) Refraction equivalents of ions and the structure of compound ions. Soc Sci Fennica Comm Phys-Mat 1:1-7

Watson RE (1958) Analytic Hartree-Fock solutions for O^-. Phys Rev 111:1108-1110

Yagi T, Mao H, Bell PM, (1978) Structure and crystal chemistry of perovskite-type $MgSiO_3$. Phys Chem Minerals 3:97-110

Yamaguchi Y, Frisch MJ, Gaw JF, Schaefer III HF, Binkley JS (1986) Analytic evaluation and basis set dependence of intensities of infrared spectra. J Chem Phys 84:2262-2278

Yu PY, Mak TCW (1978) Refinement of the crystal structure of anhydrous sulfuric acid. J Cryst Molec Struc 8:193-199

Yuen PS, Lister MW, Nyburg SC (1978) The four-center charge distribution of the carbonate ion and the lattice energies of calcite and aragonite. J Chem Phys 68:1936-1941

Zachariasen WH (1931) A set of empirical crystal radii for ions with inert-gas configuration. Z Krist 80:137-153

Zedlitz O (1939) Perovskite, uhligite, and dysanalite. Neues Jahrb Mineral A75:245-296

Zhang ZG, Boisen Jr MB, Finger LW, Gibbs GV (1985) Molecular mimicry of the geometry and charge density distribution of polyanions in borate minerals. Am Mineral 70:1238-1247

Zoltai T, Stout JH (1984) Mineralogy. Concepts and Principles. Burgess, Minneapolis, MN

Zussman J (1968) The crystal chemistry of pyroxenes and amphiboles. 1. Pyroxenes. Earth Sci Rev 4:39-67

The vita has been removed from the scanned document